Investigation of the benefits of a parallel-hybrid electric architecture in NO_x, CO and H_2O emissions in the LTO cycle for regional turboprop

Ana Marta A. S. Cabrita de Carvalho

Technische Universiteit Delft

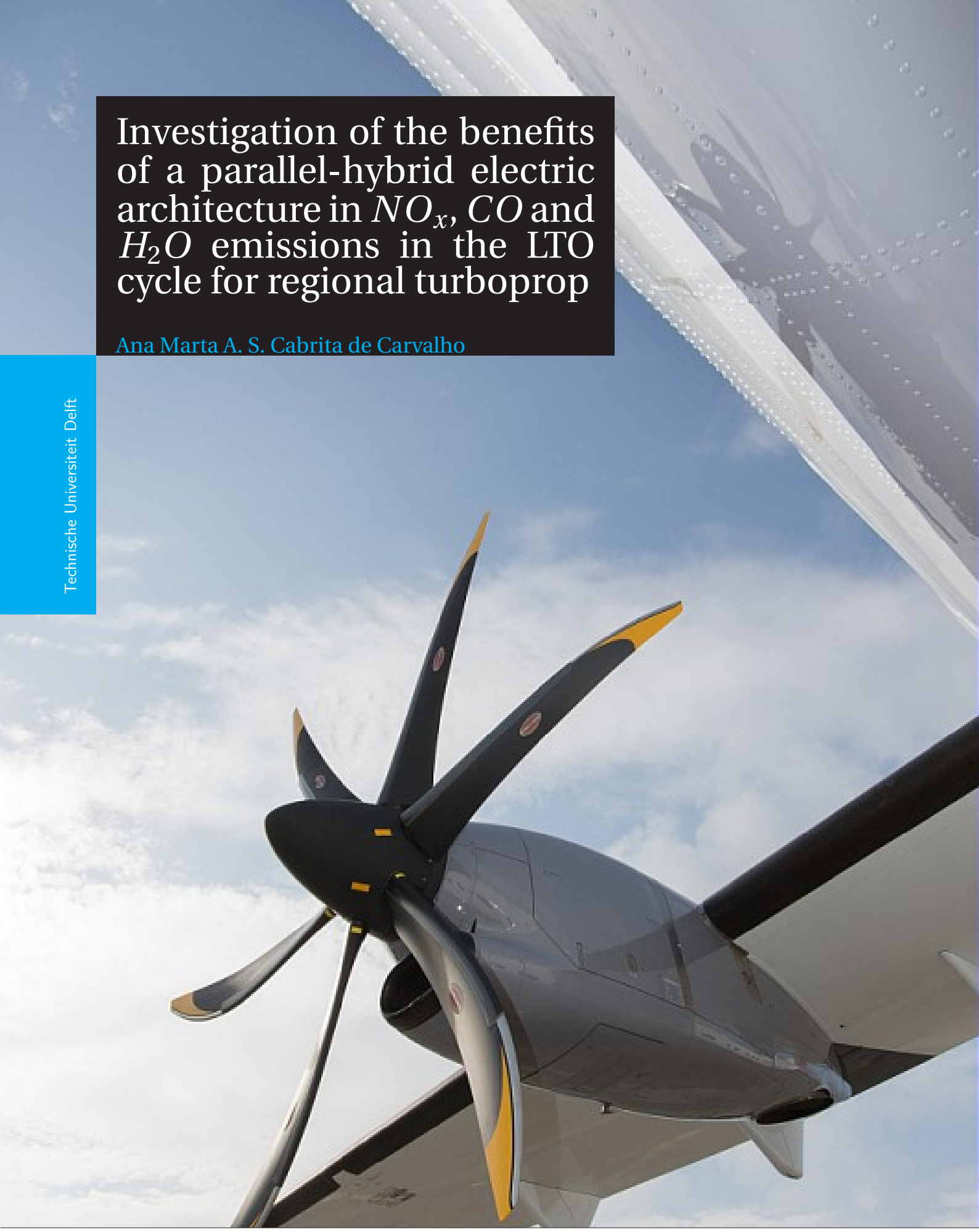

TU Delft Delft University of Technology

Challenge the future

Investigation of the benefits of a parallel-hybrid electric architecture in NO_x, CO and H_2O emissions in the LTO cycle for regional turboprop

by

Ana Marta A. S. Cabrita de Carvalho

in partial fulfillment of the requirements for the degree of

Master of Science

in Aerospace Engineering

at the Delft University of Technology,

to be defended publicly on July 24, 2020 at 02:00 PM.

Supervisors:	Dr. Maurice Hoogreef	
	Dr. Arvind Rao	
Thesis committee:	Dr. Arvind Rao ,	TU Delft
	Dr. Maurice Hoogreef,	TU Delft
	Dr. Irene Dedoussi	TU Delft

TU Delft Delft University of Technology

Abstract

In Europe, air traffic is foreseen to rise 42 % from 2017 to 2040. Consequently, aircraft emissions are expected to escalate, even under anticipated technology and operational improvements, leading to more stringent Standards and Regulations. Particularly, emissions emitted at low altitudes (vicinity of airports) play a major role in Local Air Quality, having a detrimental impact on the environment and human health and welfare. NO_x and CO emissions are examples of emissions that are monitored and regulated at low altitudes, in the so-called LTO (Landing and Take-off) cycle. This cycle targets the emissions released below 3,000 ft (914 meters), comprising taxi, take-off, climb-out and approach segments with a fixed duration and power setting.

Hybrid-electric propulsion (HEP) has been investigated as a concept that could address this problem by potentially bring a fuel burn and emissions reduction. In particular, the parallel-hybrid electric architecture has been proven to be more beneficial to integrate into large commercial aircraft and regional aircraft (regional turboprop incorporating a parallel-hybrid powertrain).

This research goal is to assess whether a parallel-hybrid electric architecture (also known as electrically assisted regional turboprop) could reduce exhaust emission gases (namely NO_x, CO and H_2O) in the LTO cycle.

To reach the research goal, a turboprop engine model, a simplified electric system sizing model, and a mission simulation and analysis routine were developed.

The turboprop model computes accurate engine performance and predicts emissions at each time-step of the mission. The electrical system model estimates its weight, based on the degree of hybridization (percentage of the electric power provided to the total shaft power), DoH, and technology maturity scenario.

The regional aircraft used as reference was the ATR 72-600, and its performance was computed across a 1000 Km fixed mission. The performance of the electrically assisted versions of the ATR 72-600 was also estimated in the same mission. Due to the focus of the research on low altitude emissions, the following flight segments were hybridized:

- Taxi-out and Taxi-in are fully (100 %) electric due to the low inefficiency of the gas turbines during this phase
- Hybrid Take-off and Climb-out (up to 3048 meters)
- Hybrid approach (below 457 meters)

In order to evaluate the sensitivity of the electrically assisted regional turboprop to the DoH and battery technology maturity scenarios, they were varied from 10 to 100 % and from 300 to 1000 Wh/kg, respectively, in the simulations.

Analyzing the LTO cycle emissions of NO_x, CO, and H_2O, this study shows that these can be reduced with a parallel-hybrid electric architecture. NO_x LTO emissions can be reduced from 29 % up to 71 %, and CO LTO from 15.4 % up to 21 %. As to H_2O produced in the LTO cycle, it can be reduced from 31 % up to 55%.

However, the results have shown that the hybridization proposed leads to an increase in the take-off weight (TOW) due to the significant weight added by the electric system, even when admitting an optimistic battery technology of 1000 Wh/kg (e_{Bat}). As a result, the benefits of a HEP in saving fuel burnt are not visible. Only 900 Wh/kg and 1000 Wh/kg of e_{Bat} 2 % of the fuel consumed during the entire mission can be reduced. The specific energy of batteries is 13 times lower than the fuel, leading to a penalty in the total energy consumed during the mission.

Acknowledgements

Another stage of my life has come to an end with the delivery of my master thesis. The past three years were challenging. It allowed me to learn not only the tools for my future engineering career but also how to deal with difficulties. I can only smile when I think about all the happy and stressful moments I have been through during my Masters.

I want to thank my daily supervisor Maurice for the availability, help, guidance, and support. His positivism and motivation helped me going through during the most challenging times. Other thanks to Arvind, also my supervisor, for our discussions and help in looking at the problems from a different perspective. I am grateful to have had such smart and kind supervisors.

No words can express how much I am thankful to all my friends, and for all I have learned with them and the happy and sad moments we shared. I would like to thank Patrícia and Kartikay for the unconditional availability and listening to all my thoughts, worries, and joys. Also, a special thanks to the Portuguese community in Delft and all the warm and familiar gatherings.

I would like to extend my thanks to my flatmates, with whom I spend the last months intensively. Thank you for the unqualified motivation and support every single day of the quarantine. They have made my last month of thesis great.

Last but not least, I want to dedicate this thesis to my parents, who have made all this come true. I am a lucky girl. There are no words to describe how much I appreciate everything you have given me. Thank you for the opportunity of doing this Masters abroad. Your love and daily support is, and will always be, fundamental in my life.

Ana Marta A. S. Cabrita de Carvalho
Delft, July 2020

Nomenclature

List of abbreviations

AC	Alternating Current
ADP	Aerodynamic Design point
APU	Auxiliary Power Unit
BPR	Bypass Ratio
CAEP	Committee on Aviation Environmental Protection
CO	Carbon Monoxide
DC	Direct Current
DOD	Depth of Discharge
DoH	Degree of Hybridisation
DP	Distributed Propulsion
EATF	Electrically assisted turbofan
EATP	Electrically assisted turboprop
EI	Emission Index
EM	Electric motor
EMS	Energy Management System
ESAR	Energy Specific Air Range
FOI	Swedish Defence Research Agency
FHL	Fuel Heating Value
GB	Gear box
GHG	Green house gases
GMF	Global Market Forecast
GSP	Gas Turbine Simulation Program
GT	Gas Turbine
HEPS	Hybrid-electric Propulsion System
HEP	Hybrid-electric Propulsion
HPC	High Pressure Compressor
HPT	High Pressure Turbine
HTS	High Temperature Superconductors
HS	High spool
ICAO	International Civil Aviation Organization
IM	Induction Machines
ISA	International Standard Atmosphere

KPI International Standard Atmosphere

LAQ Local Air Quality

LHV Lower heating Value

ITT Inter Turbine Temperature

LTO Landing and Take-off

LPA Large Passenger Aircraft

LPC Low Pressure Turbine

LPT Low Pressure Turbine

LS Low spool

MCR Maximum Cruise

MCL Maximum Climb

MLW Maximum Landing Weight

MTOM/W Maximum Take-off mass/weight

NASA National Aeronautics and Space Administration

NO_x Nitrogen Oxides

OPR Overall Pressure Ratio

OEM/OEW Operative Empty Mass/ Weight

PM Permanet Magnet

PM Particulate Matter

PMAD Power Management And Distribution

PR Pressure ratio

PREE Payload Range Energy Efficiency

PSFC Power Specific Fuel Consumption

SARPs Standards and Recommended Practices

SLS Sea Level Static

SOC State-of-Charge

SP Shaft Power

SRM Switched reluctance motors

SUGAR Subsonic Ultra Green Aircraft Research

TIM Time-in-Mode

TIT Turbine Inlet Temperature

TLAR Top level aircraft requirements

TMS Thermal Management System

TOC Top of Climb

TSFC Thrust Specific Fuel Consumption

VSV Variable Stator Vanes

UHC Unburned hydrocarbons

List of subscripts

A/C	Aircraft
bat	Battery
des	Design
div	Diversion
em	Electric motor
fuel	Fuel
gb	Gear box
gt	Gas Turbine
j	Jet
max	Maximum
ov	overall
p	Propulsive
pl	payload
prop	Propeller
req	Required
th	Thermodynamic
tip	Propeller tip
tot	Total
wet	Wetted area

List of greek symbols

η	Efficiency	[-]
γ	Flight Path angle	deg]
ω	Angular velocity	[Hz]
ρ	Density	[kg/m^3]
Φ	Power Split ratio	[-]
ϕ	Power Supplied ratio	[-]

List of symbols

D	Drag	[N]
E	Energy capacity	[Wh]
e	Specific energy	$[Wh/kg]$
FN	Propulsive Net thrust	[N]
g	Acceleration of gravity	$[m/s^2]$
H_P	Degree of Power Hybridisation	[-]
H_E	Degree of Energy Hybridisation	[-]
I	Electric current	[A]
J	Advance Ratio of the Propeller	[-]
k	Correction factor	[-]
L	Lift	[N]
M	Mach number	[-]
m	Mass	[Kg]
n	Shaft speed	[rpm]
P	Power	[W]
p	Pressure	[Pa]
p	Specific Power	[W/kg]
Q	Torque	[Nm]
S	Wing Area	$[m^2]$
R	Range	[m]
R	Electrical Resistance	[Ω]
T	Thrust	[N]
U	Voltage	[V]
W	Weight	[N]

List of Figures

List of Tables

Contents

1

Introduction

1.1. Background

The main pollutants that aircraft engines emit are Carbon Dioxide (CO_2), Water vapor (H_2O), Nitrogen oxides (NO_x, mainly consisting of NO and NO_2), Sulfur Oxides (SO_x), unburned hydrocarbons (UHC), Carbon monoxide (CO), Particulate matter (PM) and soot. These emissions undergo various chemical transformations in the atmosphere leading to radiative forcing. Radiative forcing (RF) measures the difference between the energy that is absorbed by the Earth and the energy that is radiated back to space. Alterations in the concentration of previously mentioned species cause modifications in this parameter and are ultimately responsible for climate change.

The principal greenhouse gas from aviation is CO_2, but others also have an indirect impact on climate change. Water vapor combined with aerosols leads to contrail formation and cloudiness at cruise conditions, which causes a similar effect as natural cirrus clouds causing positive RF. Although NO_x it is not a greenhouse gas, it behaves as a catalyst to produce O_3 (resulting in a positive RF) and oxidizes CH_4 through a photochemical process (decreasing its abundance and having a cooling effect).

Aviation, unlikely other transportation modes, travel at a wide variety of altitudes, and thus, its emissions have an impact on local, regional, and global air quality. In particular, airport emissions are responsible for the deterioration of the air quality of nearby communities.

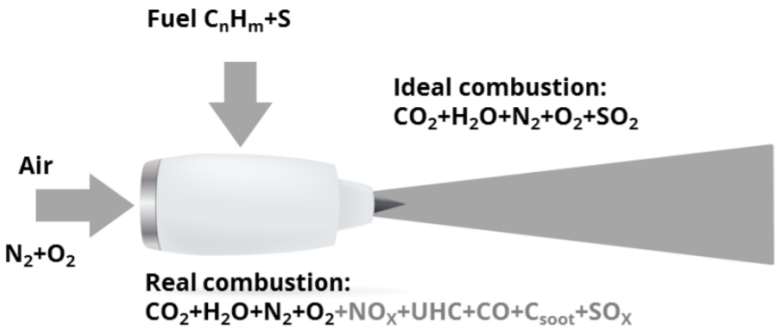

Figure 1.1: Aircraft emissions from an ideal and real combustion

ICAO's (International Civil Aviation Organization) CAEP (Committee on Aviation Environmental Protection) has been addressing aircraft and airport air pollutant emissions since the late 1970s (when there was a considerable increase in the commercial air traffic). The committee has put in place SARPs (Standards and Recommended Practices) to minimize aviation's potentially harmful effects on the environment and human health and welfare. These technology Standards can be found in Annex 16 to the Convention on Internation Civil Aviation and is divided into three volumes[7] :

- **Aircraft noise** (Volume I)
- **Engine Emissions** (Volume II): Currently regulate unburned hydrocarbons (UHC), carbon monoxide

(CO), nitrogen oxides (NO_x), smoke and non-volatile particulate (nvPM) [25] to control Local Air Quality (LAQ) near airports. The certification procedure is conducted on a single-engine in a test cell that simulates an ideal landing and take-off (LTO) cycle.

- **Aeroplane Carbon Dioxide** (Volume III) [26]

The Landing Take Off (LTO) cycle was conceived as a reference cycle for technology comparison, and it is representative of the emissions emitted in the vicinity of airports. The LTO cycle can be divided into four operational modes, characterized by different thrust settings and time: Take-off, Climb-out, Approach, and taxi. ICAO has defined the LTO cycle below a height of 3,000 ft (914 m) above ground level, and it is meant to tackle aircraft operations below the atmospheric "mixing height" (height of the vertical mixing of the lower troposphere). The pollutants emitted below that height can have a significant effect on local air quality concentrations [24].

1.2. Problem Statement

According to Airbus' Global Market Forecast 2019-2038, the world's passenger fleet will more than double to 48,000 aircraft in 20 years, with traffic growing at a resilient 4.3% per year (figure 1.2, driving a need for 37,390 new passenger and freighter aircraft [1]. In Europe, the air traffic growth estimation is 42 % from 2017 to 2040 [7].

Even though technological improvements, fleet renovation, and increased operational efficiency have been playing a role in balancing the impact of recent growth, an increase in aircraft emissions is predicted [7]. Figure 1.3 shows the estimation of NO_x emission below 3,000 ft above ground level from International aviation until 2050. This growth behavior has driven CAEP to adopt more and more stringent standards so that harmful emissions from the engines are further reduced.

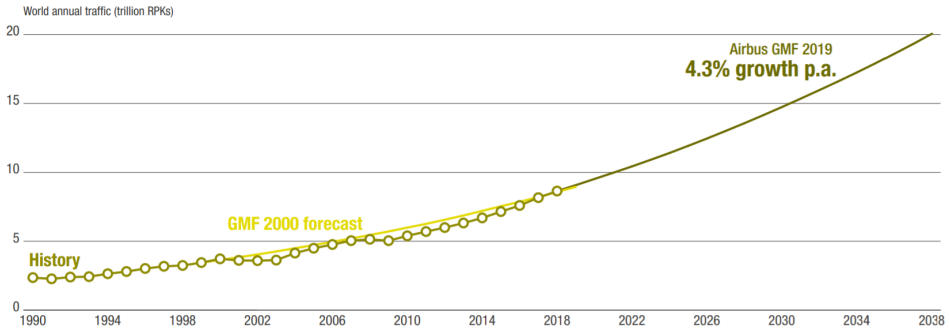

Figure 1.2: Airbus Global Market Forecast 2018-2037 [1]

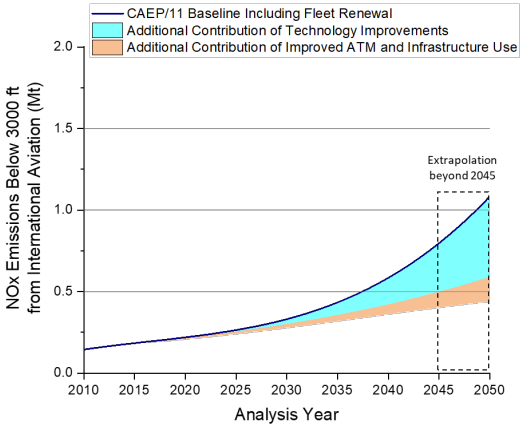

Figure 1.3: NOx Emissions below 3,000 feet from International Aviation, 2010 to 2050 [2]

For the last 70 years, engine technology evolution has been driven by a reduction in fuel burn (aiming to reduce CO_2 emissions) [27]. It was achieved by introducing new materials (so that the combustion chamber and turbine blades can withstand high temperatures and pressures) and more fuel-efficient cycles. However, attaining high temperature and pressure in the combustor increases nitrogen oxides (NO_x) emissions, which makes the combustor chamber design a challenge [28] [6]. Examples of technology aiming to reduce NO_x reduction are the Lean Burn and the Rich Quick Quench technologies.

The urge to develop technologies that reduce climate change impact on future transport aircraft led to the study of hybrid-electric propulsion. A Hybrid-electric propulsion (HEP) concept is a vehicle in which the generation and/or transmission of power relies on two or more sorts of energy sources (where at least one of energy sources is electrical). Such concept can potentially bring the following advantages [29] [30]:

- Low operational costs
- Reduce noise and carbon footprint
- Optimization of power train efficiency through electrically-assisted propulsion
- Distribute power to different locations on the airframe: enabling distributed propulsion (that arises an increased aero-propulsive efficiency)

The ideal scenario would be to develop a fully electric commercial passenger aircraft concept that would not emit any CO_2 and would deliver higher efficiency than the conventional gas turbine [31] . Although the efficiency of batteries, inverters, and electrical motors are high (90 % [32], 99.5% [33] and 93% [34], respectively), the specific energy (amount of energy per weight) of the batteries and specific power (power-to-weight ratio) of the electrical components is insufficient to supply the high power requirements of such aircraft. The main components that affect the weight of the electrical system are the batteries, the inverters, the cables, and the electric motors [30].

Therefore, significant technological advances in the energy density of electrical energy storage devices and specific power of electrical components (e.g., electrical machines) must take place to even the small range full-electric aircraft concepts become feasible to compensate for the considerable increase in take-off weight [35]. As a result, HEP has been seen as a solution for more extensive and longer-range aircraft. From all the architectures available for HEP (listed in section 2.3.1), the parallel-hybrid electric architecture (detailedly covered in section 2.3.1) is the most efficient, and it enables the powertrain to be powered by an electric motor or a gas turbine (individually or combined) [36]. A turbofan or a turboprop that incorporates parallel-hybrid electric propulsion in its powertrain is classified as electrically boosted (or assisted) turbofan/ turboprop.

The Degree of Hybridization (concept firstly introduced by Isikveren et al. [37]) is an indicator of the level of electrification of the powertrain and stands for the ratio of power provided by the electric motor and the total power (sum of gas turbine and electric power). Section 2.3 introduces the terminology and performance metric parameters related to hybrid-electric propulsion.

Many studies have explored the potential of electrically boosted turbofan, EBTF, concept for Large Passenger Aircraft, LPA, (that have high power level requirements than regional turboprop aircraft) in saving fuel and CO_2 emissions [9], [38] [39]. Pornet et al. [38] and Vratny et al. [9] show that even with the most optimistic level of the electric components' technology scenarios (specific energy of 1000 Wh/kg), a high level of hybridization throughout the entire mission is not beneficial. The long duration of the cruise translates into high energy requirements. Even a low hybridization of this segment would require an increase in take-off weight to carry the necessary batteries that would offset the benefits of HEP.

Ang et al. [39] studied the hypothesis of hybridizing an Airbus A320 incorporating an EBTF in some flight phases for a 1000 km mission. The hybridization strategy did not include cruise, and it resulted in a fuel burn saving of 7.5% with a degree of hybridization of 25% for take-off and 14% for climb, coupled with a 90% downscale of the gas turbine (assuming specific energy of 600 Wh/kg).

This problem is not associated with commercial turbofan aircraft only, the regional turboprop aircraft equipped with an electrically assisted turboprop concept has been a target of several pieces of research [40] [17] [41].

Antliff et al. [40] investigated different hybridization strategies (0%, 25 %, 50%, 75% and 100% electrification) throughout a 600 nautical miles range mission for a regional aircraft. The main findings of this research are: for that range, the specific energy of the battery needs to greater than 500 Wh/kg for the total energy consumed by the hybrid concept to be lower than the conventional configuration; the parallel-hybrid electric configuration is not economically favorable for battery specific energy lower than 500 Wh/kg [40]. However, this research did not explore the interest of this concept in reducing emissions.

Voskuijl et al. [17] have shown that HEP can reduce CO_2 emissions in regional turboprop aircraft for short-range missions (range of 1528 km assumed). When picking up a power split ratio (ratio of shaft power delivered by the electric motor and the combustion engine) of 0.34 and a battery specific energy of 1000 Wh/kg, the study claims to reduce mission fuel by 28 % and total energy consumption by 17 % when comparing to the baseline aircraft. However, such a high value for battery specific energy is too optimistic and could only be feasible in two decades [42]

The potential of a parallel-hybrid electric configuration in reducing local air quality emissions (NO_x, CO, UHC) for regional turboprop aircraft has not been assessed in the previously mentioned studies. Only CO_2 emission have been tackled. This type of aircraft fly shorter ranges, hence shorter cruise, and the LTO cycle plays a more prominent role in the total mission emissions. Therefore, hybridizing only the LTO segments can be advantageous in improving Local Air quality around the airports and on be compliant with ICAO future tighter standards (regulated in Volume II of Annex 16).

1.2.1. Research goal and questions

In the context of exploring the role of a parallel-hybrid electric concept in reducing local air quality emissions in the LTO cycle, the research question for this Master thesis can be formulated as follows:

How does a parallel-hybrid electric architecture influence NO_x, CO, and H_2O emissions on a typical LTO cycle for a regional turboprop aircraft?

Besides, to find an answer to the research question, the following sub-research questions are to be addressed:

- How to model a turboprop engine? Which is the ideal design point and relevant design variables?
- How does the turboprop engine performance model behaves in off-design?
- How to model a mission analysis sensitive to power requirements per mission phase?
- How sensitive are NO_x, CO, and H_2O emissions to technology maturity scenarios?
- How do water vapor (H_2O) emissions evolve with the degree of hybridization?
- What is the degree of hybridization, per mission segment, of a parallel-hybrid turboprop engine that minimizes NO_x emissions in the LTO cycle?
- What is the degree of hybridization, per mission segment, of a parallel-hybrid turboprop engine that minimizes CO emissions in the LTO cycle?
- What is the hybridization strategy that best compromises NO_x, CO, H_2O, and CO_2 emissions?

The goal of this research is as follows:

The goal of this research is to investigate the impact of using a parallel-hybrid electric architecture on NO_x, CO, and H_2O emissions on a typical LTO cycle for a regional turboprop aircraft

1.3. Research scope

This research focuses only on turboprop aircraft. The reason behind it is that this aircraft category is lighter than commercial turbofan (then the power level requirements are consequently lower), and it flies shorter ranges resulting in a better choice to hybridize.

Hybrid-electric propulsion enables different configurations (e.g., parallel, series, and turboelectric) as well as different types of energy supply (e.g., fossil fuel, battery, fuel cells, and capacitors). Although chapter 2

covers the HEPS architectures available and respective advantages and disadvantages, this study considers only a parallel-hybrid configuration, and batteries supply the electric energy. The main reason to pick a parallel-hybrid architecture is that it requires the least modifications in the airframe to incorporate it, and is more efficient than other configurations because fewer energy conversions take place.

An electrically assisted turboprop is a conventional turboprop incorporating an electric motor (powered by a battery) in the free turbine shaft that provides additional power for specific flight phases. For example, the electric boost can be used to compensate for peak loads in some flight phases with high power requirements (such as take-off and climb).

The baseline aircraft used in this research is the ATR 72-600 (picture in figure 1.4), which incorporates a two-spool turboprop engine PW 127-M (illustrated in figure 1.5), from Pratt & Whitney. The motivation behind this choice is the vast literature and data available for this aircraft and engine.

The electrical system modeled includes the following electrical components: electric motors, batteries, transmission cables, and power electronics (inverters). The thermal management system and a cooling system design (essential to keep the main components in their operating temperature limit) will not be included in the electric system modeling due to its complexity. However, 30 % of the electrical system weight will be added extra to account for the weight of the cooling and PMAD (Power Management and Distribution) system [43].

Figure 1.4: ATR 72-600 (Taken from ATR website [3])

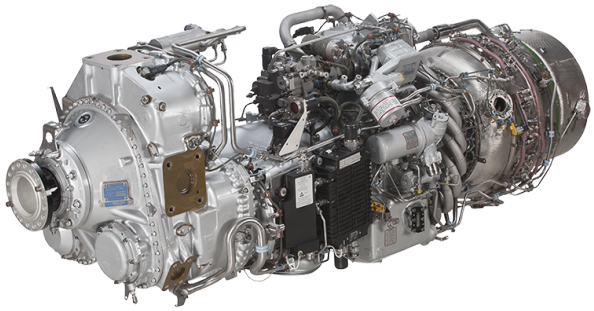

Figure 1.5: Pratt & Whitney (PW) 127-M engine (Taken from PW website [4])

Below, the assumptions and limitations of this research are listed:

- Hybridization is implemented only in the LTO cycle segments: Taxi-out, take-off, climb-out, approach, landing, and taxi-in (detailed description of all these phases in section 2.5).
- Although the origin of ground-based GHG emissions at airports is diverse (gasoline and diesel fuel for airport vehicles and ground support equipment GSE, fossil fuel for electricity and heating), this

research is going to cover only emissions originated by jet fuel.

- The re-design of the combustor chamber or investigation the introduction of a more advance combustor is out of the scope
- The geometry of the aircraft is kept fixed.
- The electrical system (excluding the batteries) is sized as a function of the maximum power requirement during the mission.
- In the Turboprop engine model, the propeller performance is obtained interpolating a performance map from a propeller similar to the ATR-72 propeller.
- Aspects as life-cycle costs and maintainability are not covered.
- The baseline turboprop engine and its design point are kept constant.
- Not all engine emissions regulated by ICAO mentioned are studied in this research. Due to the complexity of their prediction, soot, smoke, and unburned hydrocarbons are not computed.
- The Mission profile is built based on published literature values for speed and power requirements in different mission segments [44]. Detailed assumptions and mission profile characteristics can be read in section 3.1
- Energy stored in the batteries is generated from renewable sources.

The computation of NO_x and CO emissions in the LTO cycle follows ICAO emission regulations for civil subsonic turbofan engines over an operational cycle around airports. The LTO cycle represents a typical commercial aircraft operation as it climbs up to 3,000ft, and it descends from the same altitude on its approach path.

1.4. Approach

To answer the research questions it was necessary to build:

- A Mission simulation routine, responsible to compute the fuel and electric system weight required for a specific mission, for different
- A turboprop model able to compute the engine performance and emissions for a particular power requirement and inlet conditions
- A simplified electrical system model that estimates the electric components weight with power requirements
- Mission analysis suite that uses the mission simulation routine results to compute emissions, fuel and energy consumption for the specified mission profile

For each mission hybridization strategy (the degree of hybridization, ϕ, in the LTO segments) and technology scenario, the mission simulation routine runs until the fuel and battery weight converge, and a solution is obtained.

The engine model consists of a two-spool turboprop, following the PW 127-M configuration, and it was built in GSP ® (Gas Turbine Simulator). GSP is a component-based gas turbine modeling environment developed by the Netherlands Aerospace Center (NLR) and the TU Delft that allows performance prediction of both on-design and off-design analysis. The inputs data is from PW 127-M, and the model delivers as outputs the engine performance (thermodynamic properties, fuel flow, PSFC, etc.) and emissions at each time step. These results are integrated into the mission simulation routine, which is coded in MATLAB ®, and coupled to GSP ® via the API (Application Programming Interface).

The flow chart presented in figure 1.6 is a simple schematic that represents the flow of the program implemented in this research. The detailed methodology that the Mission Simulation Routine uses is presented in section 3.4.

Figure 1.7 displays a list of inputs used in the simulations. The ATR 72-600 data includes overall dimensions of the aircraft, wing data (span, aspect ratio and area), payload, cruise altitude and Mach number, Range, Approach and take-off speed, optimum climb data (speed and rate of climb), etc. A complete list of the

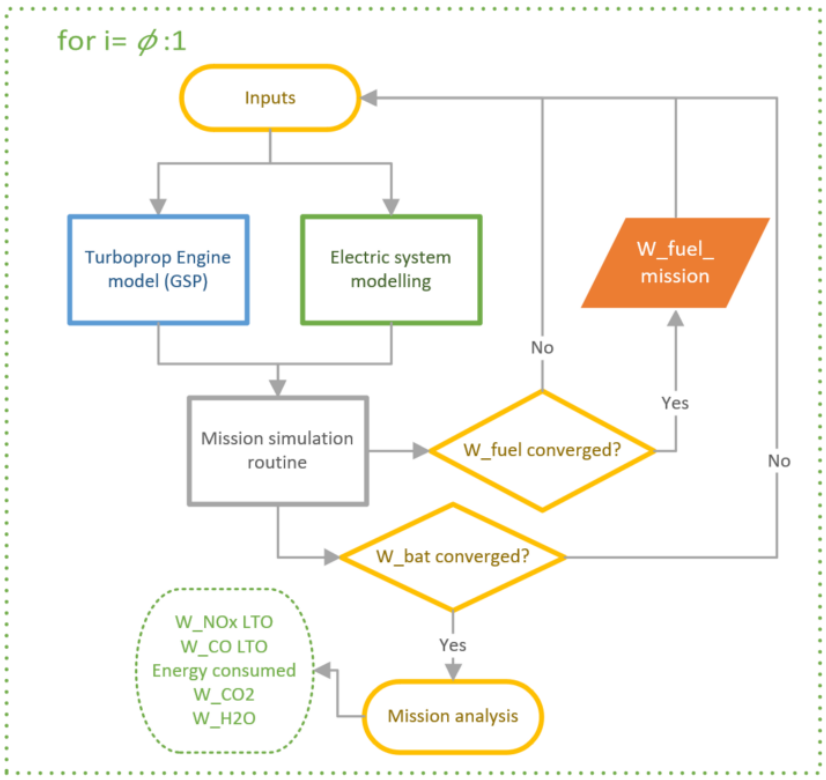

Figure 1.6: Flow chart with methodology implemented in the research

Inputs:

- PW 127-F data
- ATR-72 600 data
- Mission profile:
  - Power requirement as a function of aircraft weight
  - Range= 1000 Km
  - Operating conditions (Altitude and Mach number)
  - Propeller rotational speed (in %)
  - Power setting and time-in mode during LTO cycle
  - Degree of hybridization strategy
  - Fuel and battery weight guess
- Technology maturity level scenarios
  - Electrical system characteristics

Figure 1.7: List of inputs for the mission analysis loop

parameters and their values are reported in section 4.1. PW 127-M data includes engine limitations for maximum take-off, normal take-off and maximum continuous (maximum power and torque, maximum inter turbine temperature ITT, the maximum rotational speed of the propeller, high and low-pressure spools) and values of OPR (overall pressure ratio), fuel flow and specific fuel consumption at normal SSL (Standard Sea level) take-off. A more detailed list of PW 127-M and how it was used to calculate the design point and validate its performance is done in section 4.2.

As depicted in the flow chart, the program simulates different missions, differing in the hybridization strategy and technology scenarios. NO_x, CO, and H_2O emissions from each simulation will be compared and the configuration (strategy) will be identified.

1.5. Structure of the report

This report is divided into 7 chapters. The following 6 will present the following content:

- Chapter 2 (Background information) provides information on: Engine emissions (formation mechanisms, modelling and ICAO Standards); Conventional Turboprop engine (its working principles and main performance indicators); electrical system components and flight mechanics for each flight phase (important background for the Mission analysis set up).
- Chapter 3 (Mission Profile & Methodology) presents the mission profile, the parallel hybrid-electric powertrain schematics, the mission hybridization strategy used in this research and the detailed methodology followed
- Chapter 4 (Baseline models) explains how the models of baseline ATR 72-600, baseline turboprop, and electrical system components were set up (input parameters, methodology and design point calculation and in the case of the GSP turboprop model) and respective validation.
- Chapter 5 (Mission Simulation Results) is focused on the comparison of the results of emissions, power requirements and fuel flow during the mission of the baseline aircraft with the parallel-hybrid electric concept
- Chapter 6 (Mission Analysis Results) displays the results and analysis of the take-off mass, electric system mass, energy consumption, fuel burn, emissions during the whole mission and LTO cycle.
- Chapter 7 (Conclusions and Recommendations) provides with the main conclusions of the study and gives some recommendation for future work.

2

Background information

2.1. Engine emissions

Pollutant gases from aviation have become a greater concern due to the increase in air traffic and its harmful impact on human health and the environment.

Aircraft engine exhaust gases include carbon monoxide (CO), carbon dioxide (CO_2), water vapour (H_2O), unburned hydrocarbons (UHC), particulate matter (PM) and oxides of nitrogen (NO_x). CO_2 and H_2O are not considered as pollutants as they are products from ideal and complete combustion. The main combustion pollutants are listed in table 2.1 along with their effects.

Although CO_2 and H_2O are not pollutants, both are responsible for climate changing. Carbon dioxide has a long residence time (approximately 100 years) in the atmosphere and a long-term influence on climate, being the main responsible for radiative forcing [18] (see figure 2.1). Contrarily to other emissions, CO_2 mix globally in the atmosphere, and the results of aviation emissions are no different than those from other sources in the same quantity [45]. It is important to note that NO_x also has an indirect impact on radiative forcing, and thus on climate changing: it produces ground-level ozone and in the stratosphere causes ozone destruction (both contributing to positive radiative forcing), but accelerates methane (CH_4) destruction rate (leading to negative radiative forcing). Weighting both phenomenons, NO_x emission have a resultant positive radiative forcing, as figure 2.1 shows.

As to other aviation emissions, these have shorter residence times and tend to be condensed near flight routes, which can lead to regional radiative forcing. Water vapour, released in the troposphere, triggers the formation of line-shaped contrails and, ultimately, cirrus cloudiness. Contrails work similarly to thin high clouds, and their radiative effect depends on optical properties and the particles present in the aircraft plume and on atmospheric conditions [45].

Table 2.1: Effects of principal pollutants emitted by aircraft engines

Pollutant species	Effect
Carbon Monoxide (CO)	Toxic. Reduces capacity of blood to absorb oxygen
Nitrogen Oxides (NO_x)	Photochemical smog. Contributes to acid rain.Damages plant life. Production of Ozone in the troposphere. Depletion of ozone layer in the stratosphere
Particulate Matter (PM)	Visibility impairment. Contributes to acid rain
Unburned hydrocarbons (UHC)	Toxic. Photochemical smog (when combined with NO_x)
Sulfur oxides	Toxic and corrosive (responsible for sulfuric acid in the atmosphere)

In concentrations near 100 ppb (parts per billion), O_3 (Ozone) is likely to be responsible for respiratory problems, damaged vision, chronic headaches, and allergies [6].

CO_2, H_2O, and SO_4 emissions depend on fuel composition, and it is assumed that the emissions index of these species are constant. The Emission Index for specie i (EI_i) is a fuel property that gives the mass ratio of emitted specie i to fuel burned. CO_2, H_2O and SO_4 emission index are displayed in table 2.2. Since EIs for these species are constant, the total emissions emitted in a mission (e_i) are the product of EI and total fuel consumed throughout the mission W_{fuel} (see equation 2.1).

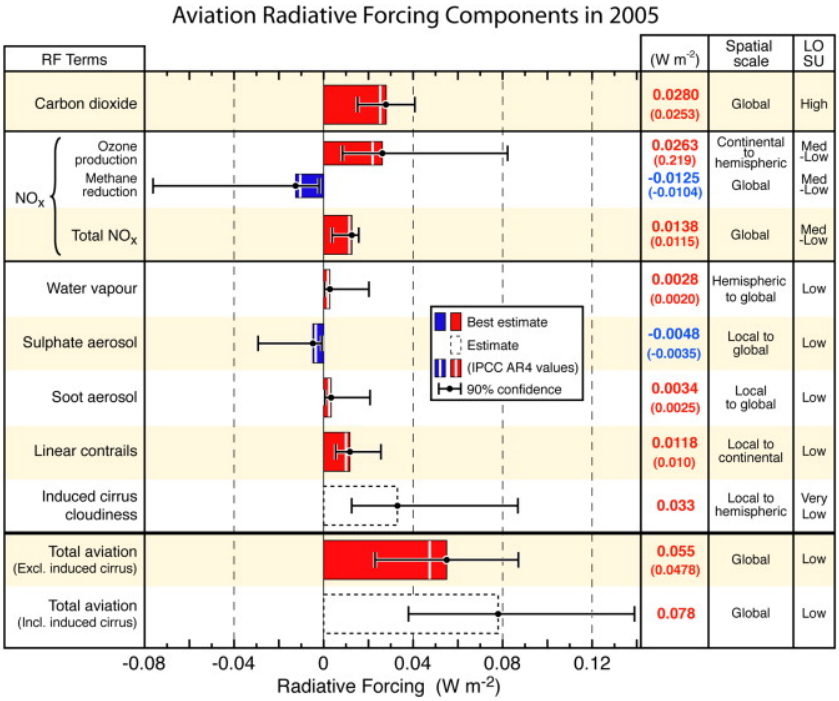

Figure 2.1: Radiative forcing decomposition from international aviation from preindustrial times until 2005. Taken from [5]

$$e_i = EI_i \times W_{fuel} \tag{2.1}$$

Table 2.2: Emissions indices [18]

Species	Emission Index $\left[\frac{kg}{kg\,fuel}\right]$
CO_2	3.16
H_2O	1.26
SO_4	2.0 e^{-4}

NO_x, CO, and UHC emissions are not constant and solely dependent on the fuel used. Instead, these differ complexly with operating conditions (temperature and pressure), engine thrust setting, and combustor type. Figure 2.2 shows the trends of NO_x, CO, UHC emissions, and smoke with power settings.

However, of all factors, the temperature of the combustion zone is the one that most influences pollutant emissions. Figure 2.3 shows CO and NO_x emission behaviour with primary zone temperature.

Analysing figures 2.2 and 2.3 the following conclusions can be drawn:

- CO and UHC are the most elevated at low-power conditions and go down at higher power levels (becoming negligible at the highest power setting)
- NO_x and soot are dominant at higher power condition (achieving the maximum at the highest power setting)

- The ideal geometry of a combustor is the one that enables a keeps combustion zones temperatures within a narrow band of temperatures overall power settings

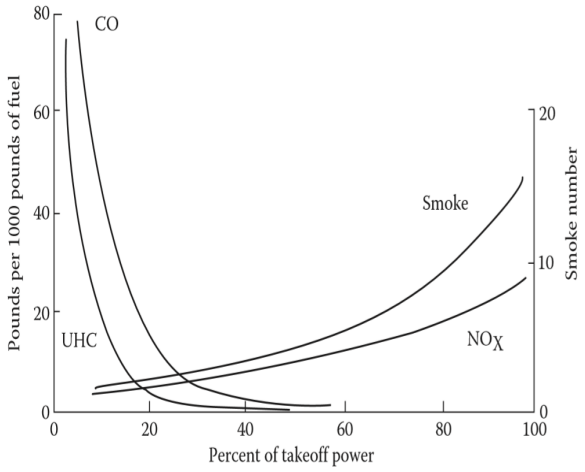

Figure 2.2: NO_x, CO, UHC and smoke emissions behaviour with power settings. Taken from [6]

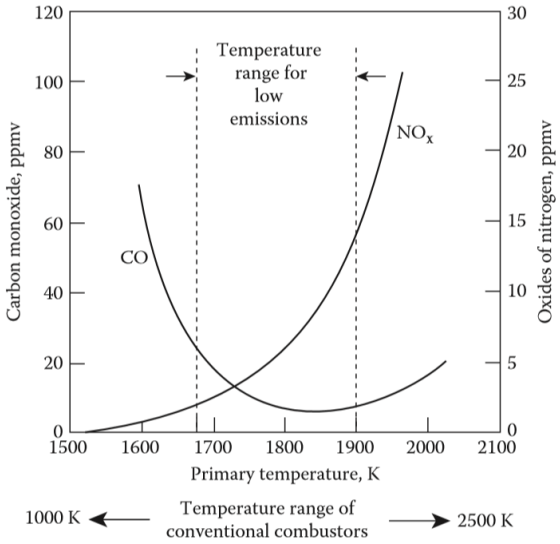

Figure 2.3: NO_x, CO, UHC and smoke emissions behaviour with power settings. Taken from [6]

UHC formation is a result of poor atomization, inadequate burning rates, or chilling effects of film-cooling air [6]. However, the reaction kinetics of this specie is complex, and for that reason, UHC formation mechanisms are not covered in the following sections.

Smoke is formed in fuel-rich zones and its composition is mostly carbon (96 %) [6] resulting from incomplete combustion. The impure carbon particles are soot. The soot formation process is complex, and thus, it is not addressed in this research.

Sections 2.1.1 and 2.1.2 enumerate and describe NO_x and CO formation mechanisms, respectively and section 2.1.3 introduces methods used to estimate these two species emissions.

Before diving into these sections, it is important to introduce the concept of equivalence ratio Φ. It is the fuel-to-air ratio divided by the stoichiometric fuel-to-air ratio. The stoichiometric fuel-to-air ratio is the amount of fuel (in g) per 1 g of air necessary for complete combustion to occur. For Kerosene ($C_{12}H_{24}$) the stoichiometric fuel-to-air ratio is 0.0676. Thus, in stoichiometric conditions, the equivalence ratio is 1.

2.1.1. NO_x formation mechanisms

Nitrogen oxides (that include NO and NO_2) production depends on factors as pressure, temperature, stoichiometric condition and residence time in the combustor. There are four main NO_x formation mechanisms : Zeldovich mechanism (section 2.1.1), nitrous Oxide mechanism (section 2.1.1), prompt NO (section 2.1.1), and fuel NO (section 2.1.1).

Zeldovich mechanism

Also known as thermal nitric oxide, this mechanism is endothermic and is mostly dictated by the flame temperature: higher production at high-temperature regions of the flame. Thermal Nitric oxide (NO) is produced by the oxidation of nitrogen present in atmosphere (N_2). The chemical reactions that lead to its production can displayed below. Note that these reactions are reversible.

$$N_2 + O \rightleftharpoons NO + N$$
$$N + O_2 \rightleftharpoons NO + O$$
$$N + OH \rightleftharpoons NO + H$$

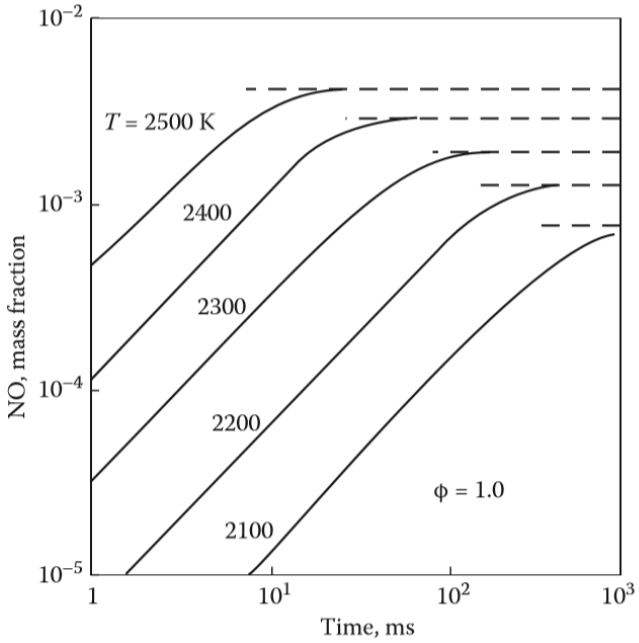

Figure 2.4: Dependence of thermal NO on flame temperature and residence time

NO peak formation happens at a slightly fuel-lean stoichiometric condition. The reason behind this is the competition between fuel and nitrogen for the available oxygen. Even though the combustion temperature is higher on the richer side of the stoichiometric point, the oxygen is tendentiously consumed by the fuel. The behavior of thermal NO with flame temperature and residence time is pictured in figure 2.4. The main conclusions taken from this experimental data (obtained from [6]) are listed below:

- Thermal NO creation diminishes as flame temperatures go down
- Little thermal NO is formed below a flame temperature of 2100 K
- In a conventional combustor thermal NO increases linearly with residence time

Nitrous Oxide mechanism

This mechanism is started by the formation of nitrous oxide that is later oxidized to NO as below reactions describe [46]:

$$N_2 + O \rightleftharpoons N_2O$$
$$N_2O + O \rightleftharpoons NO + NO$$

NO can be a result of the following reactions:

$$N_2O + H \rightleftharpoons NO + NH$$
$$N_2O + CO \rightleftharpoons NO + NCO$$

Prompt Nitric Oxide

According to Nicol at al. [46], nitrous oxide can be produced at earliest stage of combustion with HCN molecules and N atoms oxidation. HCN and N are formed with the following reaction:

$$N_2 + CH \rightleftharpoons HCN + N$$

The sequence HCN → CN → NCO → NO takes place in lean-premixed conditions meaning that NO formation does not only occur in a fuel-rich mixture [46].

Fuel Nitric Oxide

Fuel contains a low percentage (around 0.06 % in light distillate fuels and 1.8 % in heavy distillate ones) of fuel-bond-nitrogen (FBN) that can react during the combustion, and the nitric oxide formed through this process is named *fuel* NO_x.

In a study conducted by Nicol et al. [46], the relative contribution of each of the just mentioned mechanisms was analyzed for a lean-premixed combustor burning methane as fuel. From the total NO_x produced at an equivalence ratio of 0.8 and temperature of 1900 K, the contributions are 60 % thermal (Zeldovich mechanism), 10 % nitrous oxide, 30% prompt and 0% fuel. According to the same study, as the temperature and equivalence ratios decrease, the proportion of N_2O and prompt NO over the total NO_x emitted increases and at the lowest equivalence ratios [46], the N_2O mechanism is the main contributor to the total NO_x.

2.1.2. CO formation mechanisms

CO is formed with incomplete combustion of fuel (meaning that there is not enough oxygen to burn the fuel), and this phenomenon is associated with an inadequate burning rate in the primary combustor zone or a deficient mixing of fuel and air. Thus, it leads to regions where the mixture strength is too weak to enable combustion and other fuel-rich that originates high concentrations of CO.

Moreover, CO formation is influenced by the following parameters [6]:

- **Equivalent ratio**: CO emissions decrease with an increase in the equivalence ratio (Φ), achieving the minimum value around 0.8 [6]. High values of CO at low equivalence ratios are explained by the slow rates of oxidation at low combustion temperatures. As the flame temperature increases (due to an increase in Φ) the rate of oxidation rises up and CO emissions decline. The chemical reaction of CO oxidation is the following

  $$\mathrm{CO} + \mathrm{OH} \rightleftharpoons CO_2 + \mathrm{H}$$

  Nevertheless, for higher temperatures (when Φ is above 0.8), the production of CO is spiked by chemical dissociation of CO_2. As it has already been observed before, low levels of CO can only be obtained within a narrow range of temperatures (and Φ).
- **Pressure**: A rise in combustion pressure contributes to CO emission reduction.

2.1.3. Emissions modelling

It is important to be able to predict aircraft engine emissions practically and quickly. As a result, several techniques and methods have been developed to estimate aircraft emissions with combustor design, operating conditions, and fuel type as input. The techniques are classified as empirical models, semi-empirical models, simplified physics-based models, and high-fidelity simulations. The computational effort increases in the same order. Physics-based, and high-fidelity models are out of the scope of this literature review.

Empirical methods, as the name suggests, uses empirical data from a specific engine (P_3, T_3, T_4, fuel flow rate, etc.) to create a mathematical correlation with engine emissions. These models are used usually to predict NO_x emissions [47]. For single annular combustor the two following methods are available:

$$EINO_x = 0.042\left(\frac{P_{T3}}{439}\right)^{0.37} exp\left(\frac{T_{T3}-459.67}{345}\right) T_{T4} \tag{2.2}$$

$$EINO_x = 0.0986\left(\frac{P_{T3}}{101325}\right)^{0.4} exp\left(\frac{T_{T3}}{345}\frac{H_0}{53.2}\right) \tag{2.3}$$

$$EINO_x = 1.35 \times 0.0986\left(\frac{P_{T3}}{101325}\right)^{0.4} exp\left(\frac{T_{T3}}{345} - \frac{H_0}{53.2}\right) + 1.7 \tag{2.4}$$

Note that the units of pressure and temperature in equation 2.2 are in psia and deg R (Rankine), respectively [47] . Equation 2.3 was developed by NASA during its Experimental Clean Combustor Program [48] based on GE90-85B dual annular combustor performance. Equation 2.4 is an adaptation to single annular combustor from the previous correlation . For both of these two equations, the units used for temperature and specific humidity (H_0) are pascal, Kelvin, and grams of water per kilogram of dry air.

The downside of empirical models is the lack of accuracy. If a model is used for a variety of combustors with only a single set of empirical constants, the error when applied to a particular combustor can be high. Moreover, these models are no longer applicable when combustors go through modifications in the design. Empirical models are used in engine performance tools.

Another disadvantage of empirical models is related to the impossibility to detect trades between NO_x and CO. As a result, there are no empirical models to predict CO.

Semi-empirical models also use the same empirical data that empirical models do and also include parameters as primary zone temperature, combustor primary zone volume, and quenching time [47]. It brings the advantage of modeling CO and NO_x independently. However, it has the disadvantage of being sensitive to the inputs, and the accuracy of these is, in some cases, not high.

2.1.4. ICAO Engine Emissions Standards

The CAEP (Committee on Aviation Environmental Protection) helps ICAO (International Civil Aviation Organization) create new policies to mitigate environmental impacts and to put into practice SARPs (Standards and Recommended Practices). These SARPs can be related to Noise, Local air quality (LAQ), and CO_2 reduction. Volume II of Annex 16 to the Convention on International Civil Aviation (the *Chicago Convention*) presents standards for aircraft engine emissions that impact local air quality. Due to the focus of this research on Local Air quality emissions, only these Standards will be addressed.

ICAO Standards from Volume II establish limits for liquid fuel venting, smoke (foreseen to be replaced by the nvPM, non-volatile particulate matter, Standard) and the principal exhaust emission gases: hydrocarbons (HC), oxides of nitrogen (NO_x), carbon monoxide (CO) [49]. Air quality regulations and standards have become gradually more stringent as aviation is expanding, and the consequences of these emissions on the environment and human health are better understood.

The certification process for aircraft engine emissions is based on the Landing Take Off (LTO) cycle. This cycle goal is to portray the emissions emitted in the vicinity of airports (up to 915m or 3,000 ft in height above the runway) and to compare different technologies under the same operating conditions. It is divided into four operational modes, characterized by different thrust settings and duration time: Take-off, Climb-out, Approach, and taxi. Figure 2.5 illustrates the phases covered in the LTO cycle.

The variables certified are the Emission Index (EI) and Dp/Foo for each pollutant. Dp/Foo is the mass in grams (Dp) of pollutant divided by the thrust rated output (F_{00}) and can be computed with the following equation [47] :

$$DP/Foo = \sum_{i=1}^{4} EI_i \times TIM_i \times \frac{\dot{m}_{f_i}}{F_{00}} \tag{2.5}$$

This certification data is collected from engine manufacturers and saved in the public *ICAO Emission Database* [50], and the regulatory levels are set in Annex 16, Volume II.

However, ICAO aircraft engine emissions standards and regulatory levels apply only to subsonic and supersonic aircraft turbojet and turbofan engines of thrust rating greater than or equal to 26.7 KN. ICAO standards do not cover emissions from turboprop, piston engine, and helicopter aircraft or smaller business jets. As a result, turboprop emission data is not publicly available on the ICAO Engine Emissions Database.

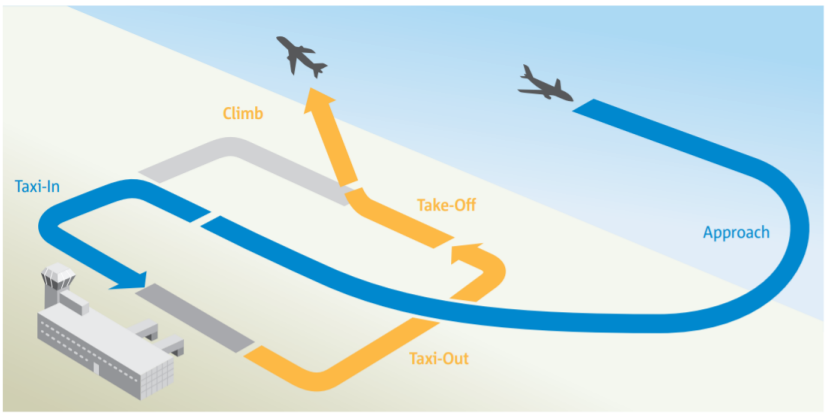

Figure 2.5: Standard engine emissions LTO cycle [7]

Table 2.3: Reference Thrust settings and TIM in LTO cycle for turbofans [7]

Mode	Thrust settings (% of rated thrust)	Time-in-Mode (Min)
Take-off	100	0.7
Climb out	85	2.2
Approach	30	4.0
Taxi	7	26

Table 2.4: Reference Thrust settings and TIM in LTO cycle for turboprops [19]

Mode	Power settings (% of rated power)	Time-in-Mode (Min)
Take-off	100	0.5
Climb out	85	2.5
Approach	30	4.5
Taxi	7	26

The Swedish Defence Research Agency (FOI) [19] is the owner of the confidential database of fuel flow and NO_x, HC, and CO emissions indices (EI) for turboprop engines [1]. Turboprop engine manufacturers provided this data to compute the take-off and landing emissions charges. This data has not been through an ICAO certification process, meaning that the unregulated test methodologies might lead to inaccuracies.

In comparison with ICAO LTO cycle characteristics, the TIM (Times in Mode) for calculating LTO emissions for turboprops differ, as well as the idle settings for turboprops. A comparison of the time-in-mode and thrust/ power settings from turbofan to turboprop is made in tables 2.3 [7] and 2.4[19] .

Both cycles are an approximation of actual operations and lie under the assumptions of abrupt power settings change from one phase to another [24].

2.2. Turboprop engine

Regional aircraft are equipped with turboprop engines. To model a turboprop, it is fundamental to understand how it works (how is the power generated), what are the main components (and their function), and how is its performance evaluated.

2.2.1. Working principles

A turboprop is a gas turbine attached to a propeller through a gearbox. In a turboprop, the power generated in the turbine is transformed into shaft power. The gearbox aims at converting high RPM/low torque output

[1] There was a tentative to have access to turboprop data but the permission was not granted by FOI

from the turbine shaft to low RPM/high torque in the propeller [51].

The propeller converts mechanical power (shaft power, SP) into thrust (T_P). The momentum difference between the air upstream and downstream the propeller generates thrust. Thus, unlikely turbofans, turboprop do not rely on jet thrust (F_g) produced by the exhaust gas expansion (at a V_j speed) [15]. The thrust required (T_{req}) at a certain point of a mission can be given by equation 2.6, assuming that both vectors present the same direction. n stands for the number of operative engines. The total output power P_{tot} in a turboprop is given by equation 2.7, η_{prop} and η_{gb} are propeller and gear-box efficiencies, respectively.

$$T_{req} = n(T_P + F_g) \tag{2.6}$$

$$P_{tot} = \eta_{prop}\eta_{gb}SP + F_g \times V_j \tag{2.7}$$

The gas turbine is composed of the following components: an axial or centrifugal compressor(s), an annular combustor, axial or centrifugal turbine(s), and a power turbine (also named as free turbine). A two-spool turboprop schematic is depicted in figure 2.6 and it is the family that engine PW-127M belongs to [15].

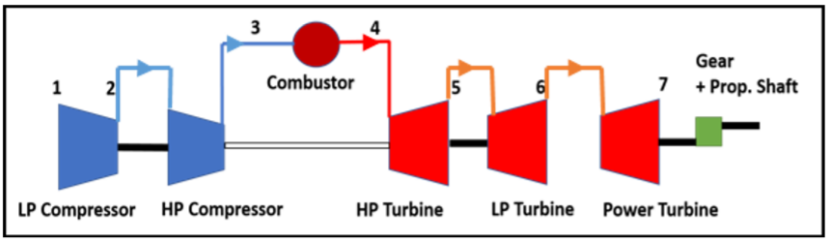

Figure 2.6: Two-spool turboprop scheme

The air is admitted through the inlet, then passed to LP (low pressure) and HP (high pressure) compressors, stations 2 and 3, where its pressure rises. When reaching the combustion chamber, fuel is included across the fuel lines and ignited, converting the chemical energy from the fuel into heat, ended up rising the fluid temperature. The maximum temperature attained in a gas turbine is at the exit of the combustor (station 4) and the inlet of HPT (high-pressure compressor). The high temperature gases expand in HPT, LPT (low-pressure turbine), and in the free turbine. While HPT and LPT's goal is to power LPC and HPC, the free turbine (or power turbine) is coupled to a power shaft and, consequently, to the propeller shaft (through a gearbox).

However, in a real gas turbine, several loss sources are important to mention [52]:

1. Both the compression and expansion in the compressors and turbines, respectively, are not adiabatic and reversible, leading to a rise in entropy.
2. Friction and heating lead to pressure losses in the combustor.
3. The combustion phenomena is not 100% complete, meaning that not all the fuel is converted into heat.
4. High temperature gases from the combustor lose energy through heat

As a result of the just mentioned losses that happen in a gas turbine cycle, it is advantageous to measure the gas turbine performance in thermal, propulsive, propeller and overall (equal to the product of thermal and propulsive) efficiencies :

- Thermal efficiency(η_{th}) evaluates the how efficient is the conversion of chemical energy stored in the fuel into output power (shaft power plus jet thrust, as equation 2.7 shows). Thermal efficiency is given

by equation 2.8 , where $\dot{m_{fuel}}$ is the fuel flow rate and LHV_{fuel} the lower heating value of the fuel.

$$\eta_{th} = \frac{P_{tot}}{\dot{m_{fuel}} \times LHV_{fuel}} \tag{2.8}$$

- Propulsive efficiency (η_p): Measures the efficiency of converting the total power output generated in the gas turbine into thrust power (TV_0). If the nozzle is unchocked, as in the majority of turboprops, and the fuel-to-air ratio is negligible, it can be simplified in the follwoing equation [51]:

$$\eta_p = \frac{TV_0}{TV_0 + \frac{1}{2}\dot{m}_j(V_e - V_0)^2} \qquad \eta_p = \frac{2}{1 + \frac{u_e}{u_0}} \tag{2.9}$$

- Overall efficiency is the product of thermal and propulsive efficiency.

Apart from efficiency, power specific fuel consumption (PSFC) is a performance indicator for turboprops that translates the fuel consumption per unit of shaft power (SP) generated (equation 2.10, units are $\frac{Kg/s}{W}$.

$$PSFC = \frac{\dot{m_{fuel}}}{SP} \tag{2.10}$$

The design of the propeller is paramount since most of the produced thrust comes from this component. The propeller allows higher propulsive efficiencies than turbofans by achieving higher values of bypass ratio (moving a large mass of air through a small change in velocity). Nevertheless, this efficiency is limited by the flight speed: due to the absence of a diffuser that reduces approach speed, above a certain subsonic Mach number, the relative blade tip speed reaches a supersonic value, which results in high propeller drag losses [51]. Besides, the propeller produces unreasonable noise at high speeds. Figure 2.7 displays the propulsive efficiency of different sorts of gas turbine engines, and it is clear the superior performance of turboprop at low speeds and as the airspeed increases the propulsive efficiency declines to undesirable values.

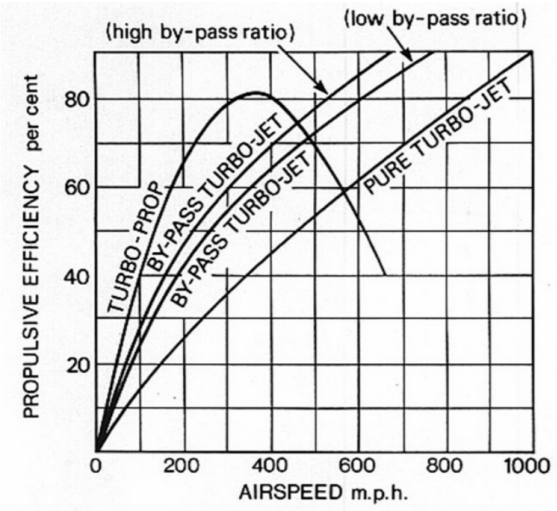

Figure 2.7: Propulsive efficiency comparison between turboprop, turbofan and turbojet (Rolls Royce, 1992)

In line with this, the propeller efficiency (η_{prop}) can be defined as the ratio of thrust power (TV_0) produced by the aircraft and shaft power (SP) of the propeller, as illustrated in equation 2.11.

$$\eta_{prop} = \frac{TV_0}{SP} \tag{2.11}$$

2.3. Hybrid-electric propulsion

A Hybrid Electric Propulsion System (HEPS) combines a combustion engine with an electrical power component to achieve a better overall performance than each sub-system would on its own.

Over the years, several HEPS concepts have been a target of research. These concepts diverge on how the gas turbine engine and electrical systems are connected and how much power originated from each energy source to drive the propellers. The different configurations of the gas turbine connection with the electric system are considered architectures. Throughout this report, the combustion engine and electrical system's energy sources are jet fuel and electrochemical batteries, respectively.

A HEP architecture comprises:

- Energy sources (fuel, batteries, etc.)
- Power converters (electric motors/generators and gas-turbine engines)
- PMAD (Power Management And Distribution) system

A PMAD system is responsible for linking the batteries, the electric motors, and the propellers. It comprises converters, inverters, and cables, and it requires a more detailed and sophisticated design than a conventional fluid-based transmission system [9].

The HEP architectures studied until today for aviation purposes, proposed by Felder [53] and later by the National Academy of Sciences, Engineering, and Medicine [8], are: electric, series, turboelectric, parallel and series-parallel (section 2.3.1 provides details on each of them).

Nevertheless, before diving into the hybrid electric power train architectures, the concept of Degree of Hybridization (DoH) will be introduced. The Degree of Hybridization (developed by Isikveren et al. [54]) can be used for power and energy. Degree of Power Hybridisation (H_P) is the ratio of total installed electric motor shaft power (P_{em}) to the total installed shaft power (P_{tot}), which includes the shaft power produced by the gas turbine (P_{gt}). Degree of Energy Hybridisation (H_E) is defined as the ratio of installed electric energy, here coming from batteries (E_{bat}) to the total installed energy (E_{tot}), that includes energy derived from fuel in the form of chemical energy (E_{fuel}).

The mathematical expressions for H_P and H_E are displayed in equations 2.12 and 2.13, respectively. Degree of Power Hybridisation is also known as the Power Split ratio (Φ).

Vries et al. [55] presents another parameter: supplied power ratio (φ). Its expression can be found in equation 2.14, and it represents the amount of power drawn from the electrical energy source compared to the total amount of power drawn from all energy sources. Note that when the battery is being charged, this parameter is negative or greater than one.

$$H_P = \Phi = \frac{P_{em}}{P_{tot}} = \frac{P_{em}}{P_{em} + P_{gt}} \tag{2.12}$$

$$H_E = \frac{E_{bat}}{E_{tot}} = \frac{E_{bat}}{E_{bat} + E_{fuel}} \tag{2.13}$$

$$\varphi = \frac{P_{bat}}{P_{tot}} = \frac{P_{bat}}{P_{bat} + P_{fuel}} \tag{2.14}$$

2.3.1. Hybrid-electric propulsion (HEP) architectures

A HEP system combines the advantages of electrical components with the advantages of gas turbine engines. However, it also brings some disadvantages such as increased weight, complexity in sizing methods, and complexity of power management. The advantages and disadvantages that different HEPS architectures

present (electric, series, turboelectric, parallel and series-parallel) are presented in sections 2.3.1, 2.3.1, 2.3.1, 2.3.1, and 2.3.2, respectively.

In general, HEP power trains can be described via H_P and H_E, but this approach has a drawback. Although all topologies can be covered with these two parameters, the architectures are not uniquely identified by them. Indeed, the parallel and series-parallel architectures are within the same range of values of H_P and H_E, as it can be checked in table 2.5.

Table 2.5: Parameter range for HEP architectures

Topology	H_P	H_E
Conventional	0	0
Universally-electric	1	1
Series Hybrid	1	$0<H_E<1$
Turboelectric	1	0
Parallel Hybrid	$0<H_P<1$	$0<H_E<1$
Series-Parallel Hybrid	$0<H_P<1$	$0<H_E<1$

Electric configuration

Also known as universally-electric, this configuration uses exclusively electrical energy (from batteries) and power (electric motors provide propulsive power) to produce thrust, see figure 2.8. Therefore, $\Phi=H_P=1$ and $\varphi=1$. Since there is no gas turbine, it does not release emissions directly. Moreover, it reduces the noise produced by the gas turbine.

The efficiency can be higher than 90 % for battery supplied architectures. However, due to the low specif energy of batteries, all-electric battery-powered aircraft configurations are limited to small aircraft in short ranges (which are not a major source of CO_2).

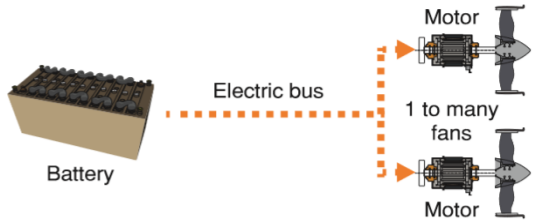

Figure 2.8: Fully electric propulsion. Adapted from[8]

Series configuration

In a series-hybrid architecture (which can comprise single or multiple gas turbines), the gas turbine and propellers are mechanically disconnected, which means that electric motors drive all the propellers. The source of electrical power, comes both from the generator(s), driven by the gas turbine(s), or batteries (electrical energy source). The series configuration is characterized by $\Phi=H_P=1$ since all the propulsive power is provided by electrical motors and $0<\varphi<1$.

This arrangement that can be checked in figure 2.9. A concept that implements a series HEPS is the E-Thrust, developed by the Airbus Group and Rolls Royce.

On the one hand, this architecture is flexible in location and amount of the propulsion units. Therefore compatible with distributed propulsion concepts. It also permits the engine to rotate at an optimal RPM during the mission since the engine shaft runs independently from the fan.

On the other hand, the extra generator that this configuration requires adds extra weight to the propulsion system. Not only that, but the efficiency can be lower due to the many energy conversions.

Another disadvantage of this configuration is that it relies on technology advancements in battery specific energy.

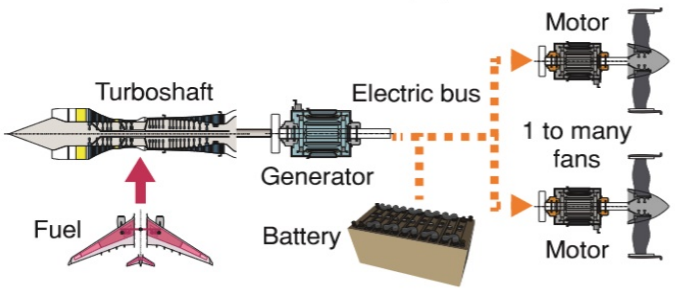

Figure 2.9: Series HEPS. Adapted from[8]

Turbo-electric propulsion system

The turboelectric architecture is a particular case of a series architecture. Similarly, the propellers are driven by electrical power supplied by the electrical motor (H_P=ϕ=1), but the energy source used is exclusively fuel. No batteries are being used (φ=0). Therefore, gas turbine engines are used to drive electric generators, which power inverters and individual direct current (DC) motors drive the propellers. The configuration can be found in figure 2.10.

This configuration, just like in the series architecture, allows flexibility in the number and position of the electric motors, thus being suitable for non-conventional concepts (e.g., Distributed propulsion and boundary layer ingestion designs). It is applied to NASA's N3-X Hybrid Wing Body (HWB).

In addition to this, since it does not incorporate an electric energy source, its application does not depend on advances in energy storage technologies. However, due to high-power requirements, it still relies on advances in superconducting electrical machines (that are cryogenically cooled) and consequently, on High-Temperature Superconductors (HTS) and refrigeration technology.

Some disadvantages of this configuration are the fact that the gas turbine engine must be sized for peak power demand and that it is less efficient (more energy conversions) and heavier when compared with the direct mechanical connection of the fan-turbine or propeller-gearbox turbine system.

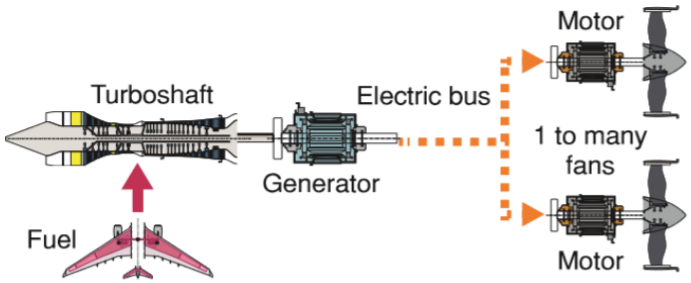

Figure 2.10: Turboelectric HEPS. Adapted from[8]

Parallel configuration

In this architecture (that can possess one or more gas turbines), the gas turbine(s) and electric motor(s) are installed on the same power shaft. This way, the propellers can be mechanically driven either by the gas turbine(s) or electric motor(s), individually or by both. This configuration can be checked in figure 2.11,

This arrangement allows power ratio between the two subsystems to be adjusted during the mission: in-flight phases that have a high power requirement, the electric motor can be used to support the gas turbine. Moreover, it enables the independent design of the power shared between both systems. Therefore, 0<H_P<1.

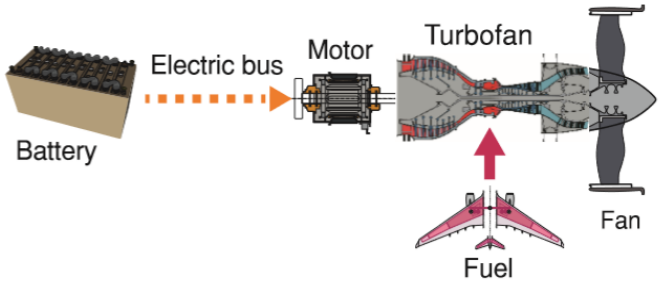

Figure 2.11: Parallel HEP. Adapted from[8]

Thus, an advantage of this architecture is that the electrical system and engine can operate independently [39].

A disadvantage of such configuration is that the engine cannot rotate at an optimal RPM throughout the whole mission because it is linked to the fan [39]. The Subsonic Ultra Green Aircraft Research (SUGAR) Volt concept that has been developed by a team led by Boeing Research & Technology to meet with the NASA N+3 goals implements a parallel HEPS on an aircraft with a large span and a high-aspect-ratio wing.

The parallel architecture, for aerospace applications, presents lower weight comparing to series configuration [56]. In a design study by Friedrich and Robinson [36], which was limited to light aircraft, it is shown that the parallel configuration provides the highest efficiency for aerospace applications.

2.3.2. Series-Parallel configuration

This architecture combines the advantages of series and parallel architectures mentioned in the previous subsections. It can be visualised in figure 2.12.

Here some propellers can be driven by a gas turbine as others exclusively by electrical motors (that can be powered by a battery or gas turbine-driven generator). Thus, the gas turbine engine is mechanically connected to the fan shaft and the generator. The electrical power output from the generator drives the electric motors, which run mechanically independent from the combustion engine.

An advantage over the parallel configuration is that the combustion engine can run at its optimal rpm and independently from the electrical part. Besides, it allows batteries to be re-charged during flight.

However, this concept ends up being heavier (additional mechanical link compared to series hybrid and additional generator compared to a parallel system) and requiring a more complex control strategy [57].

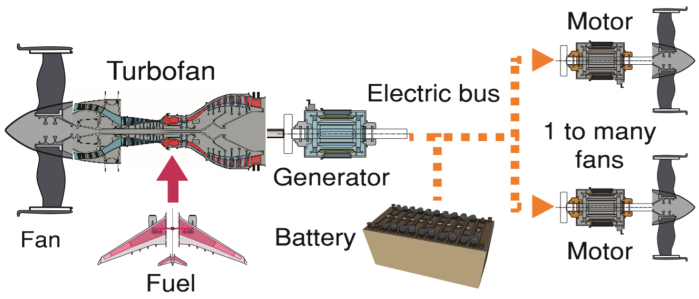

Figure 2.12: Series-Parallel HEP. Adapted from[8]

2.3.3. Hybrid-electric aircraft concepts

With new design possibilities allowed by HEP, several concepts have been developed by aerospace companies making use of the increased degrees of freedom in the design space. Below a brief introduction of the most important studies and concepts developed so far is provided. Figure 2.13 includes aircraft representatives of

hybrid-electric architectures qualitatively marked with the parameters H_P and H_E.

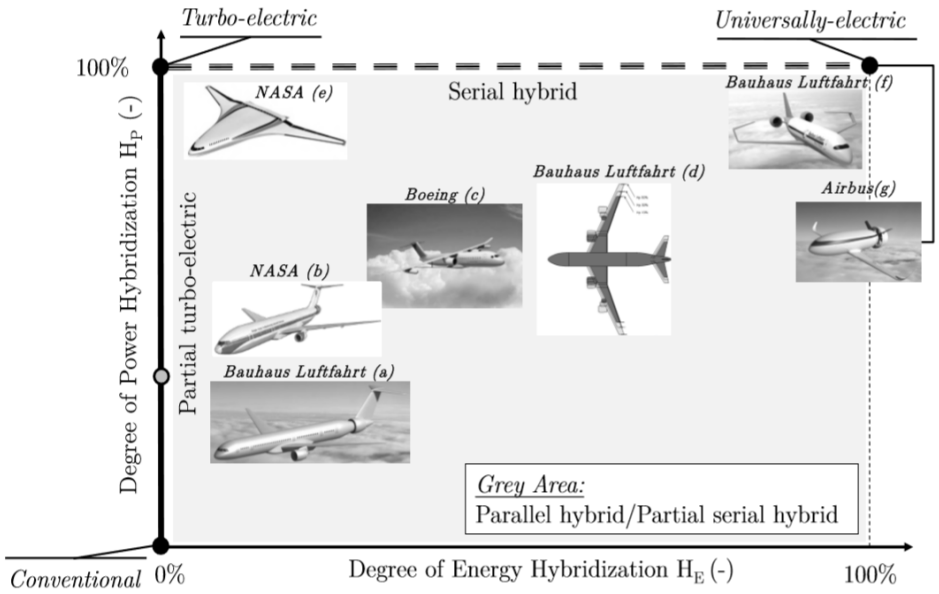

Figure 2.13: Hybrid-electric concepts with different HEPS architectures :(a)Bauhaus Luftfahrt Dispursal,(b)NASA Starc ABL, (c) Boeing Sugar Volt, (d) Bauhaus Luftfahrt Quad-Fan, (e) NASA N3-X, (f) Bauhaus Luftfahrt Ce-Liner , (g) Airbus VoltAir. Taken from [9]

- **Airbus Voltair**: It was studied both as a fully-electric and hybrid electric concept, and it is sized for 68 passengers, a 900 nm range, and a design speed of 500 Km/h. It uses electric motors to power a pair of shielded contra-rotating propellers mounted at the end of the fuselage to take advantage of the boundary later ingestion to lower the overall air resistance. Studies reveal that the reference mission can be matched with 1000 Wh/kg Li-Air batteries. HTS (High-Temperature Superconducting) technology is used for both power transmission and power conversion.
- **Airbus/RR E-Thrust**: Narrow body design for around 100 passengers. Series architecture is used, and six electrically driven fans produce the thrust. Also, the fans can be used to recharge the batteries during descent through fan windmilling partially. HTS machines and distribution systems are enabling technologies for this design.
- **Airbus E-fan X**: Hybrid-electric aircraft demonstrator developed by a partnership of Airbus, Rolls-Royce, and Siemens. In the test aircraft, one of the four jet engines is replaced by a 2MW electric motor (powered by a high power battery).
- **Bauhaus Luftfhart Ce-Liner**: All-electric aircraft, designed to handle 189 passengers over a range of 900 nm (or 1666 Km). The required specific energy of batteries is 2000 Wh/kg, based on future advances in Lithium battery technology. This concept also includes HTS technology.
- **DLR 328-LBME**: It is a small electric turboprop that can carry around 30 passengers and offers an estimated range of 1400 Km. This fully electric aircraft is the final version of a modified Dornier 328 propeller aircraft aiming to assess the potential of electric regional aircraft. The modifications made are a larger wingspan, lighter airframe structures, and inclusion of 720 Wh/kg battery.
- **ESAero/Wright ECO-150**: Aircraft designed to fly up to 150 passengers. It employs a turboelectric HEP architecture, meaning that the energy is supplied by fuel, and any battery is present. Two turbo-shafts are embedded in the wing and drive a series of small electric fans that increase the overall bypass ratio and help in filling the wake of the aircraft, decreasing the wing drag. This concept requires HTS technologies to become feasible.
- **NASA N3-X**: The NASA hybrid wing body N3-X is based on a turboelectric architecture and sized to carry 300 passengers over a range of 13,890 Km. Superconduction is applied to the electric power generators, the power distribution system, and the electric motors. Liquid hydrogen is used as fuel for the two installed turbo-shaft engines and as a cryogenic coolant. On the upper rear fuselage, 14 superconducting electric motor driven fans are installed for BLI distributed propulsion.

- **NASA/Boeing SUGAR Volt**: Hybrid-electric aircraft designed for 154 passengers, including a parallel HEP configuration where the electric motors supply to part of the power needed by the two turboprops (or turbofan in a different variant). It is characterized by a high aspect ratio braced wing with two large battery compartments hanging underneath it. Battery specific energy to become economically viable is stated in the range 750-1000 Wh/kg.
- **Zunum Aero**: Small regional aircraft incorporating a series HEP architecture where battery packs are integrated into the wing structure on both sides. Designed for 12 passengers with a range of 1126 km.

2.3.4. Electrically Assisted Turboprop concept

The low specific energy of batteries in comparison to fossil fuels, the low specific power of electric motors, and power electronics does not allow regional turboprop aircraft to become fully electric. Therefore, it is required the presence of a turboprop engine coupled with an electric motor to drive the propellers [58]. This configuration is named as Electrically Boosted turboprop (EBTP). The potential advantages associated with this concept are listed below:

- **Gas turbine optimized for cruise condition**: Due to electric assistance during take-off and climb, the conventional gas turbine does not need to be sized to fulfill the power requirements that such flight phases demand entirely. Therefore, the gas turbine can be sized to optimize its performance during cruise (the longer segment of the flight). If the gas turbine is optimized for cruise, it can become more efficient and, due to the lower power requirements of this phase, it can be downsized and enhance the reduction in pollution and specific fuel consumption.
- **Noise reduction and the potential decrease in emission near airports**: During the take-off maneuver, the electric motor can assist the thermal engine electrically. Also, taxi-out is possible to be 100% electric. Therefore, in comparison to the traditional propulsion system, fuel consumption, noise, and pollutant are lowered near the airport [39].
- **No major modifications in the airframe required**: The inclusion of a parallel-hybrid power train within a conventional regional aircraft requires least modifications to the airframe when compared to the insertion of different HEP architectures [58].
- **Potential energy recovery during descent**: Energy recovery is a traditional function of every hybrid system, as the potential energy could be recovered during the descent through the electric motor-generator moved by the propeller. Theoretically, the energy recovered can be stored in the battery and reused in the next phases, as taxi and take-off of the following mission [35]. However, this possibility is not being explored in this research.

This HEP concept has, at the same time, some disadvantages:

- **Weight penalty**: Introduction of the entire electric system and the thermal management system that this system requires adds extra weight to the conventional power plant that can off-set the benefits listed above.
- **Dependency on technology maturity levels**: As it has been stated, the feasibility of HEPS depends on the availability in the future of batteries and electric motor with considerably higher specific energy and specific power, respectively.
- **Shift in gas turbine operation line**: The volume occupied by the electrical system reduces the usable aircraft space

Since HEP is a dual-energy system, it needs different performance metrics [30]. Note that the overall efficiency (η_{ov}) of the powertrain is no longer the one described in section 2.2 but as equation 2.15 indicates.

$$\eta_{ov} = \frac{V_0 \cdot FN}{P_{tot}} = \frac{V_0 \cdot FN}{P_{bat} + P_{fuel}} \tag{2.15}$$

Figures of merit are used to assess the performance of a HEP concept, at a vehicular level. Payload Range Energy Efficiency (PREE) suggested by Bijewitz et al. [59] and Energy Specific Air Range (ESAR) developed

in [31][60]. ESAR characterizes the range of a mission per energy spent and is an instantaneous aircraft performance parameter, as it can be seen in equation 2.16. In fact, ESAR varies throughout the mission, as L/D, Speed (V_0) and aircraft mass ($m_{A/C}$) change.

PREE can be computed through equation 2.17 is translated into aircraft energy efficiency carrying a payload over a specific range and its dimensionless. $m_{des,pl}$ stands for the design payload carried over the design mission range R_{des}, where a certain amount of energy is consumed E_{des}.

$$ESAR = \frac{dR}{dE} = \frac{V_0 \cdot \frac{L}{D}}{TSPC \cdot m_{A/C} \cdot g} = \frac{\eta_{ov} \cdot \frac{L}{D}}{m_{A/C} \cdot g} \tag{2.16}$$

$$PREE = \frac{m_{des,pl} \cdot R_{des}}{E_{des}} \tag{2.17}$$

When assessing a parallel-hybrid electric architecture is relevant to compare the following parameters to the conventional configuration: Fuel burn, total energy (from both sources fuel and batteries), CO_2 emissions, pollutant emissions (NO_x, CO and UHC), Operating costs, cost per available seat /kilometer, and take-off weight.

2.4. Electrical system

This section outlines the basic working principles and the current State-of-the-Art (SOA) of batteries and electric motors, in sections 2.4.1 and 2.4.2, respectively.

2.4.1. Electric Motor

Working principle

Electric motors are required to convert electric energy (with the help of magnetic and electric fields) into mechanical energy. The efficiency of the electric machine η_{em} depends on voltage, current, required torque (Q), and rotational speed n_{shaft}. Figure 2.14 displays a Q-n diagram. The sizing point P_{des} is equivalent to the power demand during the one engine inoperative for aircraft design [10]. The electric motor's operational envelope presents three limitations as visible in figure 2.14:

- Maximum torque, illustrated by line I (the design torque)
- Maximum Power represented by P_{max} curve
- Maximum Rotational speed (n_{max})

The power of an electric motor can be determined with equation 2.18.

$$P_{des} = Q \cdot \omega_{shaft} = Q \cdot (2\pi \cdot n_{shaft}) \tag{2.18}$$

In general, electrical machines use the interaction between the magnetic fields of a rotating component (rotor) and stationary part (stator) to produce mechanical torque. The main magnetic field (typically generated in the rotor) can be constant or time-varying and can be generated using permanent magnets, soft magnetic materials (Reluctance), passive field coils ("squirrel cage") or active field coils (wound-rotor and doubly-fed machines). Electric motors and generators using the same general principles. The generator converts mechanical shaft power into alternating current (AC) electrical power, while a motor converts AC or DC into mechanical shaft power.

In a motor, windings in the stator generate a time-varying magnetic field and consume the vast majority of the electrical power of the machine. Currents in stator can be driven by sinusoidal source (AC machines) or by arbitrary, actively-controlled waveforms (DC machines). In a generator, the rotating main field induces a current in the stator coils.

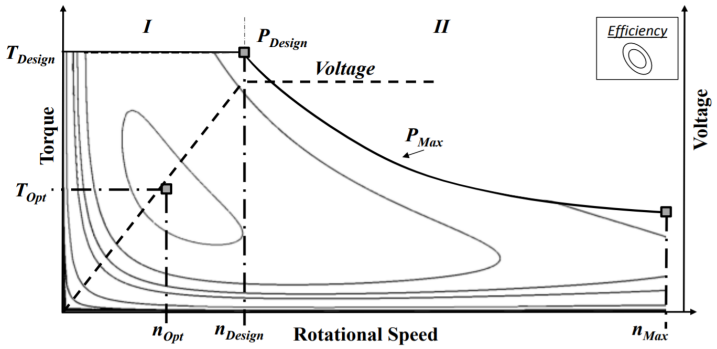

Figure 2.14: Performance map of an electric motor. Taken from [10]

There are two main sorts of electric motors: AC (Alternating current) and DC (Direct current). Within each category, there are several electric motor types as figure 2.15 illustrates. However, for aerospace purposes, Induction Machines (IM), Switched Reluctance, and Permanent Magnet machines can be considered. Table 2.6 summarizes the features of the three types of electric machine. Because of its leading performance, PMSM (Permanent Magnet Synchronous motor with alternating current) machines are the most used in aerospace research and development [20][61].

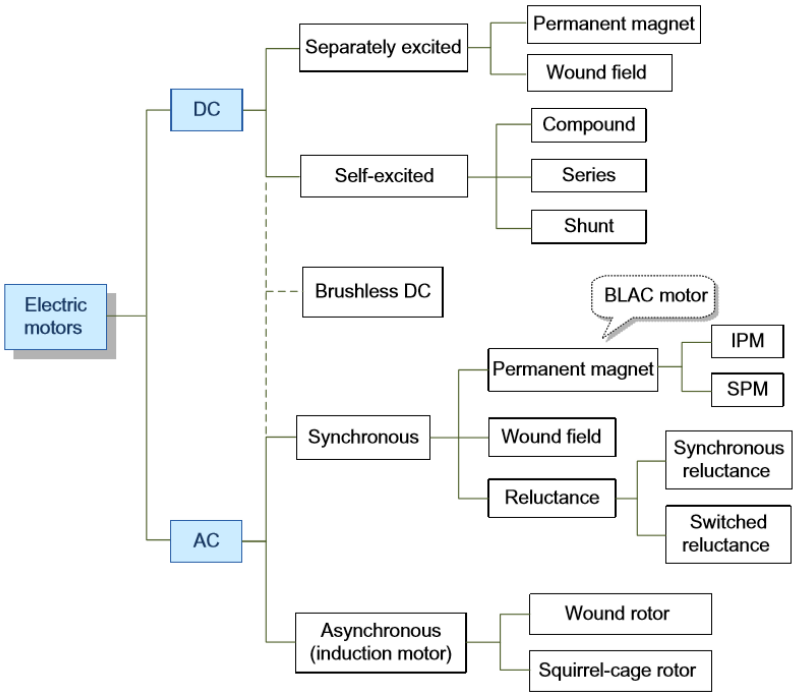

Figure 2.15: Electric motor types. Taken from [11]

However, the electric energy conversion into mechanical energy is not 100 % efficient, and thus, losses occur. The losses in an electric motor are classified as:

- **Copper losses**: Originated by the electric current due to ohmic resistance.
- **Iron or core losses**, that can be further divided into:
  - Hysteresis: Due to re-magnetisation effects.
  - Eddy current: As a result of Faraday's Law. When rotating in a magnetic field, the voltage induced causes eddy currents [11].

Table 2.6: Performance comparison of different electric motor technologies adapted from [20]

Feature	IM	SR	PM
Fault tolerance	-	++	+
Power density	Moderate	Moderate	High
Robustness	Yes	Yes	No
Efficiency	Moderate	High	High
Cost	Low	Low	High
Wide speed range	No	Yes	Yes
Open loop control	Yes	No	No
Closed loop simplicity	Yes	Yes	Yes
Torque ripple	No	High	Low
Acoustic noise	No	Moderate	Low

- **Mechanical losses (Friction and Windage losses)**: Due to drag resultant from the rotor spinning in the air, motor bearings, and lubrification.

State of the Art

The principal design characteristics that influence the applicability of specific electric motors for aerospace applications are the materials and machine topologies. Ideally, the electric motor should present high reliability, availability, and high power density to minimize operational costs, aircraft weight, and environmental impact.

NASA is sponsoring research in electric motors to achieve power densities 2-3 times higher than state of the art [57]. The research is being conducted in permanent magnet, induction, and wound field electric machines. However, only preliminary results are available, and there no final prototypes [62].

Nevertheless, there is a technology that can potential enable higher gravimetric power density: High-Temperature Superconductivity (HTS)).

The superconductivity phenomenon was observed for the first time in 1911 by the Dutch physicist Heike Kamerlingh Onnes, while studying the properties of matter at very low temperature. He noticed that the electrical resistance of mercury goes to zero below 4.2 K (equivalent to -269°) [63]. Indeed, below a certain critical temperature T_c, a critical field H_c and a critical current density J_c, materials undergo transition into the superconducting state. When a material is at the superconducting state it is characterised by offering no resistance to the passage of electrical current. When resistance falls to zero, a current can circulate inside the material without any dissipation of energy.

If either the stator or rotor from current electric motor armatures are replaced by HTS coils the specific power can raise up to 10 kW/kg, at 35.000 rpm [64]. In full HTS motors, both stator and rotor armatures are replaced by HTS material, specific power up to 40 kW/kg (not taking cooling into consideration) can be accomplished along with efficiencies greater than 99% [65].

The downside of using a HTS motor is the cooling system associated with it. HTS motor need cryocoolers to keep the HTS material at required low temperature. Such cryocoolers have a current specific power of about 0.33 kW/kg (with regard to input power) and a Carnot efficiency of 15% [65], representing extra weight in the electric system.

2.4.2. Battery

Working principle

A battery cell is a simple energy storage system consisting of an anode and a cathode separated by an electrolyte. Another definition of battery is given in [13]: *"electro-chemical cell that converts chemical energy*

into electrical energy via the energy difference between the reactions occurring at the two electrodes". It can be composed of one or more cells staked in series or parallel to provide desired output voltage, capacity, and power.

The discharge behaviour shows strong non-linearity as observed in figure 2.16 [66]. The output voltage of a battery cell depends on the discharge rate (C-rate) and DOD (Depth of discharge). For Lithium-ion batteries, the voltage decreases slowly until an abrupt drop at about 90% DOD. This voltage drop is caused by the internal resistance of a battery cell, where a part of the available voltage is consumed for internal electro-chemical processes (according to Ohm's Law). Moreover, discharging past a threshold DOD (specific to battery design) can cause shortened lifetime and thermal runaway [13].

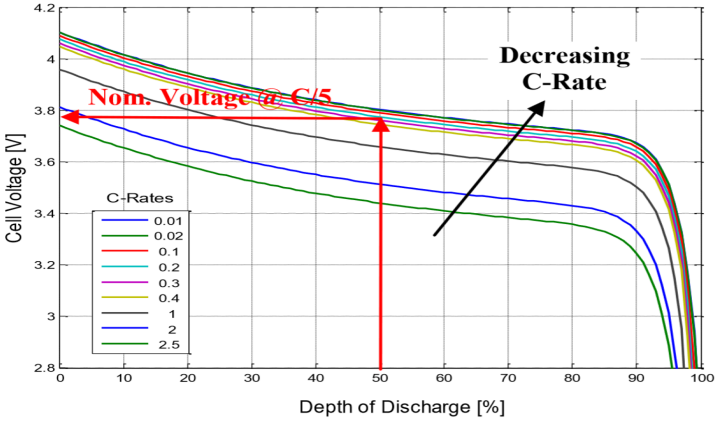

Figure 2.16: Example of a discharge behaviour model of a generic lithium based battery cell. Model according to [12]

State of the Art

Lithium-ion batteries were placed on the market in 1991, and have been used to in several applications [67]. Compared to the old rechargeable batteries, such as lead-acid, nickel-cadmium (Ni-Cd) and nickel-metal-hydride (Ni-MH), lithium-ion ones present higher energy and power density (see figure 2.17 and table 2.7). Also, lithium-ion batteries demonstrate a broad operating temperature range [68].

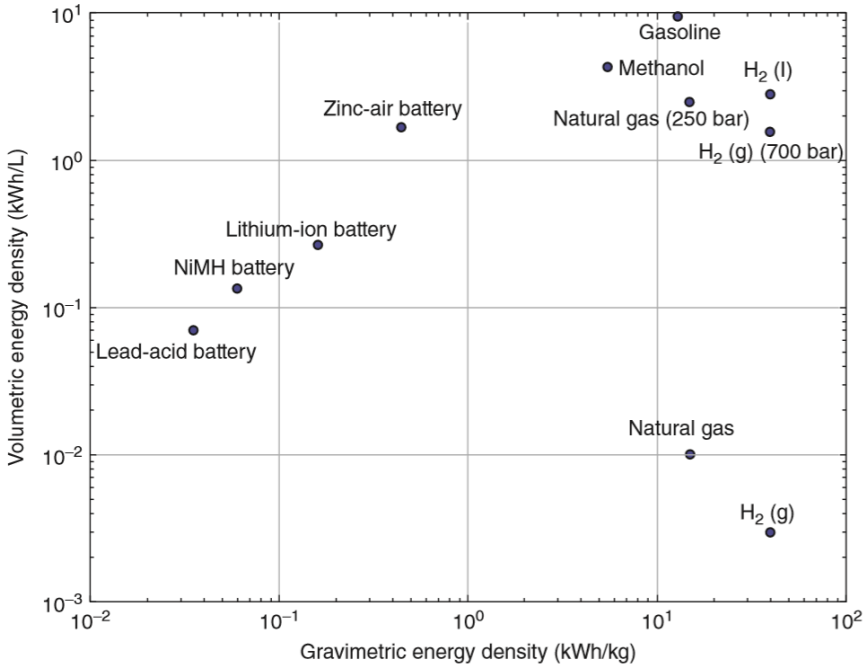

Figure 2.17: Energy density comparison of various energy-storage systems taken from [13]

Table 2.7: Overview of different battery types and their parameters adapted from [21]

Battery Type	Specific Energy [Wh/kg]	Specific Power [W/kg]
Lead-acid	25-30	80-300
Nickel-Cadmium	50-60	200-500
Nickel-metal hybrid	60-70	200-1500
Lithium	60-150	80-2000
Zinc-air	200-3000	70

The current problem with the State of the Art battery technology is the insufficient specific energy. The specific energy is computed by the ratio of the battery energy capacity to the battery mass. It is a measure of how much energy per unit mass may be stored [21]. Current Lithium-Ion batteries have a storage capacity of around 100 Wh/kg at pack level [66], compared to 12.0 kWh/kg in kerosene (see figure 2.17). Analogous, the specific power illustrates how much power can be delivered per unit mass in a battery.

2.5. Flight mechanics

This section reviews the basics of flight mechanics and the assumptions usually made when developing a mission analysis suite. Since this research focuses on the hybridization of the LTO cycle due to its regulatory character, the LTO cycle is analyzed here.

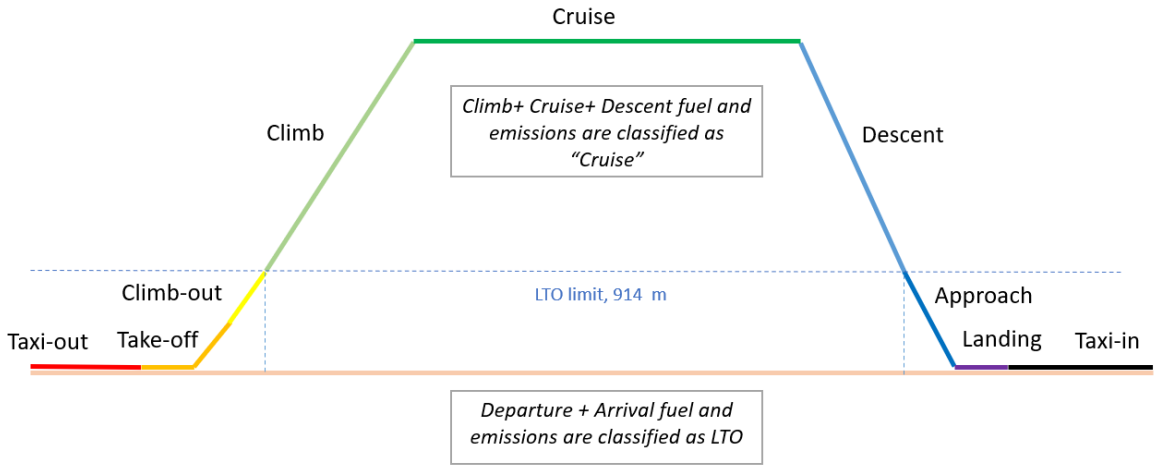

Figure 2.18: Mission profile divided in segments. Segments below 914 m (3,000 ft) are reported as *LTO* and above that height are reported as *Cruise* [14]

A regular aircraft mission is pictured in figure 2.18. It can be decomposed into the following phases [14]:

- **Taxi**: Covers the ground movements of the aircraft between the parking spot and the runway point where the take-off starts (Taxi-out) and between the landing point in the runway and the place where it parks and shuts down the engines (Taxi-in). At this phase, a relatively small thrust is required, and the propeller is trimmed at a specific ground speed to deliver thrust T_P, with F_g (jet thrust) approximately zero. The solution is such that the propeller ends up working at low efficiency, resulting in high fuel consumption. One solution adopted to overcome this issue is to have only one propeller working at a higher thrust than two propellers working at a lower thrust and low-efficiency [15]. The downside of this measure is the lateral trim of the aircraft during the ground roll and the start-up of the inoperative engine right before take-off.
- **Take-off**: Includes aircraft acceleration from taxi-out until take-off speed is reached (this speed

depends on ambient conditions and take-off weight). It is the flight segment with maximum power requirements.The acceleration of the aircraft is function of the thrust, T, the aerodynamic drag, D and the ground friction, Dg

- **Climb**: Ascending phase after take-off until the aircraft reaches cruise altitude. Usually divided into two phases: Climb-out (up to 3,000 ft altitude, LTO cycle ceiling height)) and Climb (from 3,000 ft until cruise altitude). Both phases are performed at constant CAS (Calibrated Air Speed) and it can be modelled by knowing the rate of climb vc. The governing equations to compute Thrust (T) and power (P) requirements and lift of an aircraft simplified to a point mass during climb are as follows (the free body diagram is presented in figure 2.20):

$$T - D - W\sin\gamma = m\frac{dU}{dt} \Rightarrow TU - DU - Wv_c = mU\frac{dU}{dt} \tag{2.19}$$

$$L = W\cos\gamma \tag{2.20}$$

The climb angle, for a steady climb is given by:

$$\sin\gamma = \frac{v_c}{U} = \frac{T-D}{W} \tag{2.21}$$

The climb profile suggested by ICAO is depicted in figure 2.19. In the transition of the two climb segments the aircraft accelerates at 3,000 feet to reach CAS2 (and there is slightly power increase [15]).

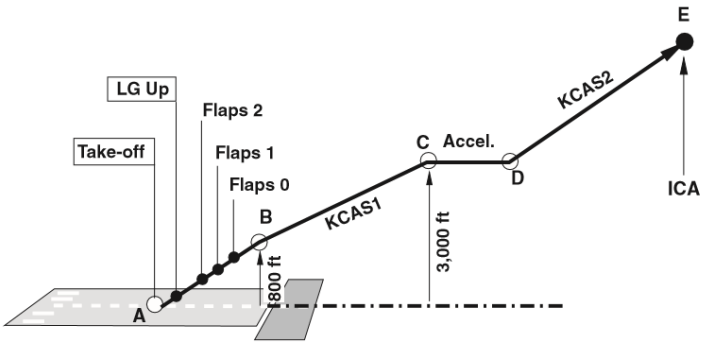

Figure 2.19: Climb profile following ICAO procedure. Taken from [15]

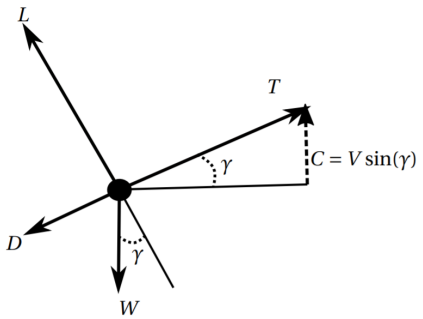

Figure 2.20: Free body diagram during climb

- **Cruise**: Usually is the longest portion of a flight (thus, where most of the fuel is consumed), and depending on operational reasons, it can be flown either at constant or variant altitude. Longer range flights enable higher altitude cruise than short-range ones. The optimum cruise altitude and Mach number depends on the type of aircraft, mission range, and take-off weight.
For modeling purposes, it is assumed a steady and constant altitude cruise (constant Mach number).

- **Descent**: Taking place after cruise, when the airplane drops altitude (contrary to climb) towards its destination. A continuous descent approach (CDA) is picked over a multi-stage approach for modeling purposes due to its simplicity and reduced fuel consumption [15]. Figure 2.21 presents a sketch of a CDA and a normal approach approach path (multi-stage). Similarly to climb, equation 2.22 the governing equation taken from a free body diagram for descent.
  The target fligth path angle is -3 degrees is the most fuel efficient option [15].

$$T - D + W\sin\gamma = m\frac{dU}{dt} \Rightarrow TU - DU + Wv_c = mU\frac{dU}{dt} \tag{2.22}$$

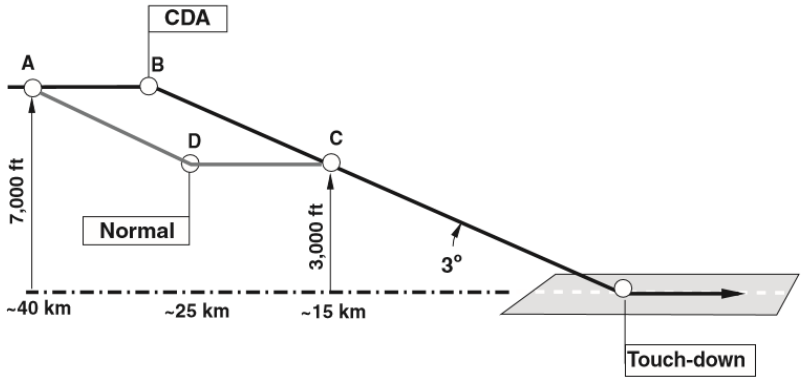

Figure 2.21: Sketch of a continuous descent approach. Taken from [15]

- **Approach**: The last segment of an aircraft's descent to landing, below 3,000 ft. The same approach as the descent is used for modeling
- **Landing**: The aircraft reaches the ground.

However, the aircraft needs to be able to perform a diversion or loiter for security reasons, and extra fuel shall be transported. Diversion occurs whenever the aircraft cannot land on the lined up airport and is re-routed to another airport.

Loiter is the hold phase of an aircraft consisting on an intentional cruise along a particular path and normally occurs before the approach to the destination airport making extra time for landing clearance to be granted by local air traffic control.

3

Mission Profile & Methodology

This master thesis' research goal is to investigate the impact of introducing a parallel-hybrid electric architecture powertrain in a Regional Turboprop Aircraft at some Local Air Quality emissions (CO and NO_x) in the LTO cycle. LTO stands for Landing and Take-off and it represents the mission segments below 914 m (3,000 ft) and, thus, the emissions released at low altitudes and in the vicinity of airports.

Among the Regional Turboprop aircraft, ATR 72-600 is the leader in the regional category with 50 to 70 seats and the one that has more literature and data available. Hence, this will be the example baseline aircraft used to hybridize.

Several studies conducted on the Electrically Assisted turbofan (EATF) [58] have shown that the hybridization during the whole mission is not advantageous due to the extra weight that it would add to the aircraft [9] and consequent penalty in the blocked fuel and overall energy consumption. Not only that, but the electrically assisted cruise have demonstrated not to bring benefits in block fuel reduction for specific energy of Batteries below 1000 Wh/kg. For a 50% electric cruise, neutral energy consumed is obtained only at a mission length of 1100 nm and battery specific energy of 1500 Wh/kg[9].

As to the research conducted with Electrically Assisted Turboprop, energy consumption reduction can only be achieved at short mission range (300 nm) with battery specific energy of 500 Wh/kg (at least) for 75 % of electrification during the entire mission. For ranges of 600 nm, the block fuel weight can be reduced but total energy of the aircraft increases in comparison to the baseline turboprop [40]. Thus, shorter range mission can alleviate the total energy storage penalty.

Although it is out of the research scope, Antcliff et al. [40] concluded that for a 600 nm (approximately 1111 km) mission range and specific energy of batteries lower than 500 Wh/kg the economics of the parallel-hybrid electric concepts were less attractive than the conventional gas turbine only powered turboprop.

The main differences between an Electrically Assisted Turboprop (targeted concept of this research) and an EATF concepts when it comes to the mission hybridization strategy are the aircraft weight, mission range, flight speed and power requirements. Turbofan commercial aircraft are bigger and also more payload can be carried along, making it heavier. With regard to the range of the missions, EATF are demanded to fly longer distances and at higher speeds. Therefore, the theoretical benefits of installing a parallel-hybrid electric powertrain in a turboprop aircraft are more likely to visible.

A HEP concept sizing is mainly sensitive to mission range, electric system technology maturity levels and degree of hybridization for power or Power Split ratio (ratio of shaft power generated by the electric motor to the shaft power that is driving the propeller). The longer the design range, the more energy is needed to carry the aircraft weight. Thus, for shorter missions the HEPS benefits are enhanced. Nevertheless, the range of the mission that will be simulated needs to be a compromise between short range and a range that the aircraft is required to fly in normal conditions.

Accordingly, to conduct this investigation it is essential to pick a Mission profile and compare the electrically assisted turboprop performance to the baseline turboprop aircraft under the same operating conditions. The mission profile and specifications are outlined in section 3.1. The mission range is fixed for simplification purposes and it is equal to 1000 km. It is important to note that the Regional Turboprop Aircraft fly short distances and the average duration of a normal commercial mission of this aircraft is close to one hour, and

range shorter than 500 km . Section 3.2 describes the electrically assisted turboprop architecture and the key performance indicators that will be used to classify and compare the different configurations simulated.

After the mission is fixed and defined, the methodology followed to simulate the entire mission for the baseline and parallel-hybrid electric powertrain concept is presented in section 3.4

The hybridization strategy picked is described in section 3.3 and it is adapted to the focus of the research: investigate the possibility of reducing emissions below 914 m.

3.1. Mission profile

In order to use a realistic mission profile, the Piano-X ®[1] tool was selected to generate it. Piano-X is a commercial mission analysis software that computes instant fuel consumption, environmental emissions (NO_x, HC, CO, CO2), drag and performance characteristics at any range and payload combination. When using Piano-X, the mission segment speeds and flight levels are inputs that the software needs to be provided.

The mission specifications used as inputs in Piano-X are presented in table 3.1. Although the maximum range of the ATR-72 600 is 1527 km, previous research has found that for such a range, the hybrid-electric propulsion is no longer beneficial due to the extra fuel or battery that needs to be carried as a result of longer cruise [40]. The benefits of HEPS are expected to take place at short-range missions, for the next two decades, with the predicted technology. Thus, the mission range picked in this research is 1000 km.

Table 3.1: Main Mission specifications

Parameter	Value	Units
Mission range	1000	[km]
Payload	5000	[Kg]
Taxi speed	40	[KCAS]
Climb-out speed	170	[KCAS]
Climb speed	170	[KCAS]
Cruise altitude	5,500	[m]
Cruise Mach Number	0.38	[-]
Take-off speed	119	[KCAS]
Fuel Block for Diversion	200	[kg]
Fuel Block for Hold	200	[kg]

The payload mass is assumed to be 5000 kg, and there is blocked fuel to perform Diversion and Holding (Loiter). Due to the main importance of these segments (and for airworthiness reasons), the reserve fuel is blocked for these two events. A mission with the characteristics displayed in table 3.1 have reserved block fuel for diversion and loiter of approximately 200 kg each, based on literature values [16]. These values that, for simplification purposes are kept constant.

The speeds (CAS in climb and take-off and TAS in cruise) and cruise altitude values were based on the optimal speeds and altitudes for an economic missions of this aircraft published by ATR [16].

Furthermore, Piano-X also computes the emissions of the generated mission by consulting the ICAO engine emissions database, but as it as been mentioned previously in chapter 2, turboprop are not included and are confidential. Thus, the source Piano-X utilizes to compute the aircraft emissions is unknown.

Moreover, the flight phases taxi-out, taxi-in, take-off, and approach are considered 'Allowances' by Piano-X, so the fuel burnt at each of these phases is computed with the power settings and Time-in Mode (inputs in the LTO cycle emissions table).

[1] https://www.lissys.uk/PianoX.html

The mission altitude, speed and Mach number profiles generated by `Piano-X` can be visualized in figures 3.1, 3.3 and 3.2, respectively. It is important to mention that the 1000 km mission that `Piano-X` defined measures the distance traveled only above 1500 ft (457 m). Taxi in and out are not represented in the figures just mentioned due to its long duration 26 minutes in total (13 accounted for each taxi)

. The climb speed true airspeed (TAS) is computed based on the constant calibrated airspeed (CAS), defined per segment.

Power off-take is considered for all the segments of the mission to represent the secondary power needs of the Aircraft since this Aircraft does not possess an APU (Auxiliary Power Unit). This power is usually required by cabin-pressurization, electric, pneumatic, and hydraulic aircraft systems.

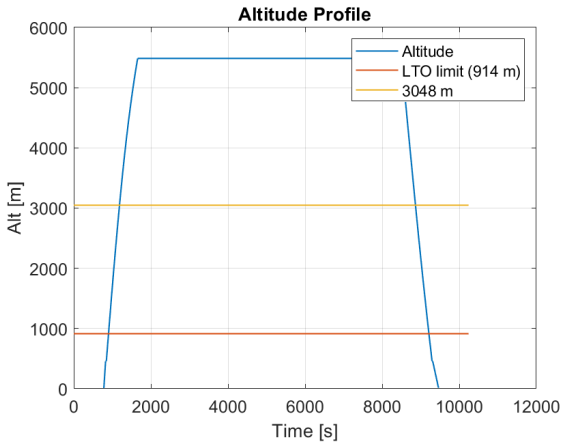

Figure 3.1: Mission Altitude profile

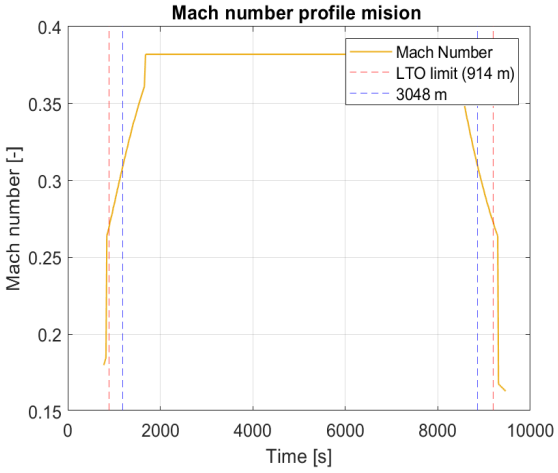

Figure 3.2: Mission Mach Number profile

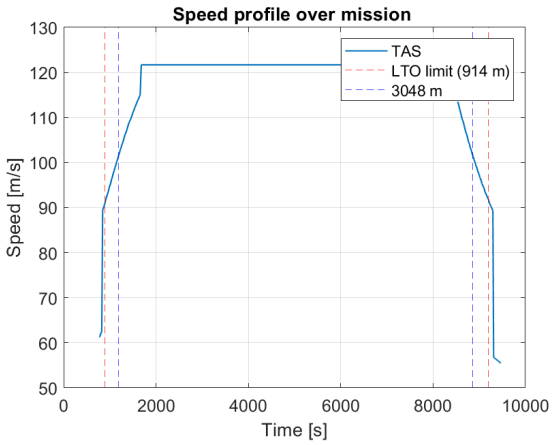

Figure 3.3: Mission True Air Speed profile

`Piano-X`, to fully define the mission, provides the user with the power settings at each flight segment. The power settings of the mission that has just been presented are outlined in table 3.3.

- The Take-off Power is the highest power required because the aircraft is accelerated to take-off speed. At this phase, the aircraft is at its heaviest configuration and has a finite distance (runway) to accelerate. The highest the power available in the engine, the shorter the runway can be, or heavier the aircraft at take-off. This power is usually limited to 5 minutes, not to degrade the engine lifespan and maintenance.

- The Maximum Continuous Thrust is relevant for the One Engine Inoperative (OEI) case. When the is a failure in one of the engines, the aircraft has to be able to fly to the nearest airport available, and it needs to be able to deliver a high amount of power (around 90%) for a continuous period.
- Maximum Climb power setting is usually the recommended power used throughout the climb phase.

Table 3.2: PW 127-M maximum power delivered in different flight phases [22]

Flight Phase	Power Setting (%)	Value [Units]
Max. Take-off Power (MTO)	100 %	2,051 [KW]
Max Continuous	90 %	1,846 [KW]
Max. Climb (MCL)	80 %	1,635 [KW]
Max. Cruise (MCR)	78 %	1590 [KW]
Idle	7 %	143 [KW]

The power settings are defined based on the reference values for Maximum Power rated for each flight segment that the Aircraft engine PW 127-M is certified to deliver: MTO (Maximum Take-off Power), Maximum Continuous Power, MCL (Maximum Climb Power) and MCR (Maximum Cruise Power). These values are exhibited in table 3.2.

Table 3.3: Power settings in Piano-X mission

Parameter	Value	Units
Power requirements		
Segment 1 (Take-off)	2,051 (100% MTO)	[KW]
Segment 2 (Climb-out)	1,635 (100% MCL)	[KW]
Segment 3 (Climb)	1,635 (100% MCL)	[KW]
Segment 4 (Cruise)	1,195 (75.2% MCR)	[KW]
Segment 5 (Descent)	143 (Idle)	[KW]
Segment 6 (Approach)	143 (Idle)	[KW]
Segment 7 (Landing)	721 (44.1% MCL)	[KW]

3.2. Parallel hybrid-electric powertrain

A parallel-hybrid electric architecture has also been selected based on a previous study that compared various HEP architectures in a turboprop aircraft, and the parallel architecture has presented the lowest sensitivity to electric component technology advancements. Thus, the only architecture that can benefit from HEP advantages for relatively lower technology levels (lower than 1000 wh/kg) [69]. More details on the theoretical benefits and disadvantages of an Electrically Assisted Turboprop (Turboprop electrically assisted by a parallel-hybrid electric powertrain) are presented in section 2.3.4

The Powertrain of a parallel hybrid-electric system (which schematic is presented in figure 3.4) can be decomposed into two sub-systems, the conventional gas turbine (upper one) powered by fuel and the electric system (lower one) where the batteries are the electric energy providers. Both sub-systems' output shaft power is added up to drive the propeller and generate thrust. Note that the gearbox is not represented in the schematics for simplification purposes, but it would be placed right before the propeller to reduce the rotational speed of the shaft and enable the propeller to rotate at tip Mach number values lower than 1.

Diving into each system, the schematic illustrates a gas turbine with the same architecture as the PW127 engine: three-shaft and twin-spool engine. The last turbine (Power turbine) displays a different color than the other turbomachines to highlight that this is the turbine connected to the propeller shaft. The gas turbine efficiency (η_{GT}) stands for the conventional engine thermal efficiency (how efficiently the chemical energy stored in the fuel is converted).

As to the electrical system part, the components mentioned in the previous sections are represented along with their efficiencies and power output.

Figure 3.4 also includes the power off-take, that is provided by the battery (that stores electric energy) instead of by the gas turbine in a hybrid configuration.

Another relevant remark is that the direction of the power flow is from left to right, meaning that it is not considered the possibility of in-flight recharge of the battery with the propeller excess power.

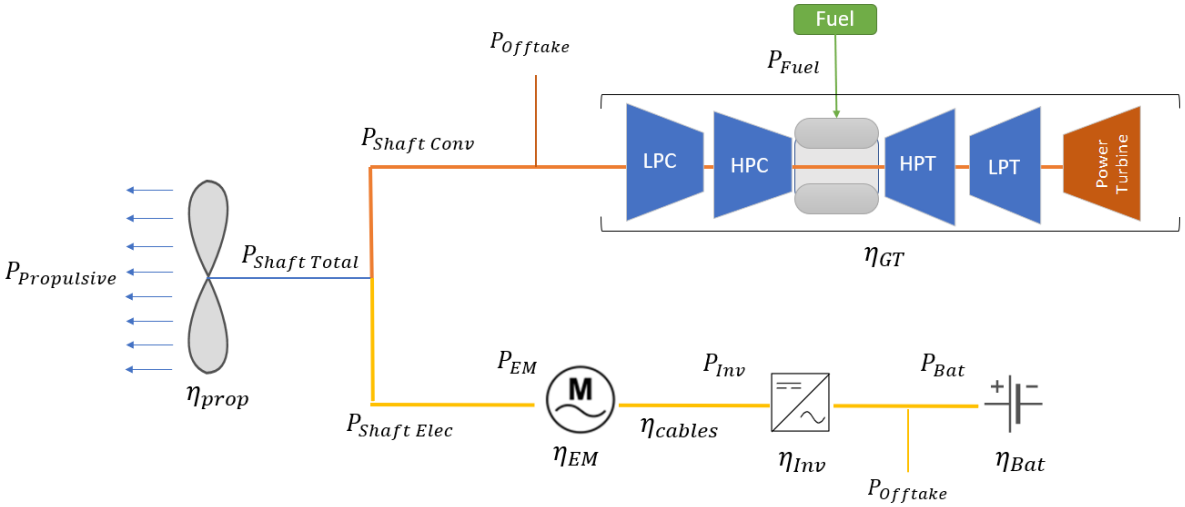

Figure 3.4: Schematic of a simplified Parallel-hybrid electric powertrain

To characterize a parallel-hybrid electric system, the concept of Degree of Hybridization for Power (or simply Degree of Hybridization for simplification purposes, DoH) is used to define how much shaft power is produced by the electric motor ($P_{Shaft_{Elec}}$) from the total shaft power that is delivered to the propeller shaft, which is the sum of the electric motor shaft power to shaft power generated by the conventional gas turbine engine ($P_{Shaft_{Conv}}$), see equation below. Power Split ratio (H_P or Φ) is used as a synonym to DoH throughout this thesis.

$$H_P = \Phi = DoH = \frac{P_{Shaft_{Elec}}}{P_{tot}} = \frac{P_{Shaft_{Elec}}}{P_{Shaft_{Elec}} + P_{Shaft_{Conv}}} \tag{3.1}$$

3.3. Hybridization strategy

After setting the mission profile, it is crucial to adopt a strategy on how much electrical assistance should be provided during each segment of the flight so that the benefits of adopting a parallel HEPS can be reached. There is a trade-off to be considered: the fuel burn ideally should be reduced with hybridization, but this also leads to a heavier electric system and more fuel is necessary to drive the more electrified Aircraft.

The strategy adopted will define the amount of energy that the batteries need to carry and the maximum power that the electric motor and inverters need to deliver to fly the defined mission. The concepts of Power Split ratio and Degree of Hybridization for Power (or Degree of Hybridization) are used as synonyms.

A parallel-hybrid electric architecture withstands a wide design space, where the Power Split Ratio can vary from 0 to 1. When zero, the propeller is driven by the conventional gas turbine engine, and when it assumes 1, the shaft power is provided by the electric motor. Moreover, there are two options when it comes to mission hybridization. The power Split ratio can be constant or varied throughout the mission. The second option permits more degrees of freedom in the mission definition and allows the exploration of various strategies.

The hybridization strategy shall depend on the aircraft category, range, and overall goal of the hybridization.

Since the goal of this research is to investigate different combinations of Power Split ratio (Φ) and Technology level scenarios in a Parallel-Hybrid electric architecture and evaluate how these two parameters influence the NO_x, CO and LTO emissions, the electric assistance focus is at low altitudes (LTO cycle altitude limit is 914 m). Moreover, the mission range picked is 1000 Km, and the Aircraft is a Regional Turboprop.

Therefore, the hybridization strategy adopted is visually represented in figure 3.5. The figure includes the altitude limits of each mission segment. Take-off and Landing take place below 457 m of altitude. The climb is divided into Climb-out (up to 3048 m) and Climb (between Climb-out and Cruise). The figure indicates whether the Aircraft is powered entirely by the electric system (Electric), by the gas turbine (Conventional). The list below describes explicitly the mission per segments:

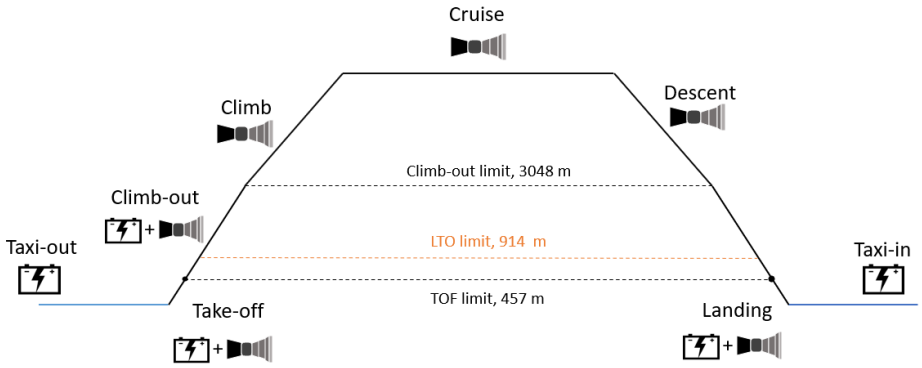

Figure 3.5: Hybridization strategy during mission

- **Taxi-out and Taxi-in**: Electric (H_P= 100 %)
- **Take-off**: Hybrid (0 < $H_P \leq$ 100 %)
- **Climb-out**: Hybrid (0 < $H_P \leq$ 100 %)
- **Climb**: Conventional gas turbine (H_P= 0 %)
- **Cruise**: Conventional gas turbine (H_P= 0 %)
- **Descent**: Conventional gas turbine (H_P= 0 %)
- **Landing**: Hybrid (0 < $H_P \leq$ 100 %)

Take-off, Climb-out, and Landing will be electrically assisted with Degree of Hybridization for Power from 10% to 100%) Taxi out and Taxi in 100% electric in all the above cases (with time-in mode or duration and power settings matching the ICAO LTO table values).

The decision to assist electrically taxi in 100 % is due to the very low efficiency of the gas turbine at idle power settings. Also, taxi is part of the LTO cycle, meaning that considering taxi fully electric will reduce fuel burnt at the airport and thus, improve local air quality. The duration of taxi and power settings match the ones defined by FOI (table [19]).

The electric system delivers the power off-takes in the hybrid configurations. Although the mission hybridization boundary is 3048 m, when computing LTO values (of NOx, CO, fuel burnt, CO2 and H2O), these are computed below 914 m (as the real LTO cycle).

For each Technology maturity scenario, the Specific Energy of the Batteries varies between 300 and 1000 Wh/kg (with intervals of 100 Wh/kg). Other parameters (specific power of e-motor and inverter, and components' efficiency) assume interpolated values of the technology predicted to 2040-year scenario. In total, 8 scenarios will be considered. The degree of hybridization varies between 0 and 100 % in intervals of 10 %.

When simulating missions for different electrical components' technology scenarios and power split ratios (Φ) the same baseline mission profile (Altitude and Mach number) and mission characteristics are used so

that the aircraft is under the same operating conditions throughout all the simulations. This way, H_P and the electrical components' performance parameters can be analysed solely.

3.4. Methodology

To reach the goal of this research, it is vital to develop a methodology that would simulate the hybrid-electric Powertrain for each of these different configurations that will be studied. Since this research deals with parallel-hybrid electric architecture, this methodology is build under the assumption of keeping the regional turboprop aircraft (ATR72-600 is used) fuselage and main design specifications as Maximum Take-off weight, wing design constant.

In order to simulate the mission for various configurations a routine was built in MATLAB ® following the methodology displayed in the flow chart in figure 3.6. The mission is divided into N time steps, and the value of each parameter at each time step is represented by the index i.

As illustrated in the flow chart, the total shaft power requirements at each time step i of the mission ($P_{Total_{Shaft_i}}$) are computed by the Drag Polar module and corrected by the propulsive efficiency, η_{prop}, (determining the Shaft Power required to produce the Required Propulsive Power, P_{req_i}, see equation 3.2).

$$P_{Total_{Shaft_i}} = P_{req_i} \times \eta_{prop} \tag{3.2}$$

The Drag Polar module is responsible for calculating the C_{L_i}, C_{D_i}, T_{req_i} and P_{req_i} (Lift and drag coefficients and Propulsive Thrust and Power Requirements at time step i) through equations 3.3 to 3.7). The details on how to compute the drag coefficient and the zero-lift drag coefficient, C_{D_0}, are exhibited in section 4.1.2.

$$W_i = W_{i-1} - \dot{W}_{fuel_{i-1}} \times (t_i - t_{i-1}) \times 2 \tag{3.3}$$

$$C_{L_i} = \frac{W_i \times \cos\gamma}{\frac{1}{2} \cdot \rho_i \cdot V_i^2 \cdot S} \tag{3.4}$$

$$C_{D_i} = C_{D_0} + \frac{C_{L_i}^2}{\pi \cdot A \cdot e} \tag{3.5}$$

$$T_{req_i} = W_i \times \sin\gamma + \frac{1}{2} \cdot C_{D_i} \cdot \rho_i \cdot V_i^2 \cdot S \tag{3.6}$$

$$P_{req_i} = T_{req_i} \times V_i \tag{3.7}$$

The output of the Turboprop model (GSP model) includes de fuel flow of the gas turbine ($\dot{W}_{fuel}$), propulsive efficiency (η_{prop}) and Emission Index of NO_x and CO (EI_{NO_x} and EI_{CO}) at each time step. Integrating these values using the trapezoidal rule it is possible to compute parameters for the total mission. This analysis is included in the Mission analysis block of figure 3.6. Total fuel burn (W_{fuel}), energy consumption (from fuel E_{fuel} and batteries E_{Bat}) and key performance indicators are examples of parameters calculated at stage of the mission analysis routine.

The total fuel mass burnt to fly the mission (W_{fuel}) is given in equation 3.8, where $(t_i - t_{i-1})$ is the time interval of each time step. The energy stored in the fuel can be computed with equation 3.9, where e_{fuel} stands for the specific energy of the fuel.

$$W_{fuel} = \sum_{i=2}^{N} \frac{\dot{W}_{fuel_i} + \dot{W}_{fuel_{i-1}}}{2} \times (t_i - t_{i-1}) \times 2 \tag{3.8}$$

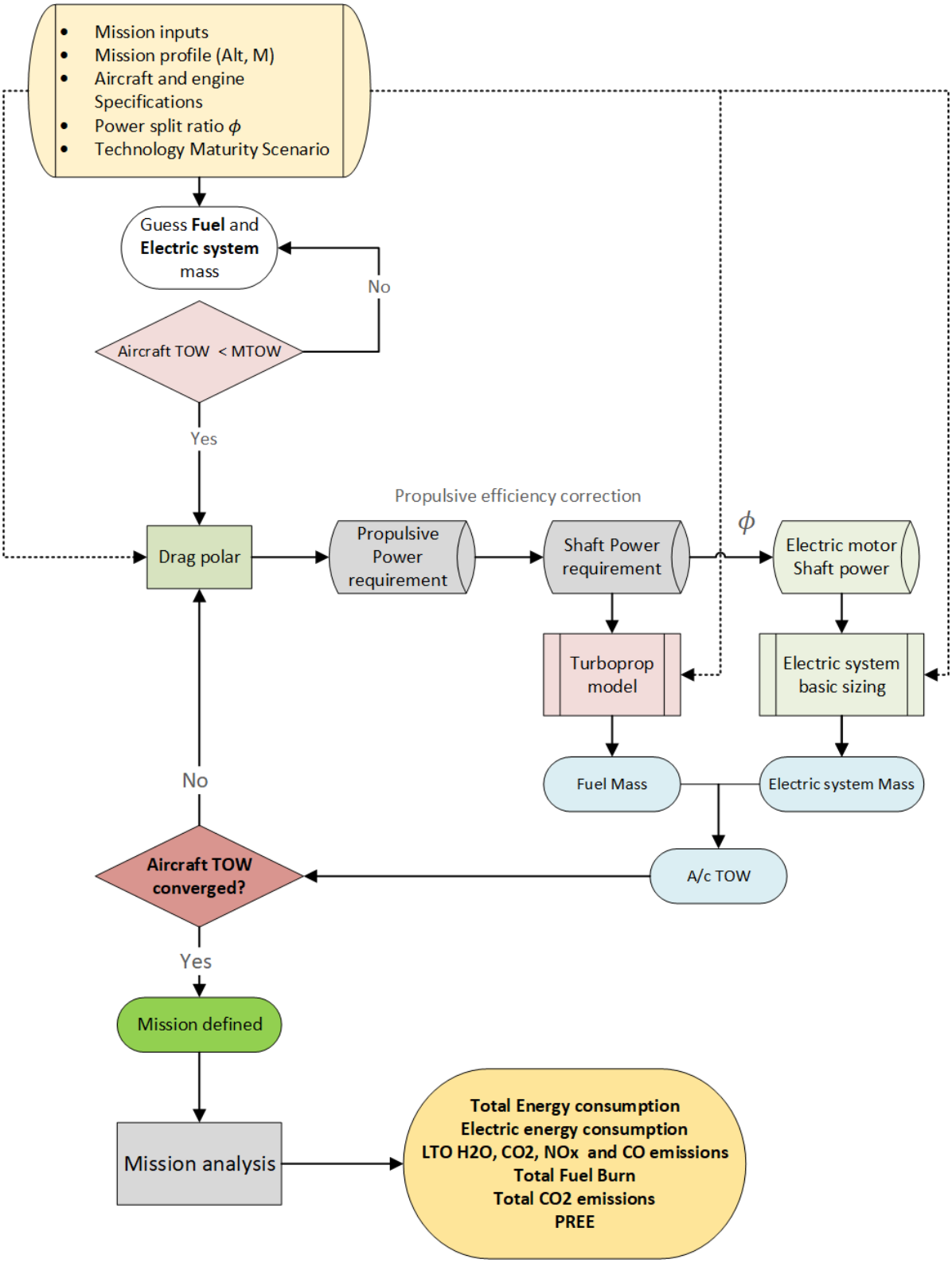

Figure 3.6: Flow chart with mission simulation methodology

$$E_{fuel} = W_{fuel} \times e_{fuel} \tag{3.9}$$

Regarding the emissions, for each specie X the mass emitted during the mission (or part of it) is estimated through equation 3.10.

$$W_X = \sum_{i=2}^{N} \frac{EI_{X_i} + EI_{X_{i-1}}}{2} \times \dot{W}_{fuel_i} \times (t_i - t_{i-1}) \times 2 \tag{3.10}$$

The electric energy stored in batteries is computed, at each time step with equation 3.11. Details on how the electric system was modeled, and the required power of the batteries P_{Bat} were estimated are displayed in section 4.3.

$$E_{Bat} = \sum_{i=2}^{N} \frac{P_{Bat_i} + P_{Bat_{i-1}}}{2} \times (t_i - t_{i-1}) \tag{3.11}$$

4

Baseline models

In order to compute aircraft performance at any mission point, it is necessary to build a baseline turboprop engine model and calculate the aircraft power requirements. Moreover, since one of the significant constraints of a parallel-hybrid electric configuration is the mass that electrical components add to the aircraft, it is critical to estimate these.

The feasibility of an aircraft to incorporate a HEPS depends highly on the degree of hybridization for power (H_P) and technology level of batteries, electric motors, power electronics and cabling systems.

This chapter includes:

- The ATR 72-600 specifications and the drag polar used as inputs in the mission analysis, in section 4.1
- The details of the engine model built along with its performance and emissions validation at Design and Off-design points, in section 4.2.
- Lastly, in section 4.3, the methodology used to size the electrical components is presented

4.1. Baseline Aircraft- ATR 72-600

ATR turboprop aircraft family is the leader in the regional category with 50 to 70 seats due to its low operational costs and high reliability [16]. This family is composed by the ATR 42-600 (48-50 seats) and ATR 72-600 (68-74 passengers). ATR 72-600 was picked for this research because it carries more passengers and is the most cost-effective turboprop aircraft in the market [3]. Some studies have analysed the potential of including parallel-hybrid architecture in this aircraft [17] [70] and they concluded that the benefits of this technology are highly dependent on the mission range, technology maturity scenarios and level of hybrizidation.

Since the parallel-hybrid electric propulsion does not include distributed propulsion, aero-propulsive interactions are neglected and the aircraft fuselage and wing designs are kept constant throughout the analysis. The aero-propulsive interactions can arise from both leading-edge and tip-mounted propellers and brings higher aerodynamic efficiency by, for instance, diminished wing area [71].

4.1.1. Top-Level Aircraft Requirements

Table 4.1 presents data from literature on ATR72-600 aircraft limitation in mass and wing characteristics. Table 4.2 exhibits data on performance and power requirements for different flight segments [72] [73].

From the mass constraints in the mentioned table the MTOM is a design constraint in the mission analysis since it limits the mass of batteries and fuel that the aircraft can carry. Indeed, the aircraft mass can be divided into 5 main parts (as equation 4.1 shows). Operating empty mass (m_{OE}) is, as the name suggests, the mass of the empty aircraft (including structures, systems, necessary equipment and propulsion systems), not accounting for payload (passengers, luggage and cargo), fuel or batteries. It is important to note that the electric system mass is not included in the Operating empty mass because it will vary for each different configuration, depending on the power split ratio and technology scenario.

It is important to highlight that, for airworthiness reasons, the aircraft needs to carry reserve fuel $m_{fuel_{diversion}}$

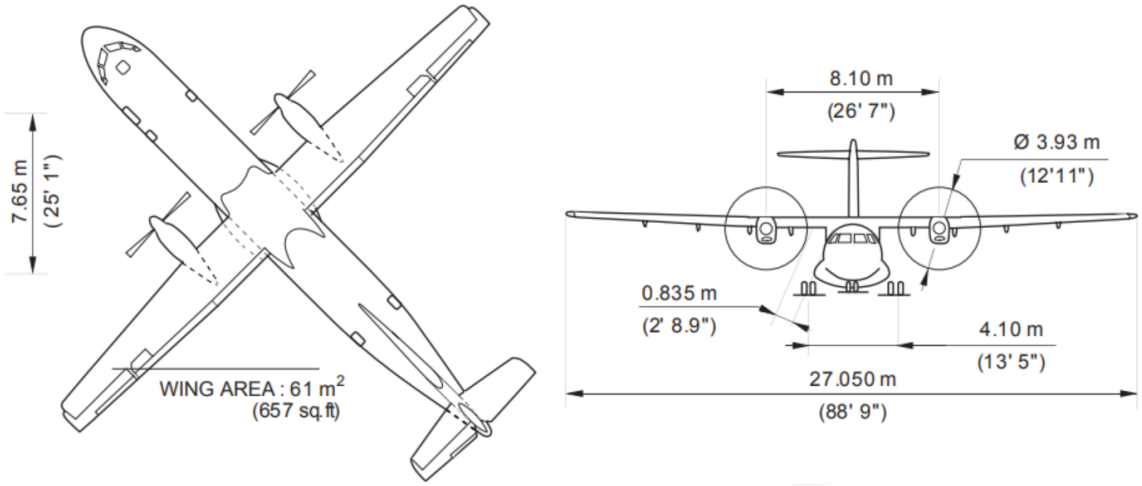

Figure 4.1: ATR 72-600 dimensions in two different views. Source [16]

to be able to perform the diversion mission if required [44]. Diversion and hold mission blocked fuel are displayed in table 3.1, and are kept constant for the different configurations.

$$m_{TO} = m_{OE} + m_{Payload} + m_{fuel_{mission}} + m_{fuel_{diversion}} + m_{electric} \tag{4.1}$$

Table 4.1: ATR72-600 specifications

Parameter	Value	Units
mass		
MTOW (Maximum Take-off Mass)	23,000	[kg]
OEW (Operating Empty Mass)	13,311	[kg]
MLW (Maximum Landing Mass)	22,350	[kg]
Maximum Zero Fuel	20,800	[kg]
Maximum Payload	7,500	[kg]
Maximum Fuel Mass	5,000	[kg]
Maximum Passengers	70	[pax]
Wing		
Wing area	61	$[m^2]$
Wing Span	27.05	[m]
Aspect ratio	12	[-]
Oswald factor for clean configuration	0.85	[-]

4.1.2. Drag polar

One of the key inputs for the mission analysis is the flight power requirement profile, that depends on the aircraft mass throughout the mission, operating conditions and aircraft configuration (flaps and landing gear retracted or not). Such profile is obtained through mechanical flight equations (presented in section 2.5) and a drag polar that estimates the drag in function of lift. Lift can be computed with the aircraft mass and flight path angle (equation 2.20).

Total drag is the sum of zero-lift drag and induced drag (drag due to lift). The first component can be decomposed into skin drag and pressure drag.

A parabolic drag polar is assumed for simplification purposes and the methods suggested in Roskam [23]

Table 4.2: Main Mission specifications

Parameter	Value	Units
Mission range	1527	[km]
Rate of climb at SL	413 m/min	[m/min]
Optimum climb speed	170	[KCAS]
Altitude ceiling	7,620	[m]
Cruise speed (at FL170, 97% MTOW)	275	[kt]
Cruise speed (at FL230, 95% MTOW)	248	[kt]
Take-off speed ($V2_{min}$ at MTOW)	116	[KCAS]
Take-off run	1,175	[m]
Landing run	1,008	[m]
Power requirements		
Maximum Take-off Power	2,051	[KW]
Normal Take-off Power (90%)	1,846	[KW]
Climb Power(80%)	1,635	[KW]
Cruise Power (78%)	1,590	[KW]

were followed. According to [23], the drag coefficient can be given by equation 4.2: C_{D_0} is the zero-lift drag coefficient, A is the Aspect ratio and e is the Oswald Coefficient (values displayed in table 4.1). The zero-lift coefficient (C_{D_0}) can be obtained by equation 4.3, where f is the equivalent parasite area and S is the wing area. The parasite area can be computed with the wetted area (S_{wet}) which depends on take-off mass [74] (see equations 4.4 and 4.5). Assuming a skin friction of c_f of 0.004 the values of a, b, c and d from the previous equations are displayed in table 4.3.

$$C_D = C_{D_0} + \frac{C_L^2}{\pi A e} \tag{4.2}$$

$$C_{D_0} = \frac{f}{S} \tag{4.3}$$

$$log_{10} f = a + b \times log_{10} S_{wet} \tag{4.4}$$

$$log_{10} S_{wet} = c + d \times log_{10} W_{TO} \tag{4.5}$$

The value of C_{D_0} obtained with equation 4.3 for the values assumed is 0.0293 . Nevertheless, depending on the airplane configuration there is an increment in the zero-lift coefficient (C_{D_0}) and a decrement in the Oswald factor as table 4.4 illustrates. The values in the table are the mean values of the ranges suggested by Roskam ([23]). Figure 4.2 plots equation 4.2 for the different configurations.

Table 4.3: Correlation coeffients for parasite area versus wetted area and Regression line coefficients for take-off mass versus wetted area

a	b	c	d
-2.3979	1.00	-0.0866	0.8099

Table 4.4: ΔC_{D_0} and e in various aircraft configurations [23]

Configuration	ΔC_{D_0}	e
Clean	0	0.85
Take-off extended flaps	0.015	0.80
Landing extended flaps	0.060	0.75
Landing gear down	0.020	-

Other performance parameters are:

- Lift-to-Drag ratio:
- Load factor ($\frac{L}{W} = \frac{L}{mg}$)
- Power-to-mass ratio ($\frac{P}{W} = \frac{T}{mg}$)
- Wing Loading ($\frac{W}{S}$), S is the wing area

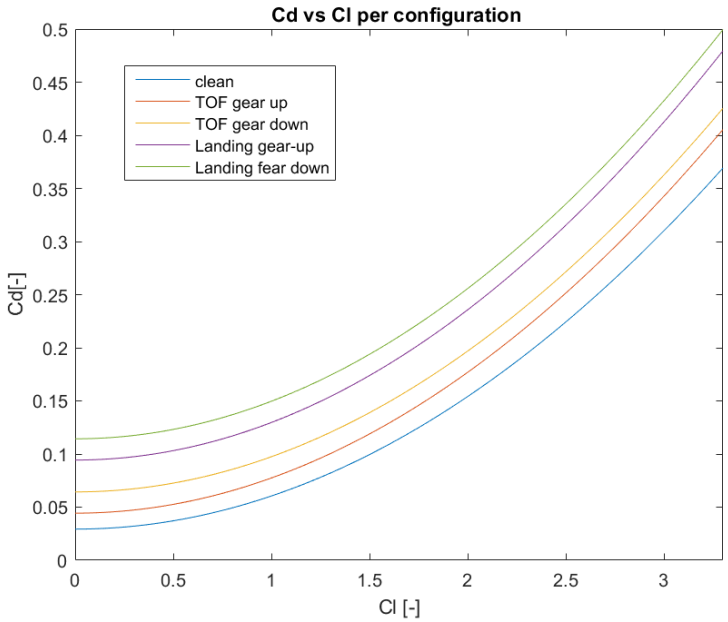

Figure 4.2: Drag Coefficient versus Lift Coefficient for different configurations

4.2. Baseline Engine- PW127 M

The PW127M belongs to the PW100 turboprop family (manufactured by Pratt & Whitney) that includes engines with power ratings in the range of 1,300 to 3,700 KW [75]. According to Pratt & Whitney, this family is the "benchmark for low fuel consumption on routes of 350 miles or less," and the fuel consumption is 25 to 40 % lower than other regional aircraft. PW127 M is a three-shaft and twin-spool engine (as mentioned in section 2.2), where each spool is driven by a single-stage low and high-pressure turbines. A two-stage radial compressor powers each of these turbines. The combustion chamber is an annular reverse-flow combustor [75]. The power turbine is a two-stage axial turbine.

The ATR 72-600 features a 6-bladed Hamilton Standard F568 propeller that operates at constant rpm. Its blades have a nominal diameter of 3.93 m and a non-linear twist with swept-back tips. Nevertheless, these propellers rotate at different rpm at different flight segments. The propeller rotational speed does not vary significantly throughout a mission, its minimum rotational speed is 70% [76].

4.2.1. Model set-up

The gas turbine simulation tool used in this thesis is GSP ® (Gas Turbine Simulation Program) [77]. It consists of 0-D modelling environment, meaning that an average value of the parameters (thermodynamic properties and gas properties) are computed at the inlet and exit of each component [78]. However, its API (Application Programming Interface) tool is useful to run the model through an external software (MATLAB ® is the one being used in this thesis).

Examples of another gas turbine modelling and simulation tools available are GasTurb [1], NPSS(Numerical Propulsion System Simulation) [2] and PROOSIS (Propulsion Object Oriented Simulation Software) [3].

[1] https://www.gasturb.de/
[2] https://www.swri.org/consortia/numerical-propulsion-system-simulation-npss
[3] https://www.ecosimpro.com/

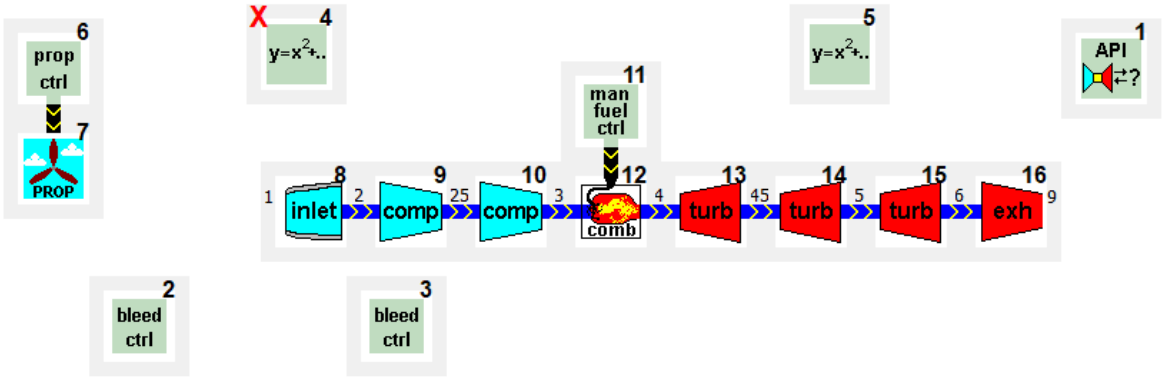

Figure 4.3: GSP model of a two-spool turboprop engine

The two-spool turboprop model created in GSP (layout presented in figure 4.3) has the following components: Propeller, Inlet, Low Pressure Compressor (LPC), High Pressure Compressor (HPC), Combustor chamber, High Pressure Turbine (HPT), Low Pressure Turbine (LPT), Free Turbine and a convergent nozzle. LPC and LPT are connected through the low pressure spool and HPC and HPT through the high pressure spool. The Free Turbine is mechanically coupled to the propeller through the free spool, and there is a gearbox that is responsible to reduce the rotational speed in the propeller since this cannot rotate at the free turbine high rotational speeds. The GSP ® computes the thermodynamic properties at the inlet and outlet of each component, and thus many stations can be identified (also visible in figure 4.3): Station 1 (inlet) , 25 (LPC's inlet), 3 (Combustor's inlet), 4 (HPT's inlet), 45 (LPT's inlet), 5 (Power turbine's inlet), 6 (Nozzle's inlet), 9 (exhaust gases).

A typical flight mission is divided into several phases, as described in section 2.5. Different operating conditions characterize each segment, and the engine needs to be able to work under the most constraining conditions. The most critical point during the mission should be identified and classified as the engine's design point. There are two main critical points to consider in design: take-off and Top of the climb. The Top of Climb is the point with maximum corrected mass flow. Take-off at hot-day is the moment where the aircraft operates at the highest spool speed and operating temperature. The design point picked for the turboprop model was take-off, where it delivers the maximum power, and it is under higher thermal stresses.

An off-design static model (equilibrium state assumed) is used to predict the performance of a designed engine (fixed geometry) when the operating conditions change (altitude, Mach number, or both). The computation of off-design performance is usually difficult because it needs a numerical solution (in complex cases, it might even require a non-linear iterative solver). GSP ® uses the Newton-Raphson solver for iterations in off-design simulations [78].

The GSP model uses a scheduling component library to schedule a controlled parameter in the simulation by assigning another parameter as an unknown (or 'free-state'). Note that this last parameter needs to affect the controlled one when changed. GSP ® iterates to a solution that results in the controlled parameter to match the desirable expression introduced in the scheduling component. Moreover, this library includes Limiters. These are important when a parameter value needs to be limited. For example, in the The Type-certification document of the PW 127-M, the Inter Turbine Temperature, is limited to 1078 K [79]. Thus, when performing iterations to match the power output scheduled, the fuel flow increase is limited by this temperature. There is no available data in the literature for the maximum TIT (turbine inlet temperature), the reason why the Inter Turbine Temperature is used instead.

Moreover, in figure 4.3 a propeller controller component is included. This controller will vary the propeller pitch angle at fixed specific rotational speed so that the power delivered can match the requirements. However, the propeller performance is not analyzed in detail since it is out of the scope of this thesis. The propeller performance map and main parameters that influence its performance are displayed in appendix B.

The gearbox reduction ratio is another parameter that is needed to be defined in the turboprop GSP model. This parameter specifies the decrease of the propeller shaft (driven shaft) rotational speed to the power turbine shaft (driving shaft) one. The literature [80] available on PW100 engines (includes PW127 engine family) reveals the reduction ratio of these engines, varying from 15.4:1 to 17.2:1 (depending on the model). The value picked was 17:1 and is kept constant.

Bleed air is also included in the model due to its importance in cabin pressurizations, airframe and engine anti-ice systems. The bleed air can be drawn out from both low-pressure and high-pressure compressors (with different pressures). This variable will not be varied during this research due to a lack of information on bleed-air for a PW127 engine. It will be assumed zero bleed air extracted from the LPC and a 5 % bleed air percentage at the HPC during take-off, climb-out and climb [80].

4.2.2. Design point

The design point evaluates the system performance at design conditions. The performance delivered at this point is computed by GSP ®. Thus the mass and energy conservation equations do not need to be solved. The engine is assumed to work at steady state, meaning that it is in an equilibrium state.

Table 4.5 presents the design values for the isentropic efficiency of the different engine components, the mechanical efficiency of the shafts, the combustion efficiency and the pressure ratio (PR) at the combustor and the inlet. Besides, the main propeller design parameters are also available in this table. Besides, these values are inputs for the design point simulation. N stands for rotor speed in rpm.

Apart from the data presented in table 4.5, more input values are necessary to fully define the design point (namely mass flow, operating conditions, Overall Pressure ratio and propeller rotational speed and power settings). These are introduced in table 4.6 and the sources of the data are [81], [79] and [73]. Note that the overall pressure ratio of the engine is assumed to be equally generated by the LPC and the HPC (Overall pressure ratio of 14.7 [81]).

The design point is determined by turning the propeller operating point (the propeller work coefficient C_p) and the fuel flow until the maximum required power output (literature value assumed) at take-off is delivered. When the design point is computed, the output parameters to analyze are: the Power output, jet thrust (or exhaust thrust), and Power specific fuel consumption. Since the turboprop exhaust emission database is confidential, the source of the PW127M performance data at Standard Sea Level for validation is a turboprop Database Handbook [81]. The validation of the performance at maximum take-off power is displayed at table 4.8.

Table 4.5: Engine component data

Component	Parameter	Value	Units
Propeller	η_{Prop}	0.7	[-]
	pitch angle	30	[deg]
Inlet	PR	0.99	[-]
LPC	η_{LPC}	0.86	[-]
	N_{LPC}	28000	[rpm]
HPC	η_{HPC}	0.86	[-]
	N_{HPC}	34000	[rpm]
LP/HP spools	η_{spool}	0.99	[-]
Combustor	η_{comb}	0.95	[-]
	Relative Pressure loss	0.07	[-]
HPT	η_{HPT}	0.88	[-]
LPT	η_{LPT}	0.88	[-]
Power Turbine	η_{PowerT}	0.88	[-]
	N_{PowerT}	20400	[rpm]

Table 4.6: Optimum input data for design point computation

Input Parameter	Value	Units
Altitude	0	[m]
Mach number	0.175	[-]
Inlet mass flow	8.48	[kg/s]
Propeller C_P	0.2167	[-]
Propeller speed N	1212	[rpm]
LPC PR	3.83	[-]
HPC PR	3.83	[-]
LPC bleed air fraction	0	[-]
HPC bleed air fraction	0.05	[-]

Table 4.7: Engine design point performance output

Output Parameter	Value	Units
Power output	2054.1	[KW]
Torque Output Q	16184	[Nm]
Propeller Thrust T_j	24.1	[KN]
Jet Thrust	1.423	[KN]
Total Thrust	25.53	[KN]
Fuel Flow	0.159	[kg/s]
OPR	14.7	[-]
PSFC	7.74×10^{-8}	[kg/s W]

Table 4.8: design point Validation

Parameter	PW127M	GSP Model	Difference
Power Output	2051 [KW]	2054.1 [KW]	0.15%
Jet Thrust	1.446 [KN]	1.423 [KN]	0.9%
PSFC	7.76×10^{-8} [kg/s W]	7.74×10^{-8} [kg/s W]	0.25%

Off-design Performance

An off-design static model (equilibrium state assumed) is used to predict the performance of a designed engine (fixed geometry) when the operating conditions change (altitude, Mach number, or both). The computation of off-design performance is usually difficult because it needs a numerical solution (in complex cases, it might even require a non-linear iterative solver). GSP ® uses the Newton-Raphson solver for iterations in off-design simulations [78].

The turboprop off-design model uses a scheduling component. The controlled parameter is the propeller power output and the free-state parameter is the fuel flow.

The GSP model predicts off-design performance using steady zero-dimensional thermodynamic analyses. The engine design point is first determined by running the model at sea-level static (SLS) conditions, and then at the different operational conditions (off-design).

The off-design performance of the gas turbine components is computed utilizing performance maps. Each turbomachine (compressors and turbines) has a typical performance map obtained with empirical data. A two-stage radial compressor, an axial turbine, a two-stage axial turbine (Power turbine), and propeller performance maps are plotted in the appendix B. Each of these maps is scaled to the design point.

Since not all turbomachines' performance maps are available in the literature, the performance maps from a compressor/turbine/propeller that operates under similar conditions can be used and scaled according to the engine's design point. The propeller map used to simulate a 6-bladed Hamilton Standard F568 is from a similar propeller. It is important to note that these propellers are classified as a fixed rotational speed and variable pitch, but the rotational speed varies with the flight segment, it is maximum at take-off (100 %) and minimum at taxi phases (80 % of maximum rpm) [76].

The **input variables** of the GSP off-design model are:

- Altitude
- Mach number
- Total Shaft Power required (P_{req})
- Power Split ratio, Φ. Electric motor Shaft Power is given by $P_{req} \times \Phi$

- Bleed Air
- EI (emission index) for taxi, take-off, climb out and approach for NO_x and CO
- Propeller Rotational Speed (N_p in %).

The **output variable**s of the GSP off-design model are:

- Fuel flow
- Thrust delivered (Propeller and Jet)
- Thermodynamic properties (Tt, Pt) throughout the gas turbine
- Emission Index for NOx and CO
- PSFC (Power Specific Fuel Consumption)
- Propulsive Efficiency
- Propeller performance

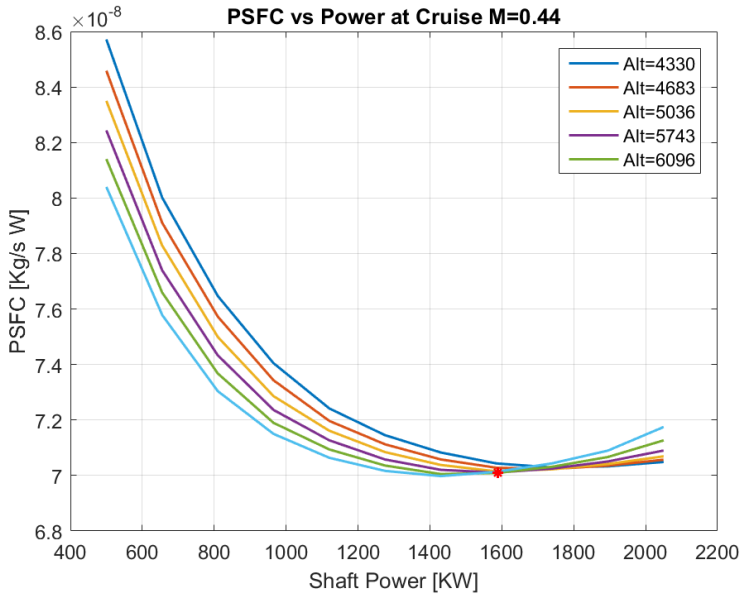

Figure 4.4: Power specific fuel consumption with shaft power for different cruise altitudes and fixed mach number

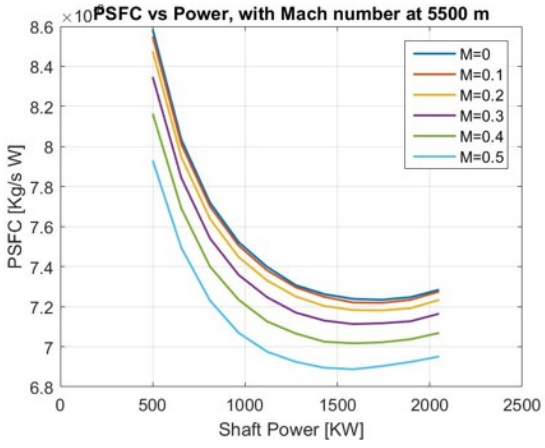

Figure 4.5: Power Specific Fuel Consumption (PSFC) variation with engine shaft Power for different Mach number and fixed cruise altitude of 5500 m

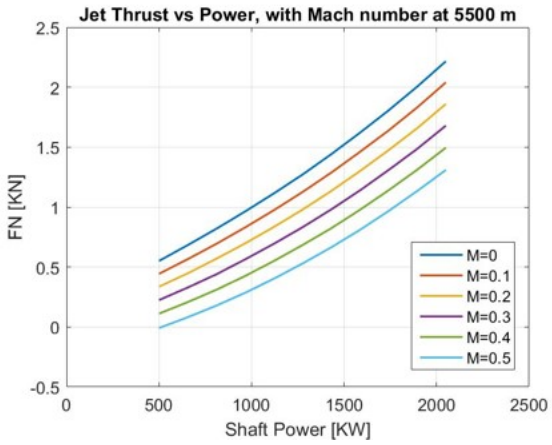

Figure 4.6: Jet Thrust variation with engine shaft Power for different Mach number and fixed cruise altitude of 5500 m

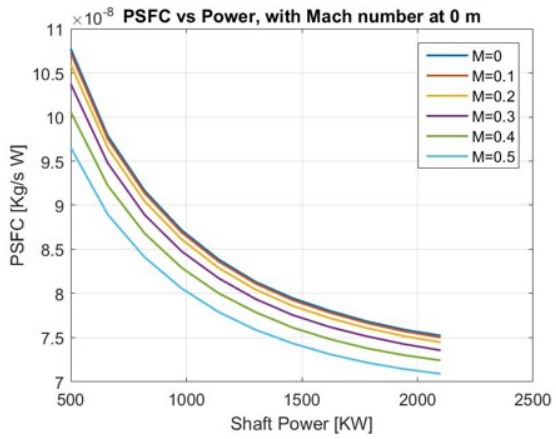

Figure 4.7: Power Specific Fuel Consumption (PSFC) variation with engine shaft Power for different Mach number and fixed at SSL

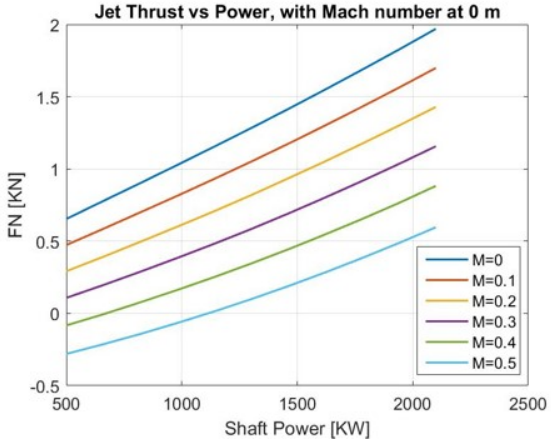

Figure 4.8: Jet Thrust variation with engine shaft Power for different Mach number and fixed at SSL

One key performance indicator of a turboprop engine is the Power Specific Fuel Consumption (equation 2.10), and a typical demonstration of engine performance is by analyzing the PSFC behavior with the engine shaft power (which translates the engine power settings). This parameter measures how efficiently the engine converts the fuel burn into shaft power (fuel flow divided by the shaft power output of the gas turbine).

In figure 4.4, it is visible the influence of the altitude on the engine performance. As the altitude increases, the density diminishes as well as the pressure. The inlet air pressure drop raises the engine's pressure ratio, and thus, a lower PSFC is obtained.

In figure 4.5, where the altitude is kept constant (constant density), and only the Mach number varies, it is seen that the lower the Mach number, the highest the PSFC. The lower the Mach number, the lower the air mass flow. The air mass flow directly influences the power delivered by the turbines since the shaft Power is given by the product of the specific power of the turbine with the mass flow. Figure 4.7 shows the same analysis, but for Sea-level altitude and the same trend is verified: higher Mach number lower PSFC.

In figure 4.4 the red dot represents the Maximum Cruise Power (MCR). Thus, the behavior plotted for shaft power above 1590 KW (MCR, as table 3.2 states) shows the penalty in the PSFC.

Figures 4.6 and 4.8 show the behavior of jet thrust at cruise altitude and at take-off, for different Mach numbers. The larger the difference between the free stream velocity and the gas turbine exhaust gases, the larger the jet thrust is. Thus, the lower the Mach number, the greater the difference in velocities obtained, and the higher the jet thrust. It is important to highlight that the jet thrust is usually less than 10 % of the total thrust.

NO_x and CO Emissions

GSP ® has 3 options to compute NO_x and CO, among them the interpolation of the ICAO emission data option was selected, that uses a T_{T3}- P_{T3} method. The input data used in GSP ® is given in table 4.9. The thermodynamic parameters T_{T3} and P_{T3} and the fuel flow presented in this table were obtained by running the GSP model in off-design for the power settings displayed. The Emission Index of CO and NO_x for the other operating points are interpolated based on table 4.9. Note that Unburned hydrocarbons (UHC) are excluded from this analysis due to the complex method to predict them and because it is only above zero for low engine power settings (3 % of lower) [22].

The Emission Index of CO_2 and H_2O is fixed, so CO_2 and H_2O are only dependent on GSP fuel flow data to be estimated.

The emission indexes of CO and NO_x computed by the GSP model for different operating points are revealed in section 4.2.3 and are compared to the literature values.

Table 4.9: Input data in GSP to compute EI NO_x and CO [22]

Mode	Power Setting (%)	Fuel Flow [kg/s]	T_{T3} [K]	P_{T3} [Bar]	EI UHC	EI CO	EI NO_x
Take-off	100 %	0.165	675.2	14.97	0	2	17.7
Climb out	85 %	0.154	649.99	14.2	0	2	16.2
Approach	30 %	0.086	570.24	8.67	0	3.7	9.8
Idle	7 %	0.051	510.24	6.083	0	9.2	6.9

4.2.3. Model validation

ICAO does not keep the turboprop exhaust emission database. Thus, validation needs to be done with this 1997 old document from ATR [22]. Although the turboprop database is confidential, it is possible to compare its values to Turbofan engines with approximately the same rated thrust, P_{T3}, T_{T3}, and T_{T4} values. A few turbofan engines that share this similarity are: PW308C, PW307D, Rolls Royce ae3007 c2 and Honeywell as907-1-1a. The emission indexes measured in the LTO cycle for these turbofan engines are close to the ones displayed on table 4.9 (which source is [22]).

Tables 4.10, 4.11 and 4.12 compare the GSP model outcome of NO_x, CO Emission Indexes and fuel flow with data from PW127F. This data is from 1997 and the only literature available.

Table 4.10: PW 127F engine NO_x emissions data. Source [22]

Flight Phase	Power Setting (%)	EI NO_x [g/kg of fuel]	GSP Model	Difference
Idle	7 %	6.9	6.93	0.41 %
Take-off	100 %	17.7	17.69	-0.015 %
Approach	30 %	9.8	9.93	1.32 %
Max. Cruise	78 %	15.6	14.28	-8.4%
Max. Climb	80 %	16.2	15.56	-3.93%
Max Continuous	90 %	16.5	16.73	1.41%

Table 4.11: PW 127F engine CO emissions data. Source [22]

Flight Phase	Power Setting (%)	EI CO [g/kg of fuel]	GSP Model	Difference
Idle	7 %	9.2	9.09	-1.15%
Take-off	100 %	2.0	2.0	0.0%
Approach	30 %	3.7	3.60	-2.65 %
Max. Cruise	78 %	2.2	2.00	-9.09%
Max. Climb	80 %	2.0	2.00	0.0%
Max Continuous	90 %	2.0	2.00	0.0%

Table 4.12: PW 127F fuel flow data. Source [22]

Flight Phase	Power Setting (%)	Fuel Flow [kg/s]	GSP Model	Difference
Idle	7 %	0.0510	0.028	-44.7%
Take-off	100 %	0.165	0.155	-6.20 %
Approach	30 %	0.0858	0.057	-33.4%
Max. Cruise	78 %	0.138	0.111	-19.26%
Max. Climb	80 %	0.139	0.125	-10.38 %
Max Continuous	90 %	0.154	0.141	-8.09%

The values for the Emission Index of CO and NO_x estimated by the GSP are close to the literature ones. Only

at Cruise (at the maximum cruise power setting) a more substantial difference is detected, with a relative error of 9.1 % and 8.4 % for EI CO and NO_x, respectively. The deviation of values for cruise is related to the speed and altitude at which the aircraft was being operated, which are not specified.

Regarding the fuel flow results, at idle (assumed at 7% power setting, similarly to LTO cycle taxi mode), the GSP model underestimates the engine's fuel flow. The off-design performance is computed through interpolation and scale of performance maps of similar turbomachines, but, at lower power settings, the performance extrapolated from the maps might not correspond to the reality. Note that idle is the furthest point away from the design point regarding power settings. Moreover, the off-take power was not taken into account in the GSP model, which can justify the lower fuel flow at this segment.

Due to the ambiguity of the conditions at which the fuel flow presented was measured (altitude and speed), it is impossible to make a strong validation. Nevertheless, it can be concluded that the GSP results for the emissions indexes are reasonable and within a 10 % deviation (even at cruise power settings).

More reasons can be related to the mismatch between the literature and the model values. The lack of literature data on ATR72-600 bleed air and power off-takes results in using estimated values for these two last parameters.

The last data documented by ICAO regarding the LTO emissions of turboprop aircraft (including the ATR 72-600) are from 2012 in [24]. This document divulges the total emissions emitted and fuel burnt during the LTO cycle. Table 4.13 displays the values from ICAO and the GSP values along with the relative difference between both.

Note that the GSP model values presented in the table were obtained after the baseline mission computation and already includes the off-take power (60 KW). This can be why the power delivered by the engine model differs from the experimental one, and, thus, the fuel flow and emission index of NO_x and CO. Although the relative difference of NO_x, fuel and CO_2 emitted in the LTO cycle is small (below 8.5 %), CO exhibits a larger difference. This deviation can be related to the high sensitivity of EI at low power settings (as figure 2.2 indicates). The power off-take addition shifts the power of the engine to an higher setting and the EI of CO decreases considerably. On top of a decrease in CO EI, the lower fuel flow estimated by the GSP also plays a role in the estimated low CO emitted during the LTO cycle.

Nevertheless, this research aims to assess the change in emissions by introducing a parallel-hybrid electric powertrain in an ATR 72-600. Therefore, the absolute value of the emissions is not crucial, but the relative difference between the different configurations instead.

Table 4.13: ATR72 LTO emission data validation [24]

LTO parameter	Units	FOI database	GSP Model	Difference
NO_x	[kg/LTO cycle]	1.82	1.836	+ 0.9%
CO	[kg/LTO cycle]	2.33	0.959	- 58.84 %
$Fuel$	[kg/LTO cycle]	200	183	- 8.42 %
CO_2	[kg/LTO cycle]	620	578	-6.65%

4.3. Electric system module

The gas turbine can use another sort of energy as input, a device capable of converting this energy (electric, in this case) to mechanical energy (to be further converted in shaft power) is needed: the electric motor. However, this component requires more electrical components to work:

- **Battery** to provide the electric motors with electric power
- **Distribution System** to conducts the power from the battery to the electric motor (transmission cables)
- **Inverter** to convert the battery output direct current (DC) to alternating current (AC)

- **Thermal management system** in charge of keeping the temperatures of the devices within admissible values

A simplified sketch of the electric system is displayed in figure 4.9. Note that the thermal management system is not represented in the just mentioned figure.

The sizing of the electric system is relevant to estimate the electric system mass, and it is key to assess the benefits and feasibility of a hybrid-electric configuration.

The electric system mass depends highly on the degree of hybridization for power (H_P) and technology level of batteries, electric motors, power electronics, and cabling systems. It impacts the gas turbine power delivered, fuel flow, and, consequently, emissions (NO_x, CO, CO_2 and H_2O).

Equation 4.6 shows how the electrical system mass is decomposed in this research. The additional 30 % of the total electrical system is accounted for due to the cooling and power management and distribution system (PMAD) [43]. The reasoning followed to compute the electric motor, battery, inverter and cables masses follow in sections 4.3.1, 4.3.4, 4.3.3 and 4.3.2, respectively.

Section 4.3.5 is dedicated to the different technology level scenarios for electrical components in the State of the Art and the expected in 10 and 20 years from now (2030 and 2040, respectively).

$$m_{electric} = 1.3 \times (m_{Bat} + m_{emotor} + m_{inv} + m_{cable}) \tag{4.6}$$

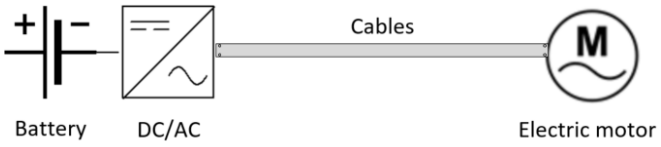

Figure 4.9: Simplified sketch of the electric powertrain

It is important to highlight the assumptions of electric system modeling:

- The electrical system is assumed to be sized for a constant 3 KV DC voltage system, as recommended by Vratny et al. in [61].
- The electrical components will be treated as black boxes since no detailed performance will be analyzed.
- The Batteries and the inverter are placed in the aircraft fuselage
- The electric motors are located in the gas turbine, with its output shaft connected to the propeller shaft
- Due to the complexity of sizing a thermal management system it is out of the scope of this research

4.3.1. Electric motor

The power delivered by the electric motor (P_{emotor}) is computed based on the total shaft power required by the Aircraft and Power Split ratio. However, an electric motor has an associated efficiency (η_{emotor}), meaning that the input electric power is not totally converted into mechanical shaft power (desired output). As observed in section 2.4.1, the efficiency of this component depends on the rotational speed, voltage, and torque. An electric motor's efficiency needs to be computed to determine the amount of electric power needed as input.

The efficiencies used are based on Zamboni's work [69], which estimates the efficiencies of an electric motor running at similar operating conditions, power requirements, and rotational speeds.

The electric motor is sized for the maximum installed power. Being p_{emotor} the specific power of the electric motor, its mass is given by:

$$m_{emotor} = \frac{1}{\eta_{emotor} \cdot p_{emotor}} max(P_{emotor}(t)) \tag{4.7}$$

4.3.2. Transmission cables

The transmission cables are responsible for distributing the electric current throughout the electric system, connecting the battery, the inverters, and the electric motors. As stated at the beginning of the chapter, batteries and inverters are assumed to be located at the fuselage of the aircraft and the electric motors at the engines, see figure 4.10. Therefore, the cable length can be computed with equation 4.8 as suggested in [43].

Another assumption made is that all the components are aligned. Thus, located at the same y and z coordinates, and the components $|y_{bat} - y_{e-motor}| + |z_{bat} - z_{e-motor}|$ in equation 4.8 are assumed to be zero.

Moreover, since the cabling system carries alternating current (AC), each cable assumed to be composed of three wires, which justifies factor 3 at the beginning of equation 4.8.

The electrical system is assumed to be sized for a constant 3 KV DC voltage system, as recommended by Vratny et al. in [61] and the efficiency of the cable to be constant throughout its operating conditions.

$$L_{cable} = 3 \times \sum(|x_{bat} - x_{emotor}| + |y_{bat} - y_{emotor}| + |z_{bat} - z_{emotor}|) \tag{4.8}$$

Stückl [82] came up with an expression (equation 4.9) in his dissertation to estimate the cross-sectional area of a copper cable in function of the current (that can be computed with the power and voltage). In order to assess the electric cabling system mass per kilometer, the linear regression proposed by Hoogreef et al. [43] is applied. This correlation is presented in equation 4.10 since the cable mass is directly proportional to its cross-sectional area.

$$A_{cable_{copper}} = 0.0144 \times I^{1.4642} \tag{4.9}$$

$$m_{cable_{copper}}[kg/km] = 58.196 + 11.044 \times A_{cable_{copper}}[mm^2] \tag{4.10}$$

4.3.3. Power electronics

The inverter is sized for power requirements. The inverter mass and output power are presented in equations 4.11 and 4.12, respectively. p_{inv} stands for the specific power of the inverter. The efficiency of the inverter (η_{Inv}) and cables (η_{cables}) are assumed to be constant throughout its operating conditions, for simplification purposes.

$$m_{inv} = \frac{1}{\eta_{Inv} \cdot \eta_{emotor} \cdot \eta_{cables} \cdot p_{inv}} max(P_{emotor}(t)) \tag{4.11}$$

$$P_{inv} = \frac{P_{emotor} \cdot \eta_{cables}}{\eta_{emotor}} \tag{4.12}$$

4.3.4. Battery

The main constraints in battery mass sizing are the specific energy (e_{Bat}) and the specific power (p_{Bat}). Thus the battery mass will be the maximum obtained by energy requirement ($m_{Batenery}$) or power requirement

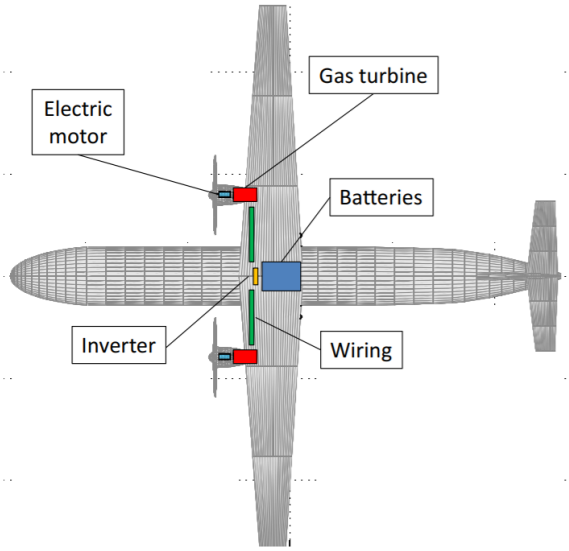

Figure 4.10: Electric components location on the aicraft fuselage. Adapted from [17]

($m_{Batpower}$) criterion (see equation 4.13). Thus, depending on the flight segment, the battery can either be sized for energy or power. The battery will be treated as black boxes since no detailed performance will be analyzed.

$$m_{Battery} = max(m_{Batenery}; m_{Batpower}) \tag{4.13}$$

For simplification purposes, a simple model will be used where the Battery efficiency (η_{Bat}) will be kept constant. According to [83], the battery mass constrained by energy and power requirements can be computed by equations 4.14 and 4.15, respectively. These expressions take into account the state-of-charge (SOC) of the battery to guarantee that the amount of energy stored does not go below the limit (SOC_{limit}). SOC_{limit} is assumed to be 20 % [84]. P_{emotor} stands for the power delivered by the electric motor to the propeller shaft. The electric energy stored in the Batteries is given by equation 4.16.

$$m_{Battery_{energy}} = \frac{1}{\eta_{Bat} \cdot \eta_{Inv} \cdot \eta_{cables} \cdot \eta_{emotor} \cdot e_{Bat} \cdot (1 - SOC_{limit})} \int_{t_{initial}}^{t_{end}} P_{emotor}(t) dt \tag{4.14}$$

$$m_{Battery_{power}} = \frac{1}{\eta_{Bat} \cdot \eta_{Inv} \cdot \eta_{cables} \cdot \eta_{emotor} \cdot p_{Bat} \cdot (1 - SOC_{limit})} max(P_{emotor}(t)) \tag{4.15}$$

$$E_{Battery} = \frac{1}{\eta_{Bat} \cdot \eta_{Inv} \cdot \eta_{cables} \cdot \eta_{emotor} \cdot (1 - SOC_{limit})} \int_{t_{initial}}^{t_{end}} P_{emotor}(t) dt \tag{4.16}$$

4.3.5. Technology maturity scenarios

In a parallel-hybrid electric configuration, the propeller shaft is driven both by the gas turbine and the electric motor. As mentioned previously, Jet A-1 is used to power the turboprop engine, and batteries are the source of electrical energy for the electric motor.

Nevertheless, the mass and efficiency of the entire electrical system depends on the level of technology available and it is vital to study in what extent these parameters influence the feasibility of a parallel-hybrid electric system.

The values of electrical components' characteristics (such as specific energy, specific power, and efficiency) from three main technology maturity scenarios (2020, 2030 and 2040) are presented in table 4.14. These

values are based on the most advanced scenario that assumes the implementation of HTS technology and cryocoolers.

Among all the below-mentioned components, battery specific energy is the most predominant factor in the hybrid-electric propulsion concept performance and, ultimately, on its possibility to become advantageous. As a result, in this research a sensitivity analysis based on different battery gravimetric specific energies (within the range between 300 Wh/kg and 1000 Wh/kg) will be performed, as mentioned in section 3.3. Cabling mass is negligible when comparing to the overall mass of the electric system. As so, the cabling technology is not being updated in the different technology maturity scenarios.

Table 4.14: Technology maturity level scenarios

Component	**Parameter**	2020 (SoA)	2030	2040
Battery	Specific energy [Wh/Kg]	300 [85]	600 [86]	1000 [86]
	Efficiency [-]	80	85	95
	Minimum SOC [%]	20	20	20
Electric motor	Specific power [KW/Kg]	4 [87]	15 [87]	20 [87]
	Efficiency [%]	95 [87]	98 [87]	99 [87]
Inverter	Specific power [KW/Kg]	2 [88]	15 [86]	20 [86]
	Efficiency [%]	90 [88]	96 [86]	98 [86]

5

Mission Simulation Results

After running the simulation routine described in chapter 3 (section 3.4) for all the proposed configurations, the turboprop engine performance can be analyzed at each time step of the mission. A configuration is a unique combination of a DoH (Degree of Hybridization for Power) and a Technology Maturity Scenario (mainly represented by battery specific energy, e_{Bat}, since the battery is normally the heaviest component in the electric system). This chapter focuses on the power and thrust requirements computed and engine performance delivered during the mission.

It should be emphasized that the concepts of power split ratio and Degree of Hybridization are used as synonyms.

This chapter is divided into two main sections. The first (section 5.1) shows the baseline ATR72-600 aircraft mission analysis results (no electrical assistance provided) and its comparison with Piano-X data. The baseline case is of significant importance since the different hybrid configurations will be compared to it. The focus is on analyzing how much each parameter varies (in percentage) relatively to the baseline configuration one, instead of the absolute value.

The second section (section 5.2) displays the mission simulation routine results (how parameters evolve with the mission) of an ATR72-600 incorporating a parallel-hybrid electric powertrain with different power split ratios and technology maturity scenarios.

5.1. Baseline mission ATR72-600

Figure 5.1 depicts the shaft power requirements corrected for propulsive efficiency throughout a typical mission of ATR 72-600 powered by a conventional turboprop engine. This power required profile is computed through the methods described in section 3.4.

It can be observed that the maximum power is required at Take-off and that it decreases throughout the climb. At cruise, the power requirement decreases slightly due to the fuel that is burnt during the mission. Moreover, the power requirement drops to power levels lower than idle.

Figures 5.2 and 5.5 compare the thrust and the fuel flow computed by the mission simulation routine and the ones provided by Piano-X. It can be concluded that both are similar and that the GSP turboprop model delivers performance close to the Piano-X performance prediction. There are two main points where the performance predicted by the GSP diverges from the Piano-X data, which are related to an underestimation of the power required during the approach phase and overestimation during descent. Piano-X admits idle power settings for the descent.

Figure 5.3 decomposes the total thrust into Propeller and Jet thrust. As expected for turboprop engines, the thrust produced by the jet is less than 10 %. It is important to highlight that these plots refer to one engine's values.

The conventional ATR 72-600 weight throughout the defined and fixed mission is as figure 5.4. The take-off weight of this aircraft to fly this mission is 20,112 kg, considerably lower than the Maximum Take-off mass admissible 23,000 kg and fuel required is 1,400 kg, excluding the fixed fuel for the diversion and loiter phases. The aircraft mass decreases with time as fuel is being consumed.

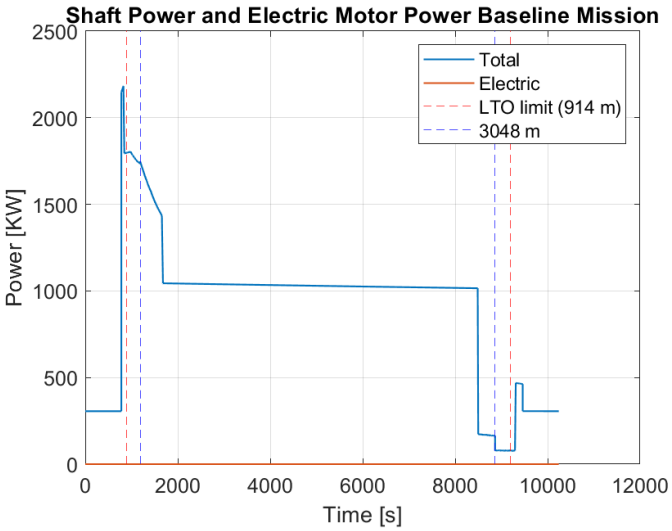

Figure 5.1: Corrected Shaft Power Requirement for Baseline Mission

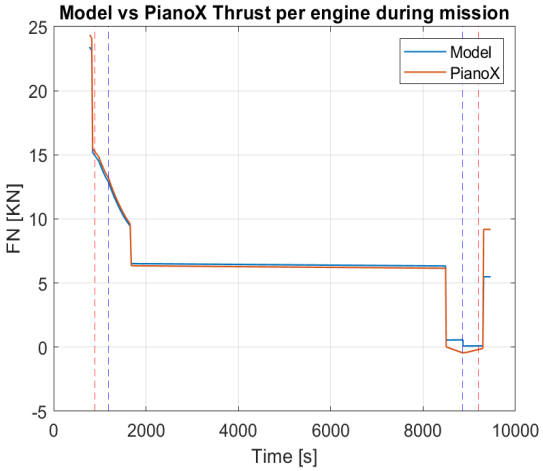

Figure 5.2: Thrust delivered by model vs Piano-X, for Baseline Mission

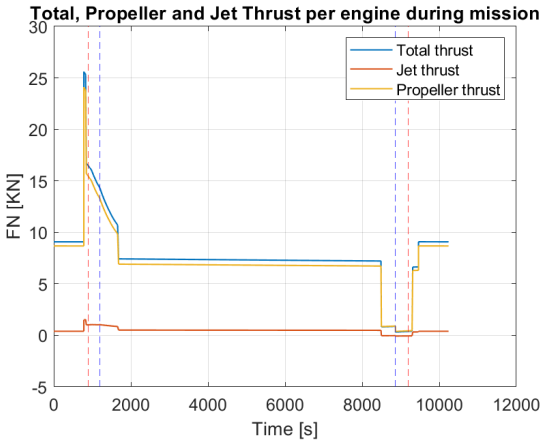

Figure 5.3: Total thrust delivered decomposed in Propeller and Jet Thrust, baseline mission

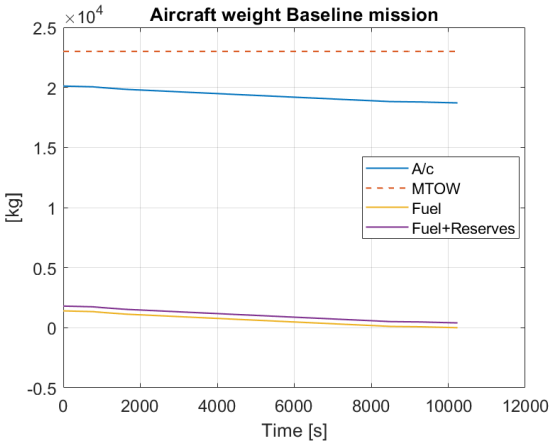

Figure 5.4: Aircraft weight throughout the baseline mission

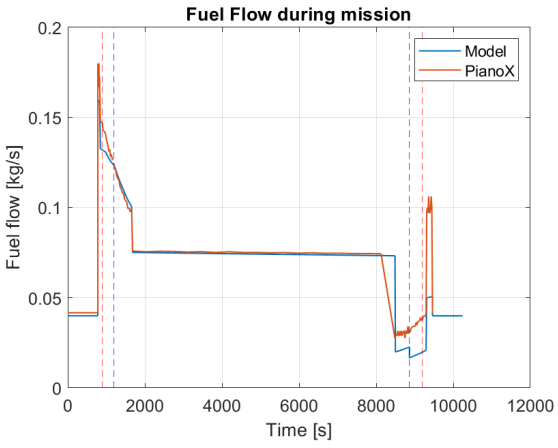

Figure 5.5: Fuel flow predicted by GSP model vs Piano-X

It is important to look at the propeller rotational speed and propeller efficiency (figures 5.6 and 5.7), since it influences the total aircraft performance. The propeller efficiency measures the capacity of the propeller to convert the propeller shaft power into propulsive Power ($U_0 \times T$), and it is used to compute the corrected shaft power requirements. The propeller efficiency is obtained by interpolating the propeller map in GSP (as explained in section 4.2). The maximum propeller efficiency is achieved during cruise, where the advance ratio presents higher values than in the remaining segments.

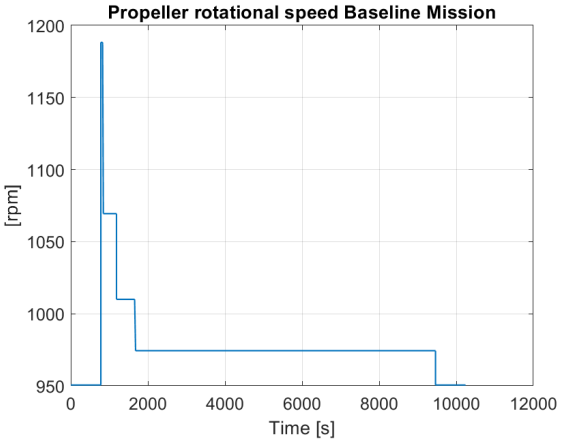

Figure 5.6: Propeller rotational speed during baseline mission

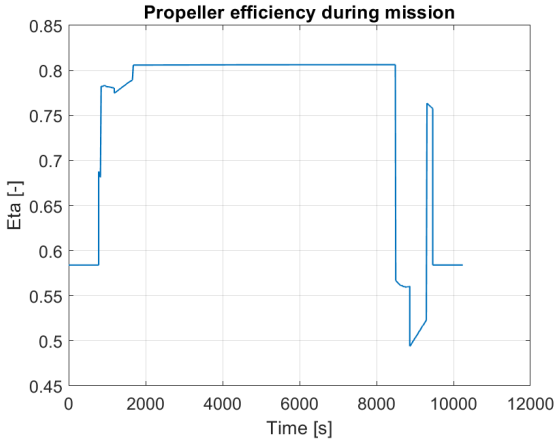

Figure 5.7: Propeller efficiency during baseline mission

Analyzing NO_x and CO behavior, it is noticeable that the NO_x Emission Index (EI) profile follows the power settings trend. NO_x includes both NO and NO_2, but most of the chemical reactions lead primarily to the formation of NO, nitric oxide. Nitric oxide is formed at high temperatures. Thus, at the highest power setting conditions (take-off), where the fuel flow is maximum (then so it is the flame temperature), the nitric oxide emissions achieve the maximum value.

The Carbon Monoxide emissions are a result of incomplete combustion of fuel. Therefore, as the power settings and fuel flow are reduced, the flame temperature decreases, and CO increases. It should be noted that the taxi values of CO are lower than descent because for taxi a 7 % power setting is being assumed, plus power off-take to be used by other aircraft systems. In descent, the power required computed is lower than 7 % (as figure 5.1 also illustrates).

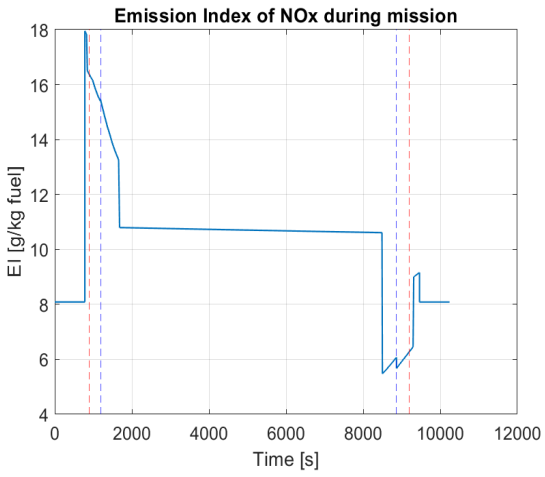

Figure 5.8: Emission Index of NO_x throughout baseline mission

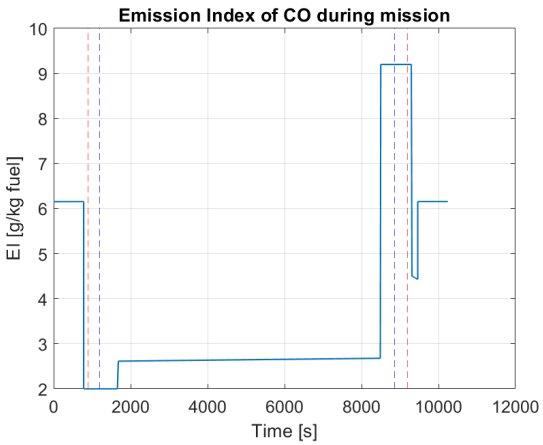

Figure 5.9: Emission Index of CO throughout baseline mission

A key performance indicator of the conventional powertrain is the PSFC, which is the ratio of the fuel flow to the shaft power delivered by the gas turbine. It can be seen a correlation with the propeller efficiency behavior. The lowest PSFC takes place at the highest propeller efficiency (in cruise) and the highest PSFC (greater ratio of fuel flow for the shaft power delivered) at the lowest propeller efficiency point (during descent). At low power settings the gas turbine is less efficient at converting the chemical energy into useful shaft power (propeller shaft power).

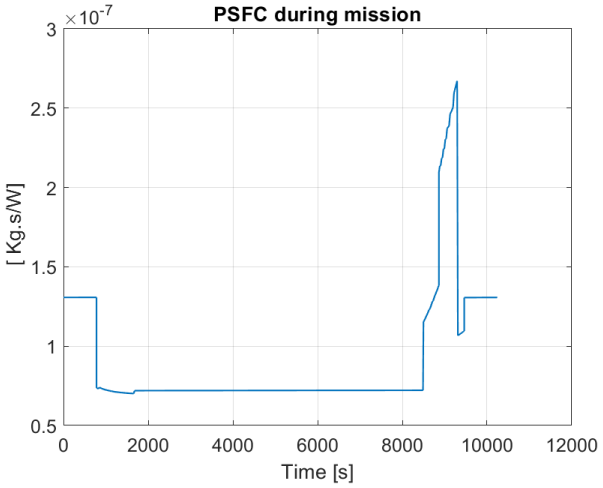

Figure 5.10: PSFC for Baseline Mission

5.2. Parallel-hybrid ATR 72-600

To determine the impact of hybridizing a regional aircraft in reducing LTO cycle emissions, the mission simulation routine has been run for the different power split ratios (H_P) under the hybridization strategy explained in section 3.3. Different technology levels have been analyzed to measure the general performance of the parallel-hybrid electric architecture and its sensitivity to them.

During the Mission simulation routines, the same mission profile and operating conditions were used to allow a fair comparison of all the configurations by isolating the main design variables: The power split ratio (H_P) and Technology Maturity Scenarios (e_{Bat}).

Before diving into the analysis of the results, it is useful to recall that a technology maturity scenario is identified by the specific energy of the battery because this is the heaviest component of the electric system. Nevertheless, all the electric component parameters were updated accordingly (as section section 4.3.5 explains).

Figure 5.11, 5.12 and 5.13 illustrate the shaft power decomposition for different DoH cases (20 %, 60 % and 100%) for a fixed technology scenario. The total propulsive power (propeller shaft power, but in the figures' legend, it is simplified as Propeller Power) is displayed with the blue line. It is relevant to notice that the maximum power peak (at take-off) increases as the power split ratio rises. More hybridization leads to a a heavier electric system that automatically increments the aircraft weight and, thus, the power requirements.

Also, it is pertinent to note the limits of the LTO and Climb-out in these figure and how the hybridization is only being done below the 3048 meters limit. Moreover, in the electric configurations, the power delivered by the gas turbine does not reach zero, which can be explained by the fact that the power turbine does not stop rotating, even when it is in its lower power setting.

The total thrust delivered for two different technology maturity scenarios (intermediate 600 Wh/kg and advanced 1000 Wh/kg) are displayed in figures 5.14 and 5.15. The higher the power split ratio, the heavier the aircraft and, consequently, the thrust required to propel the aircraft is higher. However, it is noteworthy that under the most optimistic battery technology scenario, the thrust requirements are lower for a particular

hybridization percentage. The Take-off Thrust, particularly, is reduced from almost 31 KN to 27 KN, per engine for the 100 % DoH case.

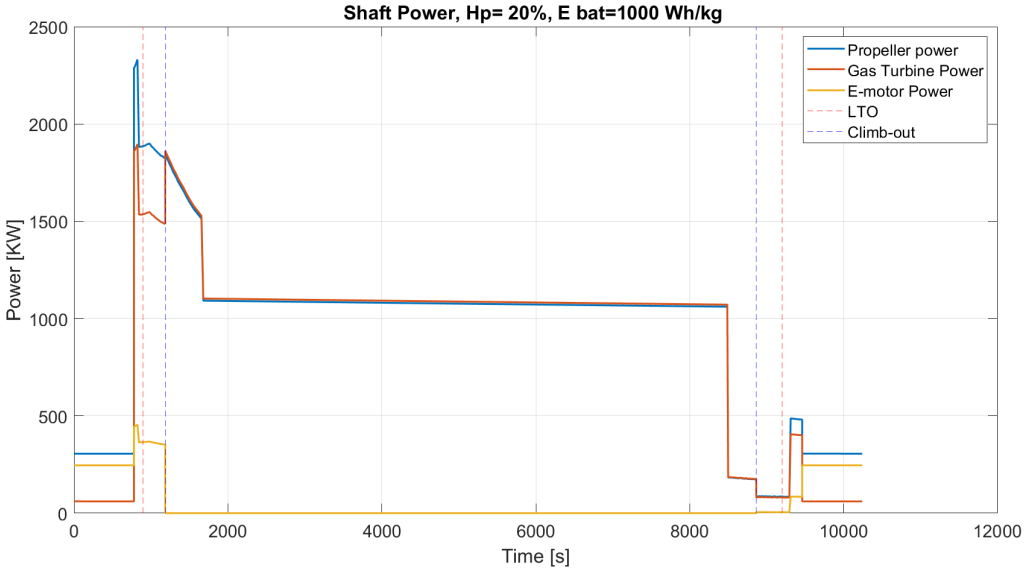

Figure 5.11: Propeller shaft power decomposition with e_{Bat} of 1000 Wh/kg for power split ratio of 20%

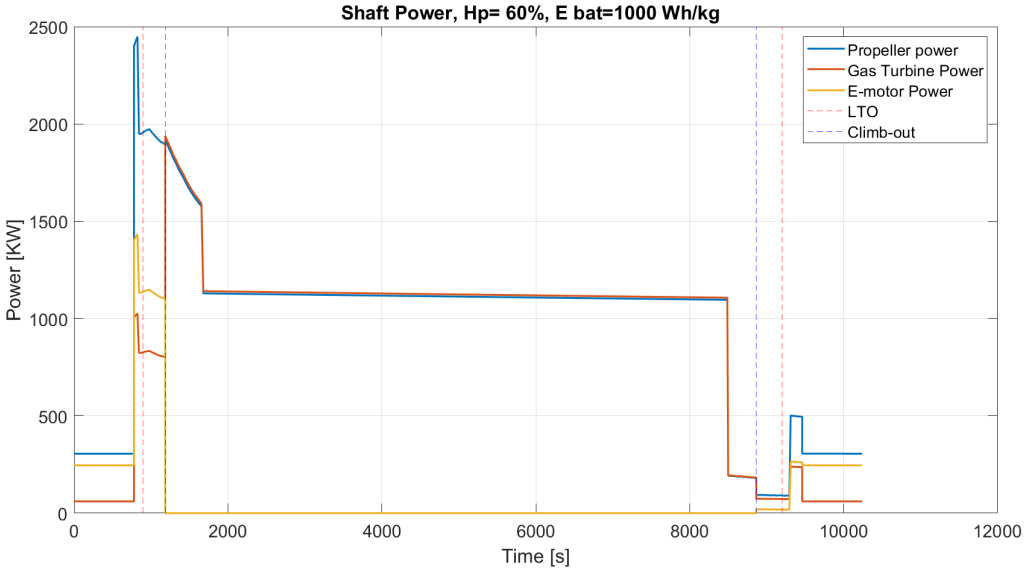

Figure 5.12: Propeller shaft power decomposition decomposition with e_{Bat} of 1000 Wh/kg for power split ratio of 60%

For a fixed technology scenario, the fuel flow during the mission decreases as the DoH increases, and the shaft power required is partially provided by the electric motor. As a result, less power needs to be delivered by the conventional gas turbine engine as the powertrain becomes more hybridized. However, it is interesting to note that when the DoH is 100 % (for example, in the taxi segments), the fuel flow does not reach zero. This is related to the architecture of the PW127, which possesses 3 turbines, and only one's shaft is connected to the electric motor. As a result, even with the 100% power split ratio in the parallel-hybrid architecture, the high-pressure and low-pressure turbines will still rotate (and the compressors as a result). Thus a minimal amount of fuel is released in this situation because the gas turbine does not stop rotating. The minimum value that the fuel flow achieves is 0.02 kg/s.

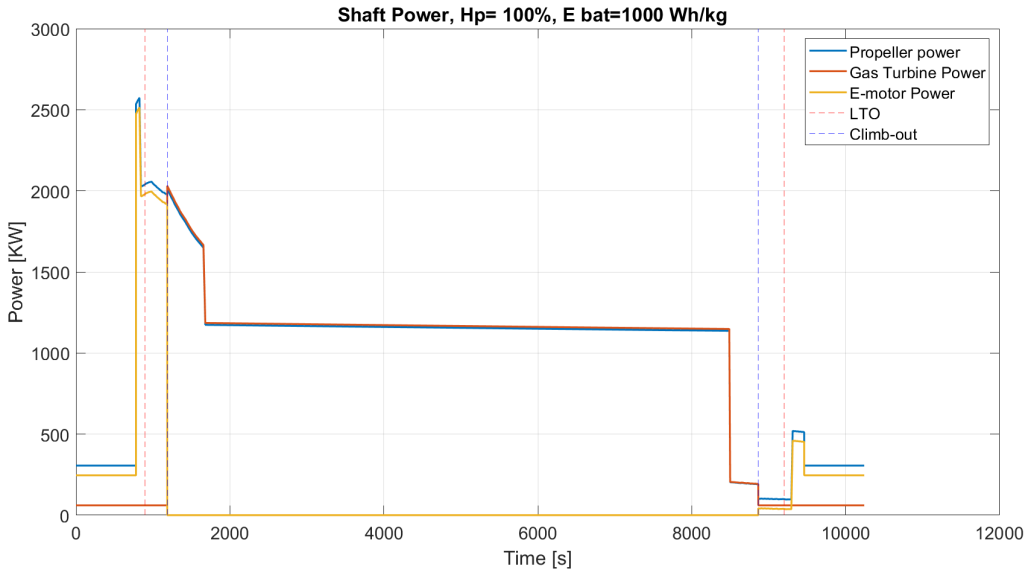

Figure 5.13: Propeller shaft power decomposition with Battery Specific Energy of 1000 Wh/kg for power split ratio of 100%

By analyzing the fuel flow behavior for three different technology scenario, the same trends are observed: The higher the DoH, more fuel is required so that more shaft power is generated and the aircraft power requirements are satisfied. The lines presented in figures 5.16 5.16 and 5.17 present only some power split ratio configurations (the 10 %, 20 %, 40 %, 60 %, 80% and 100 %). There is a non-linear increase in the disparity of fuel flow value as the DoH is incremented: The difference from 80 to 100 % is larger than from 40 to 60 %.

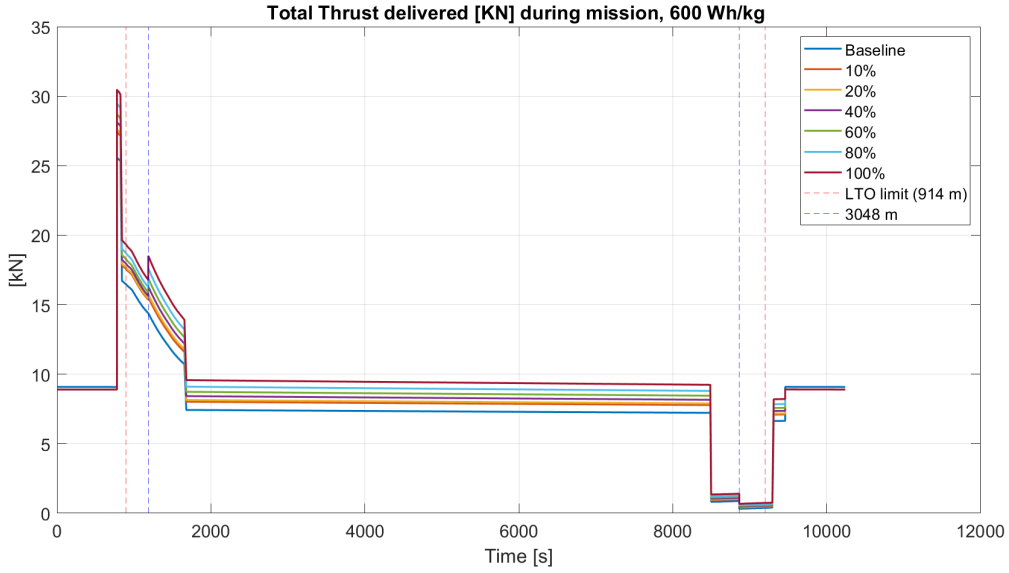

Figure 5.14: Thrust delivered by the propeller during mission with e_{Bat} of 600 Wh/kg

During the remaining flight segments that are not electrically assisted, the heaviest aircraft configurations are the ones that will require more shaft power from the gas turbine to fly the same mission at the same operating conditions, and thus, the highest fuel flow. The heaviest configuration for a fixed technology maturity level is the all-electric one (100 %). Also, for larger ranges (where the cruise is longer and not electrically assisted) it is expected a higher take-off weight since more fuel would have to be carried. This is why, for longer ranges, the hybrid-electric concept brings fewer advantages.

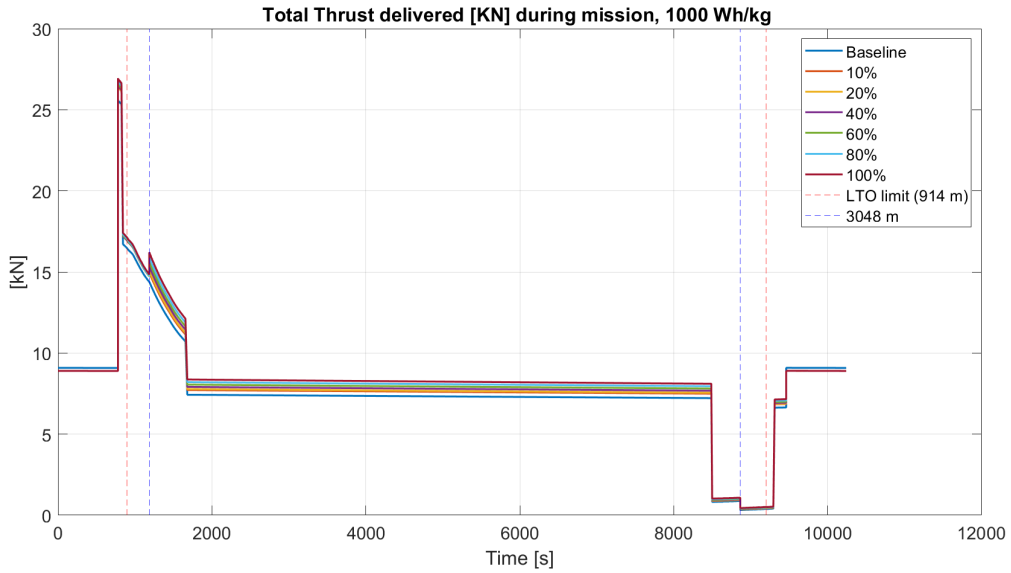

Figure 5.15: Thrust delivered by the propeller during mission with e_{Bat} of of 1000 Wh/kg

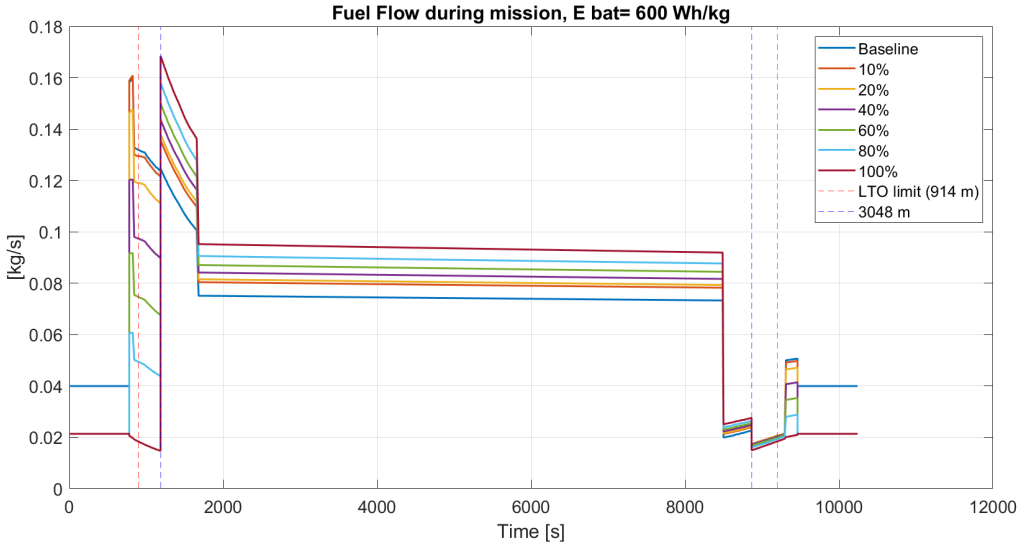

Figure 5.16: Fuel flow during mission with e_{Bat} of 600 Wh/kg

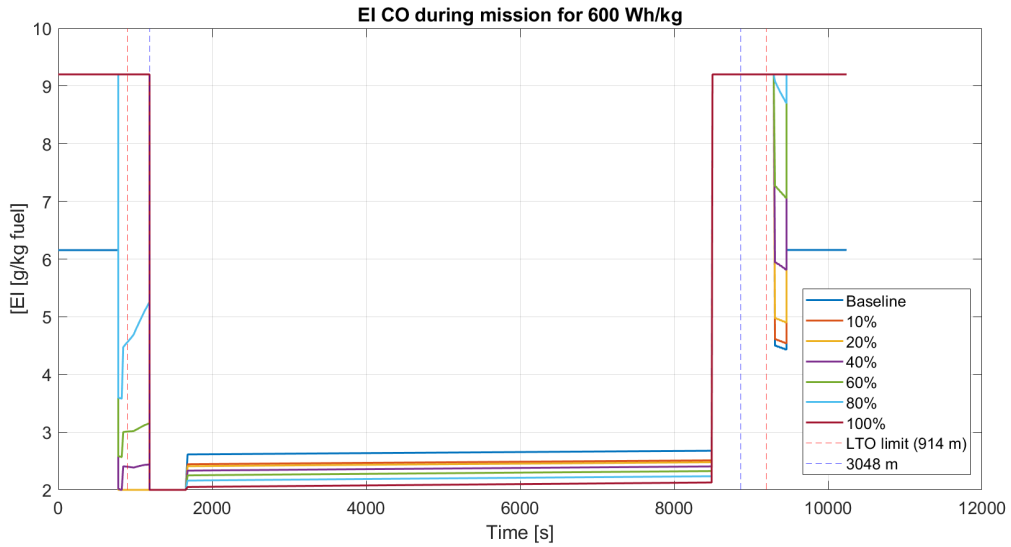

Figure 5.18: Emission Index of CO during mission with e_{Bat} of 600 Wh/kg

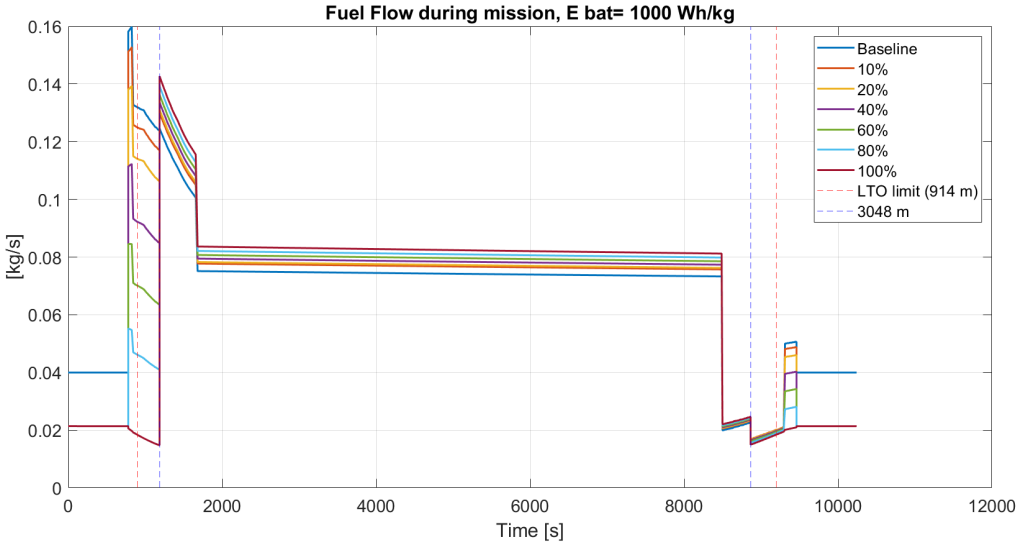

Figure 5.17: Fuel flow during mission with e_{Bat} of 1000 Wh/kg

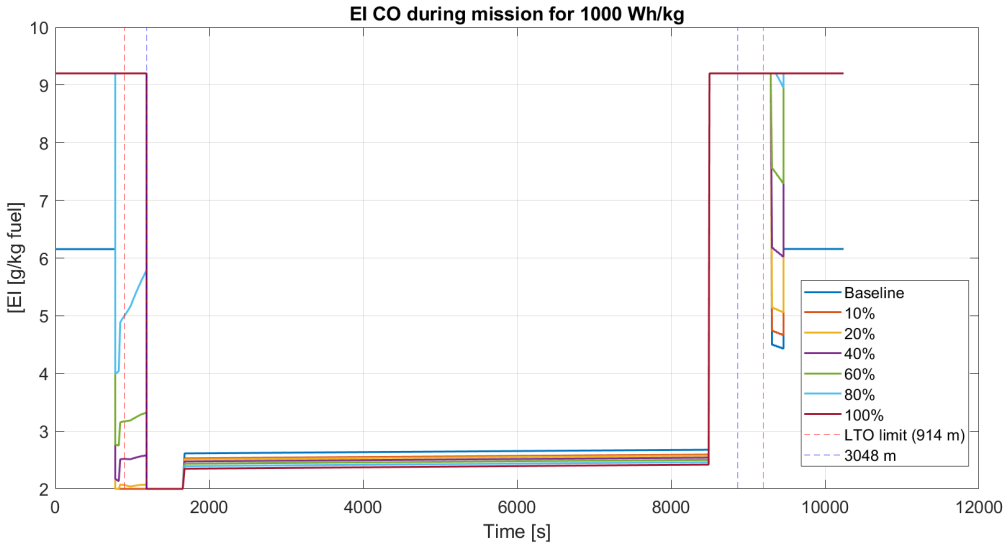

Figure 5.19: Emission Index of CO during mission with e_{Bat} of 1000 Wh/kg

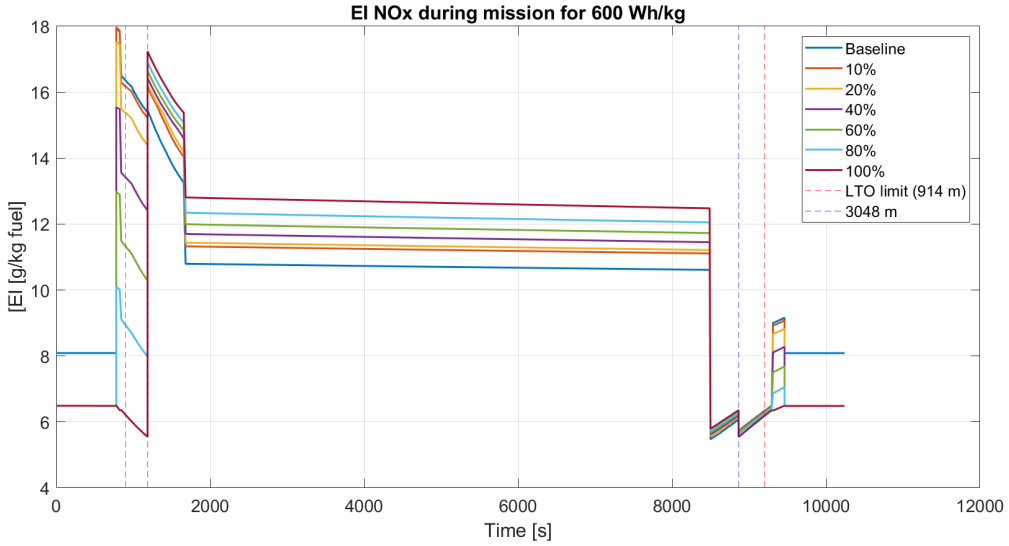

Figure 5.20: Emission Index of NO_x during mission with e_{Bat} of 600 Wh/kg

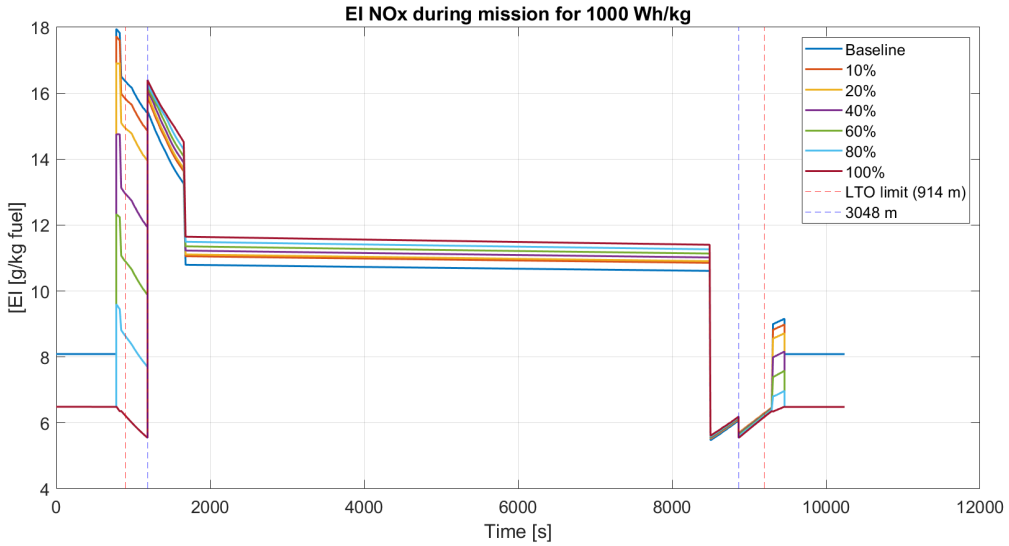

Figure 5.21: Emission Index of NO_x during mission with e_{Bat} of 1000 Wh/kg

The Emission Index (EI) of CO for battery specific energy (e_{Bat}) of 600 and 1000 Wh/kg are displayed in figures 5.18 and 5.19, respectively. It can be noticed that since the taxi phases are fully electric, the Emission Index are the same, independently on the DoH used in the climb-out and approach segments.

The electrification of taxi results in an increase in the EI, in comparison with the baseline case. This is in line with the prediction since the power settings of the gas turbine are lowest, as it has been observed with the low fuel flow in this segment. The lowest power settings lead to the highest Carbon Monoxide emissions. Apart from the taxi, also during descent (where the power level is low), the emissions of CO per kg of fuel achieve its maximum.

Focusing on the EI behavior at the climb-out and approach segments, the lowest the DoH, the highest the power setting at which the gas turbine is working, and thus, the lowest the EI of carbon monoxide. The distinct peak in take-off is visible as in this segment, the maximum shaft power is delivered.

The major differences between figures 5.18 and 5.19 are caused by the conventionally powered flight phases: climb and cruise. Here, the aircraft incorporating 600 Wh/kg battery technology emits slightly lower CO per kilogram of fuel burnt than when carrying the most advanced batteries. Because it is heavier, the power requirements are greater, and the CO is released is lower for the same hybridization strategy.

NOx and CO emissions are enhanced at different operating conditions. The Emission Index (EI) of NOx for battery specific energy (e_{Bat}) of 600 and 1000 Wh/kg are displayed in figures 5.18 and 5.19, respectively. NOx production is amplified at high power settings when high temperatures and pressures are obtained within the combustion chamber. Maximum at take-off, where the maximum temperature in the combustion chamber is achieved (maximum fuel flow and flame temperature). As the percentage of electric shaft power provided increases, the fuel flow declines, and the NO_x emissions follow the same trend.

Also, it is essential to notice that the two parameters that mainly influence the emissions follow similar trends of fuel flow and Emission Index. Figures 5.22 and 5.23 show the total pressure and temperature at the combustion chamber inlet.

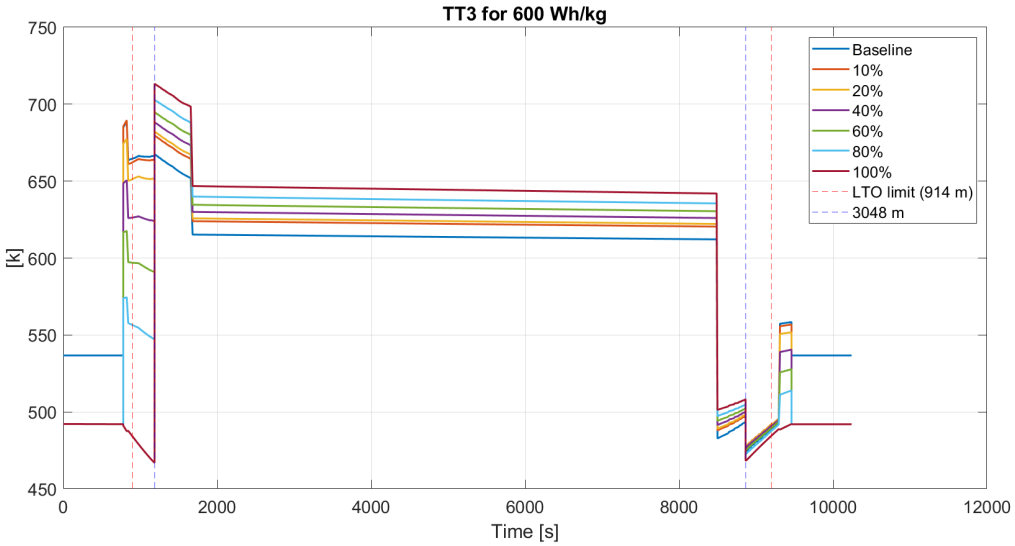

Figure 5.22: Total Temperature at the combustion chamber inlet during mission for a e_{Bat} of 600 Wh/kg

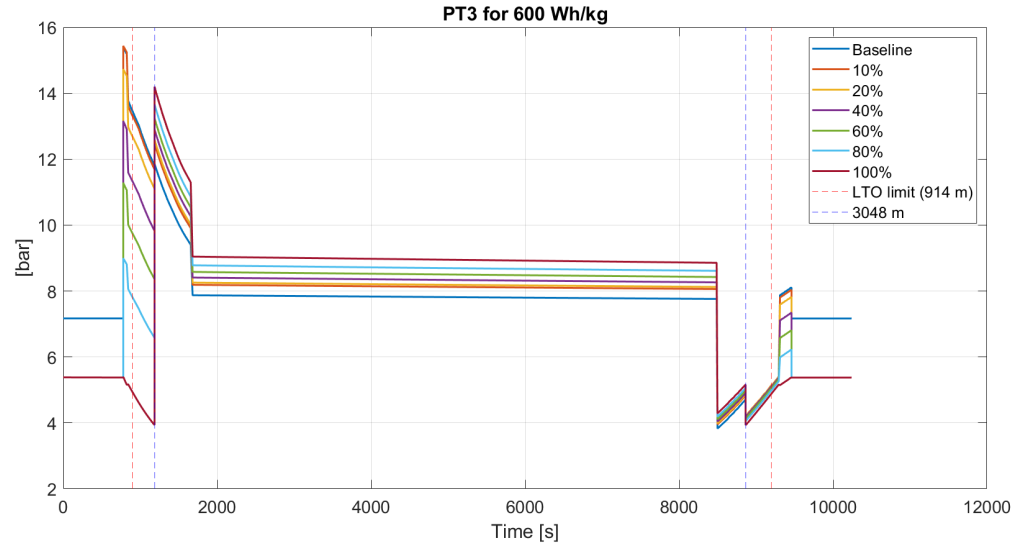

Figure 5.23: Total Pressure at the combustion chamber inlet during mission for a e_{Bat} of 600 Wh/kg

6

Mission Analysis Results

In the previous chapter, a close analysis of the engine performance during the whole mission allowed to observe the behavior of fuel flow and Emission Index of NO_x and CO in different flight phases and how these varied with different Power Split ratios (H_P) or Degree of Hybridization (DoH), for a particular battery specific energy (e_{Bat}).

This chapter gives special attention to the mission parameters and Key Performance indicators in function of both DoH and e_{Bat}.

The following parameters will be analysed for all different configurations:

- Aircraft Take-off mass (section 6.1.1)
- Fuel mass required (section 6.1.2)
- Electric system mass in its totality and per individual electrical component (section 6.1.3)
- Aircraft Energy consumption (section 6.2). This section quantifies the total and the electric energy consumed and the PREE for each configuration
- Aircraft Emissions (section 6.3). Namely NO_x, CO, CO_2 and H_2O during entire mission and NO_x, CO and H_2O emissions in the LTO cycle. This section includes a sensitivity analysis to technology maturity scenarios.

6.1. Aircraft Weight breakdown

The Aircraft Take-off weight in the hybrid-electric configuration is the sum of the Operating Empty Weight (OEW), Payload, Fuel, and Electric System weight. As the OEW, Payload, and fuel to perform a diversion mission are kept constant, only the fuel and electric components vary between the different configurations.

6.1.1. Aircraft Take-off mass

When comparing the Take-off mass of different configurations (figure 6.1), a non-linear behavior in the increase of the aircraft mass is observed as the DoH varies from zero (baseline configuration) and 100 %, for a specific technology scenario. Also, when looking at a fixed DoH, a non-linear trend is noted. The reason behind this behavior is that the aircraft gets heavier by carrying more massive batteries (as more electric power is required with DoH increase), but because the power required rises as a result, leading to quicker growth of the take-off weight.

As the technology level of the electric system gets more mature (translated in the figure into an increase in e_{Bat}) the increase rate of the aircraft take-off mass is slower due to the effect of hybridization: less fuel is required by the aircraft to be carried as the aircraft is partially being powered by electric power.

Another important point to highlight is the distinction between the configurations. When the take-off mass is higher than the Maximum Take-off Mass (MTOM) certified by the ATR 72-600 (23,000 kg), the configurations displayed in figure 6.1 are classified as impossible. The aircraft is not being retrofitted for a parallel-hybrid electric powertrain. Thus, the MTOW requirement of the baseline ATR 72-600 is being kept.

It can be concluded that the State of the Art of Batteries (with specific energy of 300) does not permit an ATR

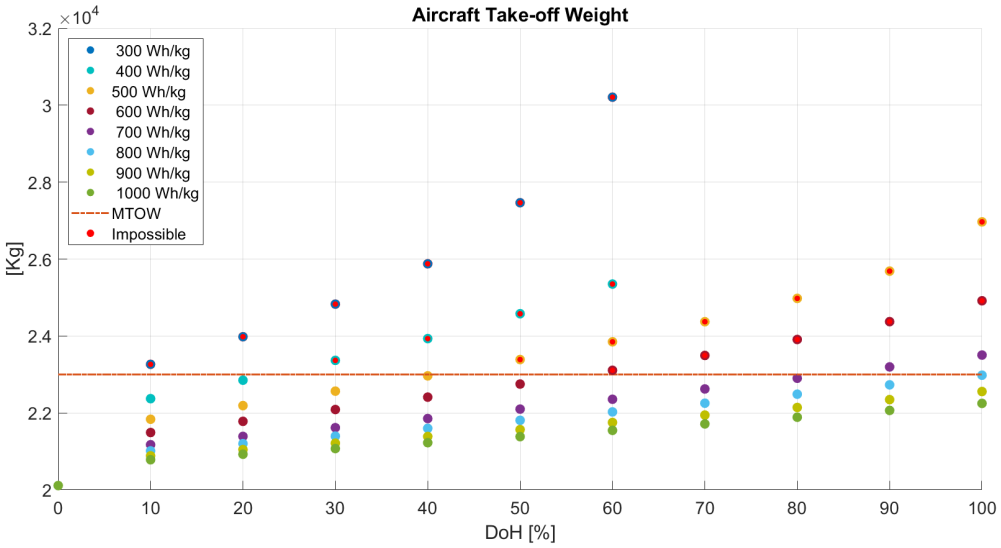

Figure 6.1: Aircraft Take-off mass (in kg) in function of the DoH for different Technology maturity scenarios

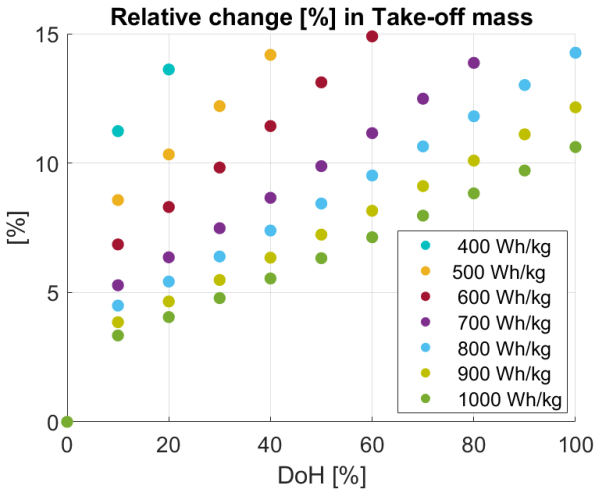

Figure 6.2: Relative change in the Take-off Weight, for the possible configurations

72-600 (not retrofitted) to be hybridized up to an altitude of 3048 m with a parallel-hybrid electric architecture powertrain. Only batteries possessing specific energy values of 800 Wh/kg or higher could afford to have a fully electric LTO cycle and climb out (up to 3048 m).

It is worthy of underlining that for the two lowest technology scenarios (300 and 400 Wh/kg) a mission with a power split ratio of Hybridization of 60 % during take-off, climb-out and approach (coupled with electric taxi) is not possible to simulate due to divergence of GSP when computing the turboprop performance. The divergence is related to the required shaft power that these configurations demand, which is higher than the maximum take-off power defined in the design point of the baseline turboprop engine model. As a result, the engine cannot withstand delivering such high power, and it does not converge.

Lastly, the non-linear behavior must be noted for power split ratios lower than 10 %. The sudden jump from the baseline case to the low hybridized configuration (a change in 10%) is steeper than when the DoH rises up by 10 %, for DoH > 10 %. The explanation is related to the hybridization strategy adopted (described in section 3.3). For all the hybrid configurations, the taxi phases are fully electric, due to the low efficiency of the gas turbine at this segment and considerable impact on the LTO cycle (emissions emitted below 914 m). Since all hybrid configurations have a fully electric taxi, the difference between them is lower than when compared

to the baseline scenario (where there is no electrification of taxi).

In order to facilitate the sensitivity of the Take-off mass to the battery technology scenario (e_{Bat}) and power split ratio, figure 6.2 depicts how much the take-off mass varies (increases, in this case) in percentage, comparatively to the baseline configuration. In this figure only the possible configurations (which Take-off weight is lower than ATR 72-600 MTOW).

6.1.2. Fuel mass

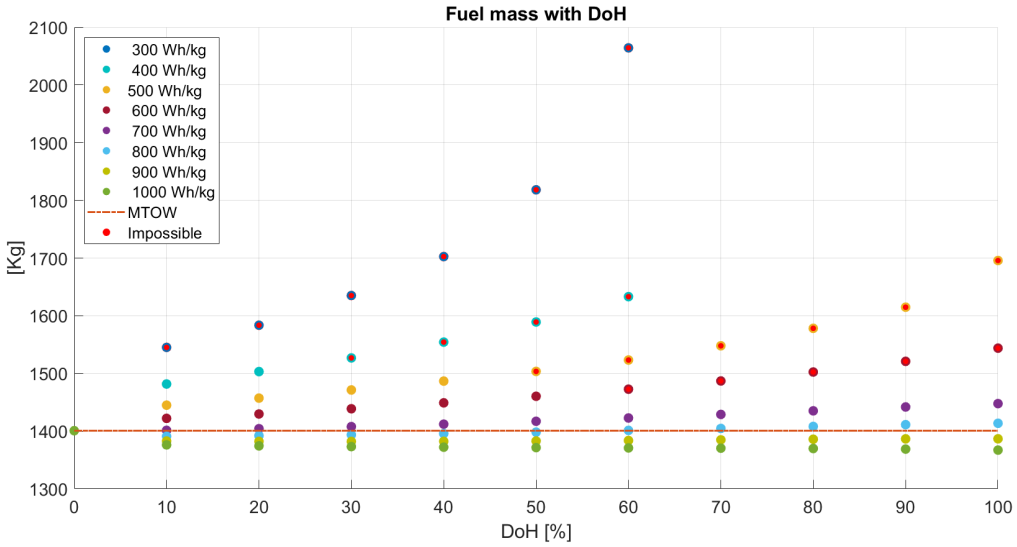

Figure 6.3: Fuel mass (in kg, excluding reserves) in function of the DoH for different Technology maturity scenarios

As it has been stated, if the electric system technology is advanced enough, the gas turbine power requirements would decrease due to more electric assistance. Moreover, a lighter electric system can compensate for the power requirement increase due to heavier aircraft (baseline ATR 72-600 is the reference) and result in fuel mass saving.

However, to observe fuel burn savings during this mission, for any DoH, a e_{Bat} of at least 900 Wh/kg is required. For 800 Wh/kg batteries, it is possible to notice fuel savings in the whole mission for power split ratio lower than 50 %. As the DoH goes beyond 50 %, the power required by the gas turbine increases due to the quick rise in the electric system weight, offsetting the benefits of having an electric system delivering part of the required power.

In figure 6.3, the behavior of the mass of fuel burnt during the mission is displayed. Also, the configurations whose MTOW is higher than the baseline aircraft are marked with a red dot. The reserves are excluded from the graphics because they are a fixed amount for all the configurations.

6.1.3. Electrical components mass

The electric system mass behavior follows the same trend as the aircraft take-off weight (TOW) with the remark it grows quicker than the TOW for e_{Bat} higher than 900 wh/kg. It can happen due to the alleviation of fuel burn mass for these configurations that slow down the rate of the TOW. The electric system weight can breakdown into its components. Figures 6.5 and 6.6 display the electric motor, cooling (assumed to be 30% of the total electric system weight), inverter, cables, and batteries, for two different technology level scenarios: 600 Wh/kg and 1000 Wh/kg, respectively. As expected, the battery is the heaviest component, followed by the cooling, and the third heaviest part is the electric-motor.

The pie charts below (figure 6.7 and 6.8) show the admitted variable parameters in the Aircraft Weight to analyze the proportion of fuel (reserve fuel for diversion mission not included because it is assumed to be constant) and the electric system as the Power Split ratio and Technology Maturity levels change. In other

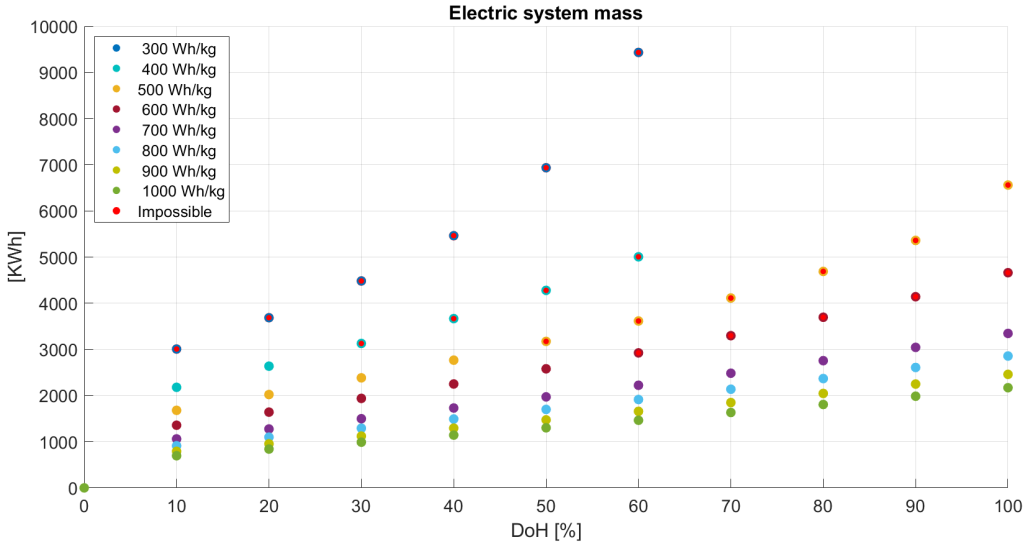

Figure 6.4: Total Electric system mass (in kg) in function of the DoH for different Technology maturity scenarios

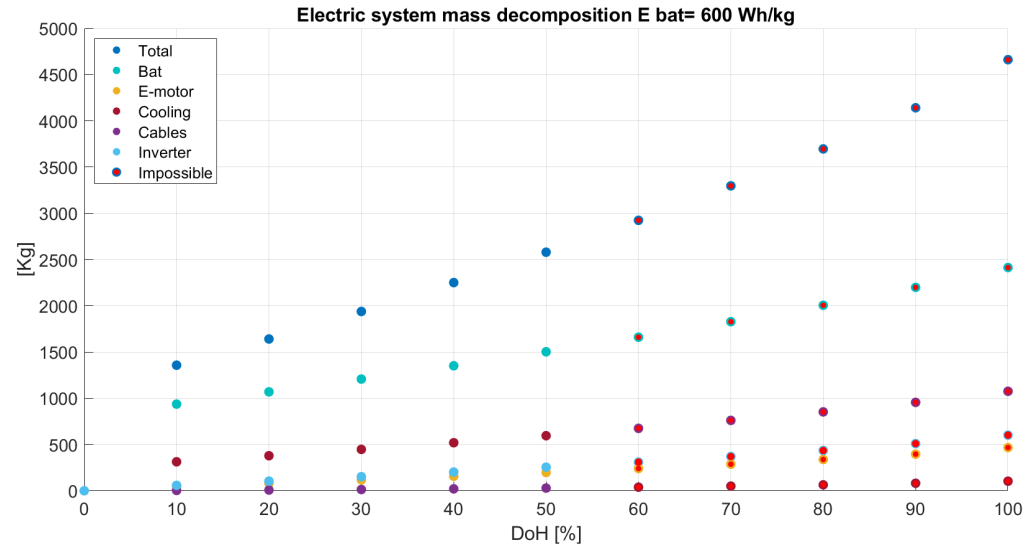

Figure 6.5: Electric system components mass (in kg) in function of the DoH for e_{Bat} of 600 Wh/kg

words, the mass of fuel burn and the electric components are represented.

It can be noticed that for 400 Wh/kg Batteries, the electric system weight is higher than the fuel weight required to fly the whole mission, for a DoH of only 20 % (figure 6.7). As the technology maturity improves, the percentage of fuel mass increases, reaching almost 70 % of the total electric system plus fuel weight for 1000 Wh/kg Batteries (figure 6.8).

In appendix A more pie charts with the proportions of fuel and electric components weight for different Power Split Ratios and Technology Maturity levels are shown.

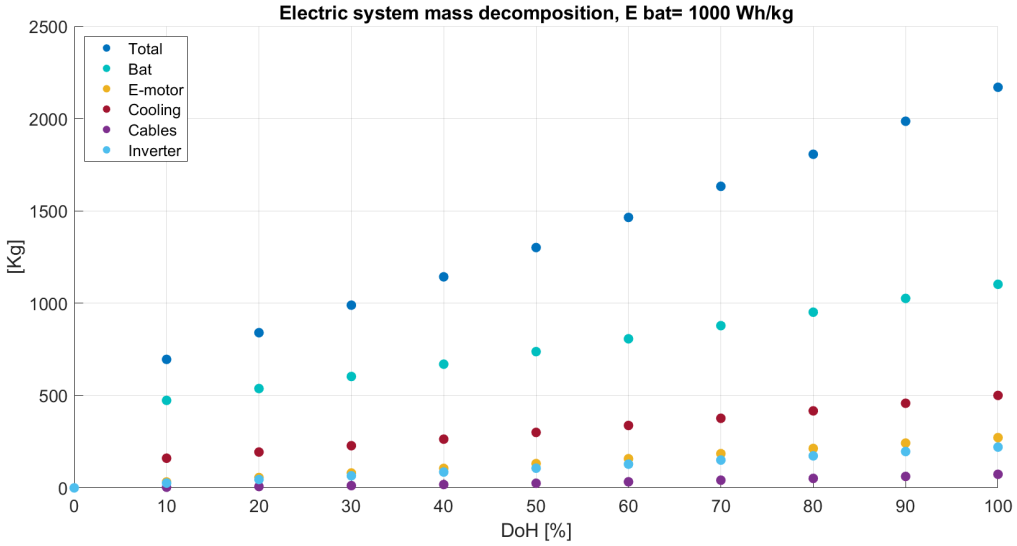

Figure 6.6: Electric system components mass (in kg) in function of the DoH for e_{Bat} of 1000 Wh/kg

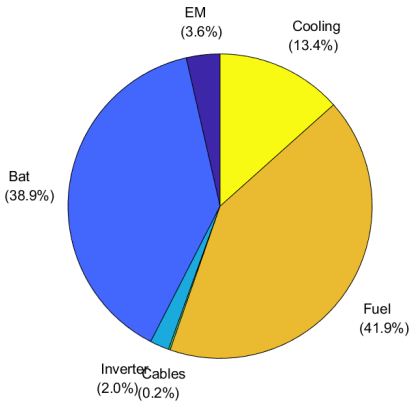

Figure 6.7: Electric system plus fuel (excluding reserves) weight percentage for DoH of 20% and e_{Bat} of 400 Wh/kg

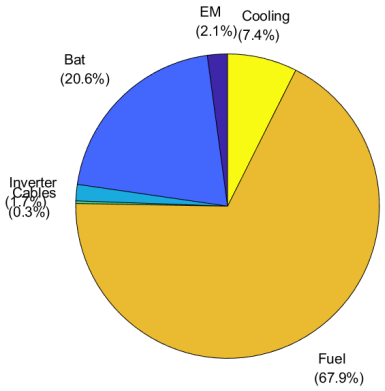

Figure 6.8: Electric system plus fuel (excluding reserves) weight percentage for DoH of 20% and e_{Bat} of 1000 Wh/kg

6.2. Energy consumption

The total energy consumption tends to increase as the degree of hybridization (DoH) increases. The specific energy of the fuel is, even under the most optimistic technology scenario, 13 times higher than the batteries. Thus, to store the same amount of energy, the batteries would weight at least 13 times ore then the fuel. Therefore, even in the configurations where the fuel mass declines with the DoH (for e_{Bat} higher or equal to 900 Wh/kg), the overall take-off weight of the aircraft will still increase with the DoH in comparison to the baseline value, as observed in figure 6.9.

The parallel-hybrid electric aircraft consumes more energy than the gas-turbine powered aircraft for all the configurations simulated and technology scenarios considered. The electric energy stored within the batteries is illustrated in figure 6.10, and it is clear that the significant proportion of this sort of energy on the total aircraft energy consumption as the DoH is increased.

To analyze the sensitivity of the total aircraft energy consumption to the battery technology (e_{Bat}) and DoH, figure 6.11 shows how much, in percentage, the total energy increases regarding the baseline aircraft. As predicted, the most advanced technology scenario enables the least increase in total energy required, reaching the minimum increase at the minimum Hybridization (10 %) due to the small proportion of electric

energy being using in this configuration.

The Performance Indicator PREE (Payload Range Energy Efficiency) of each configuration is shown in figure 6.12. Figure 6.13 depicts the relative difference between the baseline PREE value and hybrid configurations. This indicator expresses how efficiently a design payload can be carried over a certain range (regarding the amount of energy used). Since the payload and the range are fixed parameters in this research, only the energy required for each configuration to fly the mission influences the PREE. PREE is inversely proportional to the total energy consumed. Consequently, the higher the PREE, the less energy was consumed for the same payload and range.

The configuration with the highest PREE matches the one with the lowest energy consumption (10 % DoH and e_{Bat} of 1000 Wh/kg), as predicted.

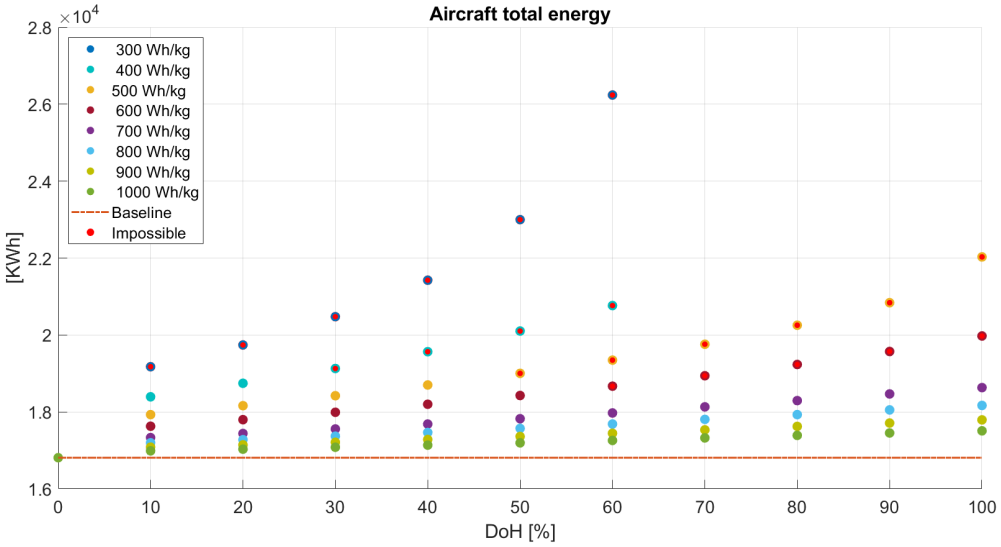

Figure 6.9: Aircraft total energy consumed during mission for different technology scenarios and DoH (DoH)

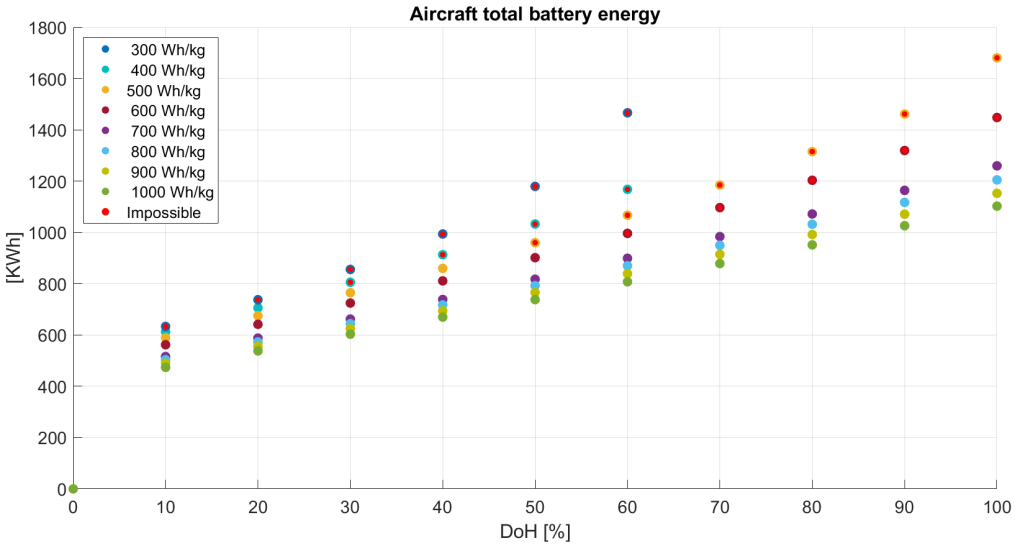

Figure 6.10: Aircraft total electric energy consumed during mission for different technology scenarios and DoH

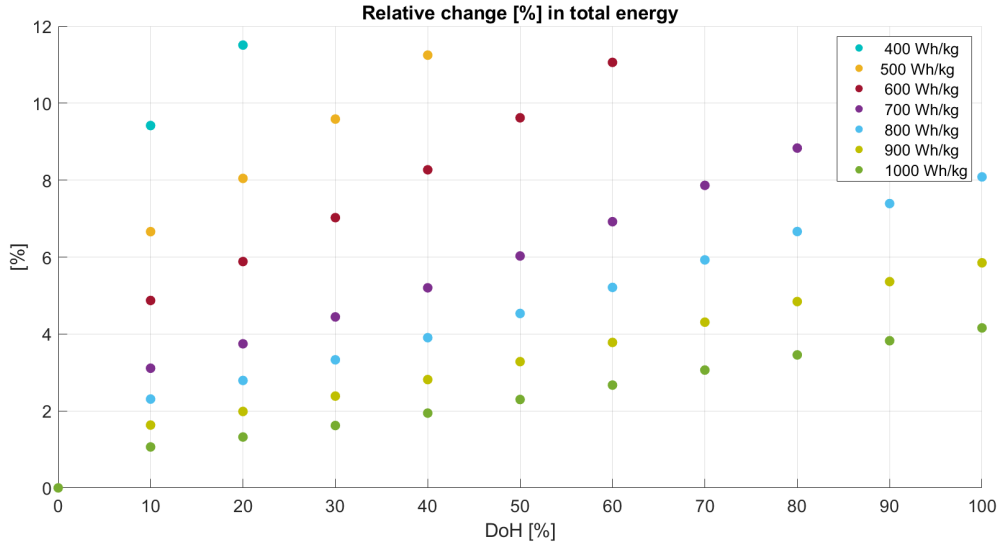

Figure 6.11: Relative change in total energy consumed during the mission for different technology scenarios and DoH

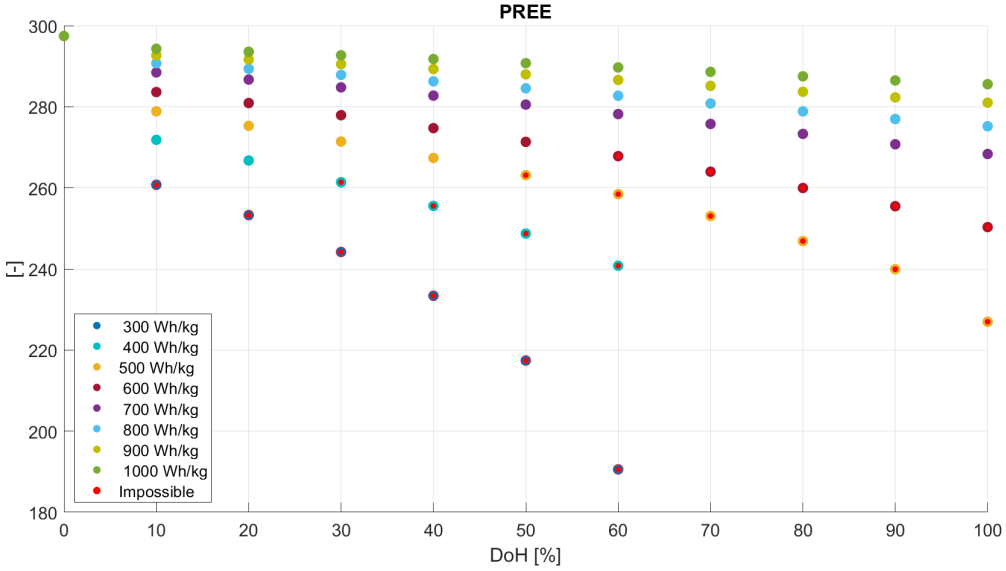

Figure 6.12: PREE for different technology scenarios and DoH

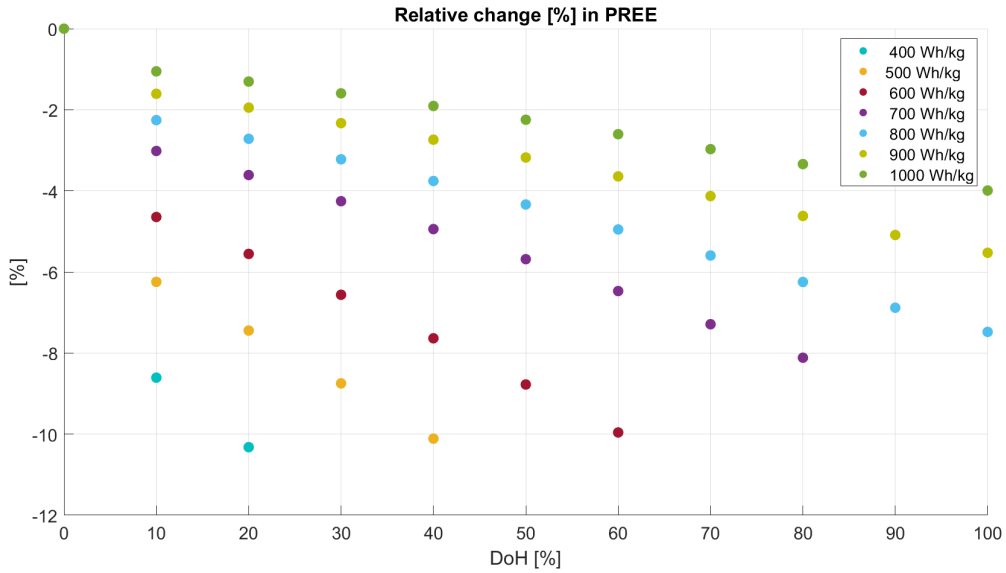

Figure 6.13: Relative change in total energy consumed during the mission for different technology scenarios and DoH, for the possible configurations

6.3. Engine emissions

The focus of this research is to investigate whether a parallel-hybrid electric powertrain could play a role in reducing Local Air Quality emissions (NO_x and CO) and H_2O at low altitudes (section 6.3.2). However, it is also vital to observe CO_2, H_2O, CO and NO_x emissions released during the mission because of its impact on climate change. The analysis of these four species throughout the mission is conducted in sections 6.3.1 (CO_2 and H_2O) and 6.3.3 (CO and NO_x).

6.3.1. CO_2 and H_2O emissions

The CO_2 emissions are computed assuming that the electric energy production is clean and no CO_2 emissions are released during the batteries life-cycle.

The CO_2 and H_2O emissions are proportional to the fuel burn (the emission indexes are constant for these species). Therefore, the trend of these emissions follows the behavior of fuel flow, as can be verified when comparing figures 6.3, 6.14 and 6.15. Furthermore, it can be observed that only configurations with e_{Bat} superior or equal to 800 Wh/kg can accomplish a decrease in the total CO_2 emissions.

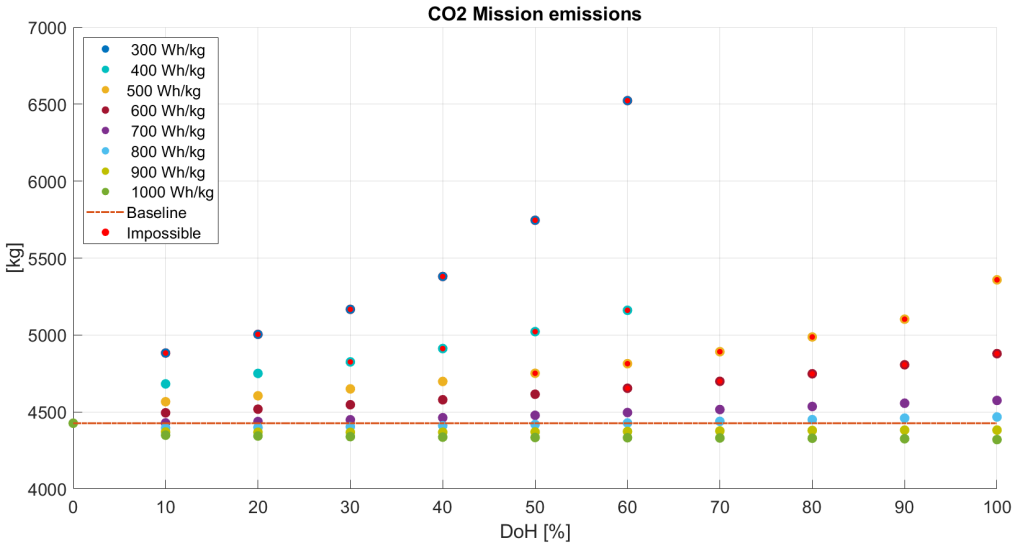

Figure 6.14: CO_2 emissions during mission (in kg) in function of the DoH for different e_{Bat}

An outcome of the analysis of these parameters is that this short electrification during the mission (only taxi, take-off, climb-out, and approach are being hybridized) does not bring significant benefits on reducing CO_2 emissions when taking into consideration the entire mission, for this range (1000 km). Looking at the sensitivity of CO_2 to power split ratio and technology scenarios (figure 6.16), it is clear that the maximum reduction is not substantial (slightly more than 2 %) regarding the Baseline aircraft. Additionally, if accounted for the total life-cycle of a battery, most likely, no advantage using this mission strategy would be attained. It is important to point out that the points exhibited in figure 6.16 are the configurations that enable a take-off mass below the MTOW of the baseline aircraft.

6.3.2. LTO cycle Emissions

This section gives emphasis to Engine Emissions NO_x and CO during the LTO cycle (stage where ICAO standards are implemented). By observing how these two species emissions vary in the LTO cycle (figure 6.17 and 6.18), it is detected low sensitivity to electric components technology.

CO behavior is worth to be commented on. It can be noticed that there is an approximately 15 % drop in LTO CO emissions at the lowest power split ratio scenario. Afterward, it keeps a roughly constant value (then, there is no major sensitivity to either DoH or e_{Bat}). With the increase of DoH, the power settings of the conventional turboprop engine are reduced, and so, CO would tend to increase its production. The CO Emission Index is

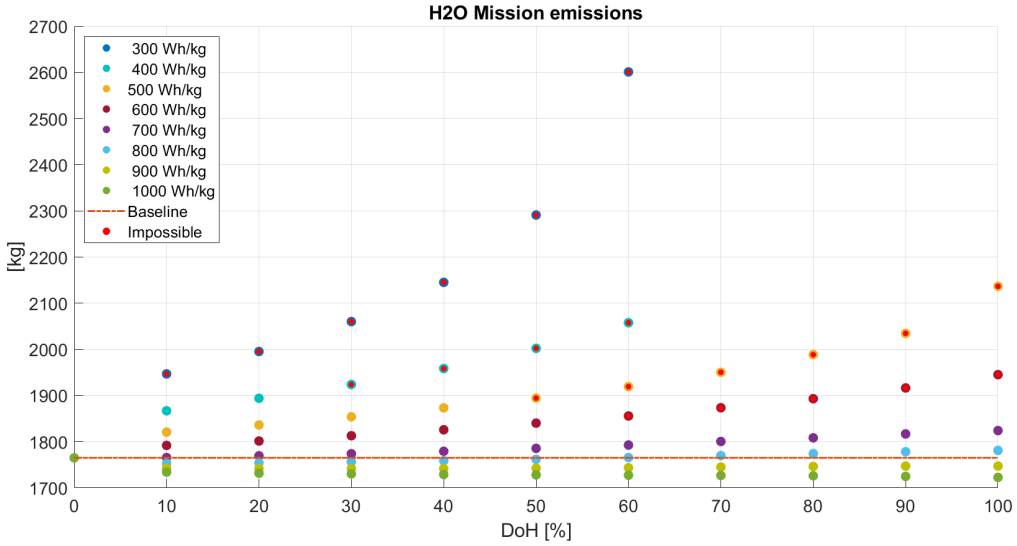

Figure 6.15: H_2O emissions during the mission (in kg) in function of the DoH for different e_{Bat}

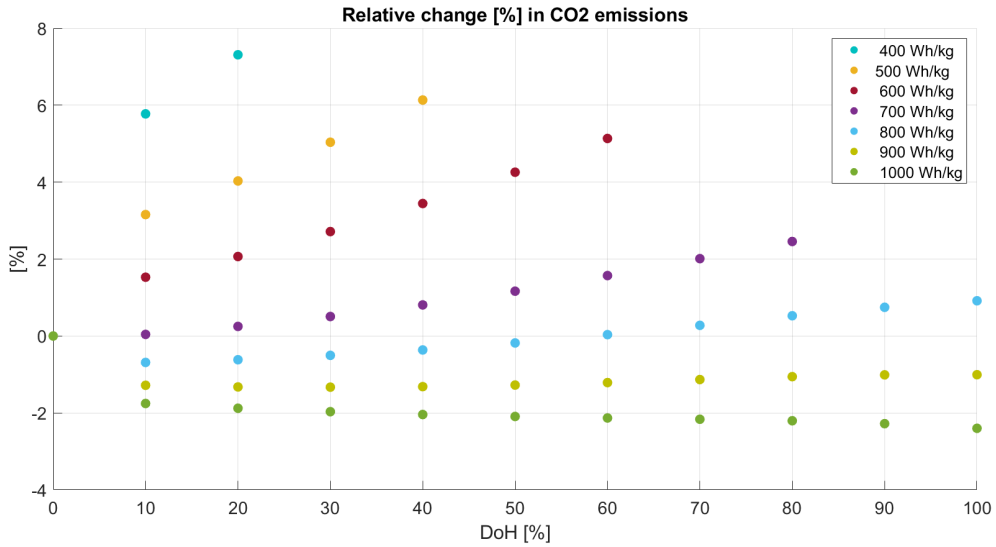

Figure 6.16: Relative change in total CO_2 emitted during the mission, for the possible configurations

displayed in figures 5.18 and 5.19, in section 5.2. However, the fuel flow is decreasing simultaneously. As a result, the product of EI CO with fuel flow (which equals the total CO emitted) is almost constant.

The fall of CO emissions within the LTO cycle for the 100 % electric LTO cycle is explained by the small fuel flow (not zero, nonetheless) that the gas turbine consumes. Although the Emission Index is maximum throughout the LTO cycle, the extremely low fuel flow (0.02 kg/s) offsets the relatively high value of the EI.

Drawing the attention to NO_x emissions within the LTO cycle, as the electric motor delivers more power to the propeller shaft, the power setting of the gas turbine is reduced, and the Emission Index of this pollutant is reduced (figures 5.20 and 5.21 exhibit this behavior). Not only the Emission Index is reduced (due to a decrease of flame temperature and pressure in the combustion chamber), but also the fuel flow diminishes as the Hybridization is enlarged. Both play a role in the NO_x emissions and both are responsible for the decrease of its emissions with the Hybridization (figure 6.17). Likewise, in figure 6.17, one can see that the emissions do not vary significantly with different e_{Bat}. The sensitivity is even lower as the hybridization increases.

It can be inferred that the hybridization strategy studied in this research does play a positive role in the LTO cycle emissions of NO_x and CO since these emissions can be reduced up to 71 % and 21 % (in the 100 % DoH configuration), respectively. Even at lowest hybridization level tested (10 % of Power Split ratio) NO_x emissions can be reduced between 29 % and 34.3 % (with 400 and 1000 Wh/kg of e_{Bat}, respectively) and CO emissions lowered within the 15.4 % - 16.4 % range (depending on the advancement of battery technology).

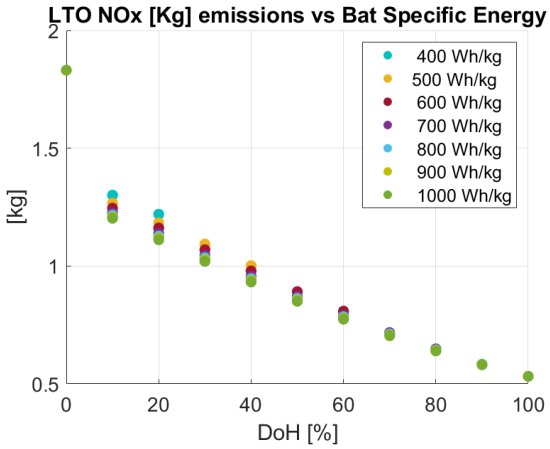

Figure 6.17: Sensitivity of LTO NO_x emissions to technology scenarios and DoH, for the possible configurations

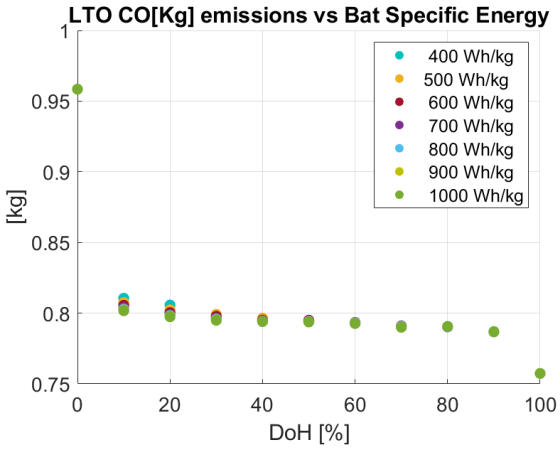

Figure 6.18: Sensitivity of LTO CO emissions to technology scenarios and DoH, for the possible configurations

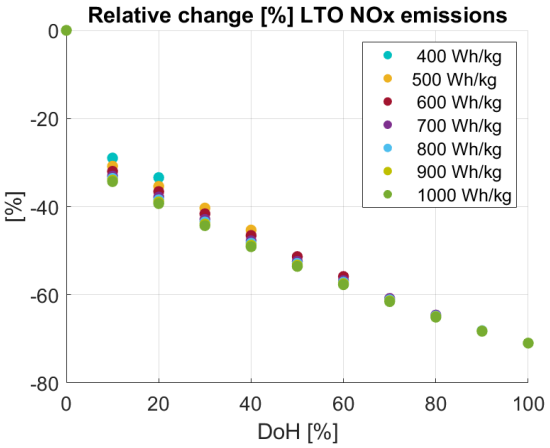

Figure 6.19: Relative change in NO_x emitted during the LTO cycle, for the possible configurations

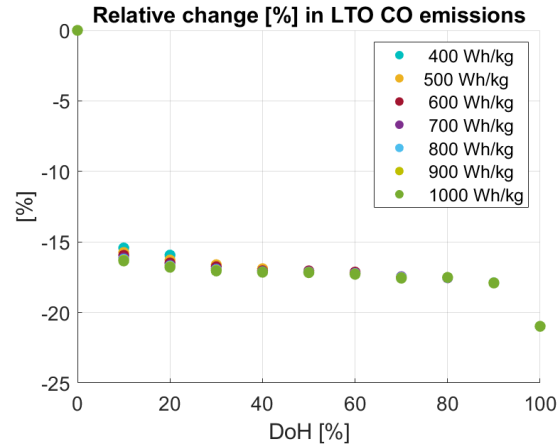

Figure 6.20: Relative change in CO emitted during the LTO cycle, for the possible configurations

After analyzing the impact of the hybridization strategy being tested in the overall H_2O and CO_2, it is substantial to take a closer look at the emissions released during the LTO cycle, which is the goal of this strategy and research. In figure 6.21, it is visible that in the LTO cycle, H_2O emissions are reduced, reaching up to around 55 % decrease for the fully electric LTO cycle and aircraft concept carrying the most advanced battery technology. The big decrease already observed with 10 % of DoH in take-off, climb-out and approach is due to the electric taxi-in and taxi-out that is occurring at every configuration. The minimum reduction obtained is observed at 400 Wh/kg, 31 %, (since lower values of e_{Bat} do not allow any configuration that complies with the MTOW criteria), with the minimum percentage of electric assistance, as the aircraft is heavier and the power requirements are higher than the baseline aircraft. As the difference in fuel flow with different technology scenarios does not change significantly during the targeted segments for Hybridization, the sensitivity of LTO H_2O emissions to that parameter is not meaningful. Besides, as the hybridization percentage increases, the sensitivity declines further.

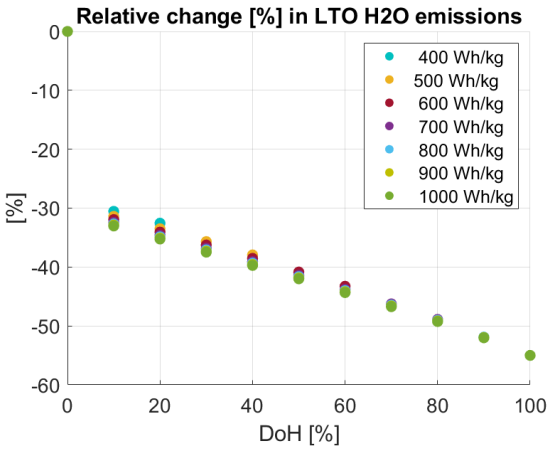

Figure 6.21: Relative change in H_2O emitted during the LTO cycle, for the possible configurations

6.3.3. CO and NO_x emissions

Figures 6.22 and 6.23 present the CO emitted during the entire mission (in grams) and its relative difference compared to the baseline value, respectively. It is visible that for all the possible configurations, the total CO emitted is reduced. The maximum reduction with this hybridization strategy is approximately 5 % and it is achieved at a DoH of 100 % and e_{Bat} 1000 Wh/kg. Although the CO emitted during the LTO can be diminished up to 21 %, the CO emitted throughout the whole mission cannot be reduced substantially. It is relevant to note that the trend of the total CO is the same as the LTO CO (compare figures 6.22 and 6.18). This can be explained by the constant values of EI in the non-hybridized segments, resulting only in an increase of magnitude and keeping the LTO trend.

Figures 6.24 and 6.25 present the NO_x emitted during the complete mission (in grams) and its relative difference compared to the baseline value, respectively. In contrast to the CO emitted, the mission hybridization strategy picked leads to an increase in the overall NO_x emissions. Even though LTO NOx decreases with the DoH for any technology scenario, the total NO_x can only be reduced with 1000 Wh/kg batteries (e_{Bat}). Besides, even this reduction is negligible (approximately 1 %). The observed increase in the total NO_x is due to higher power requirements from a heavier aircraft during the non-hybridized segments, offsetting the significant reduction observed in the LTO cycle (figure 6.17).

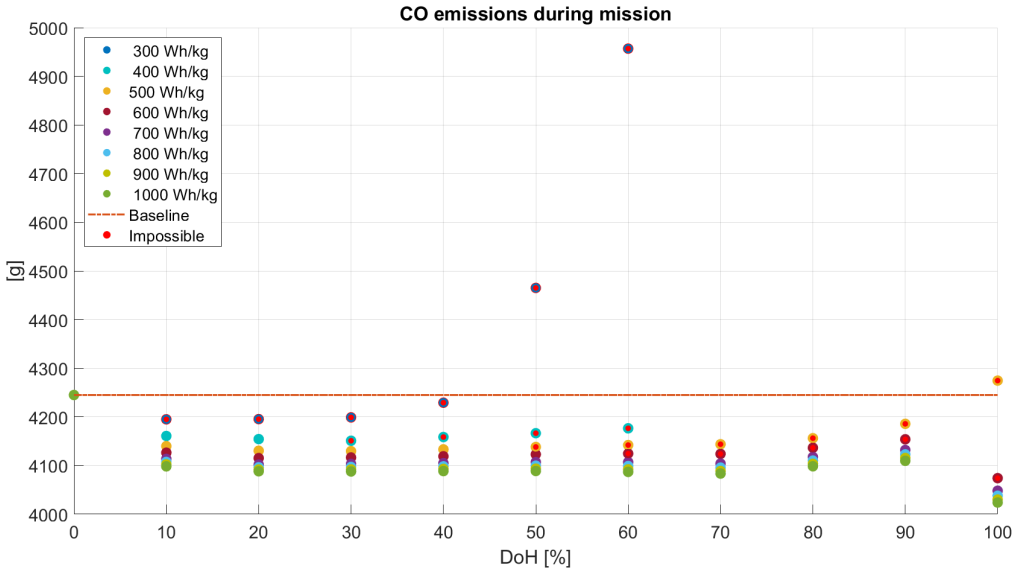

Figure 6.22: CO emissions during mission (in kg) in function of the DoH for different e_{Bat}

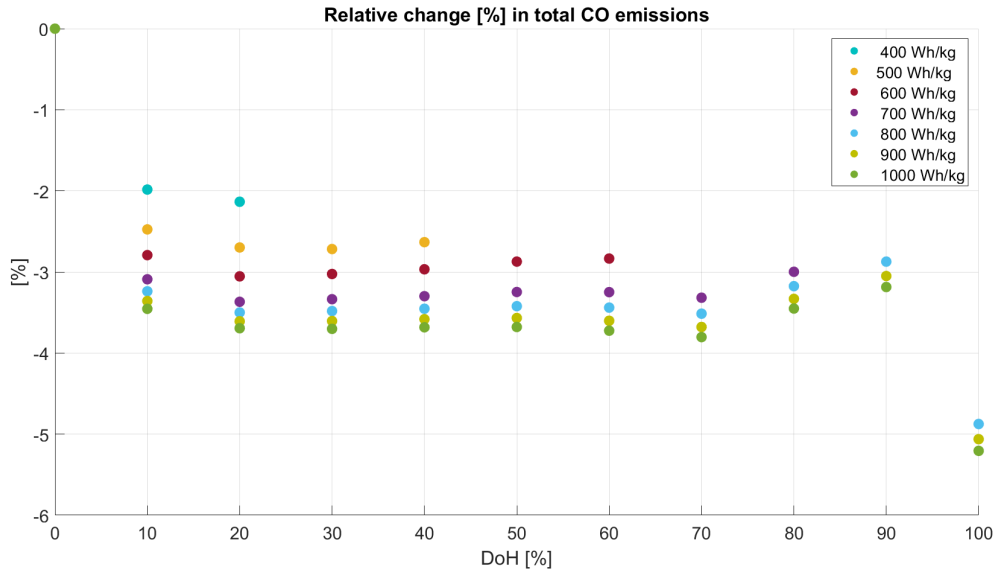

Figure 6.23: CO emissions during mission (in kg) in function of the DoH for different e_{Bat}

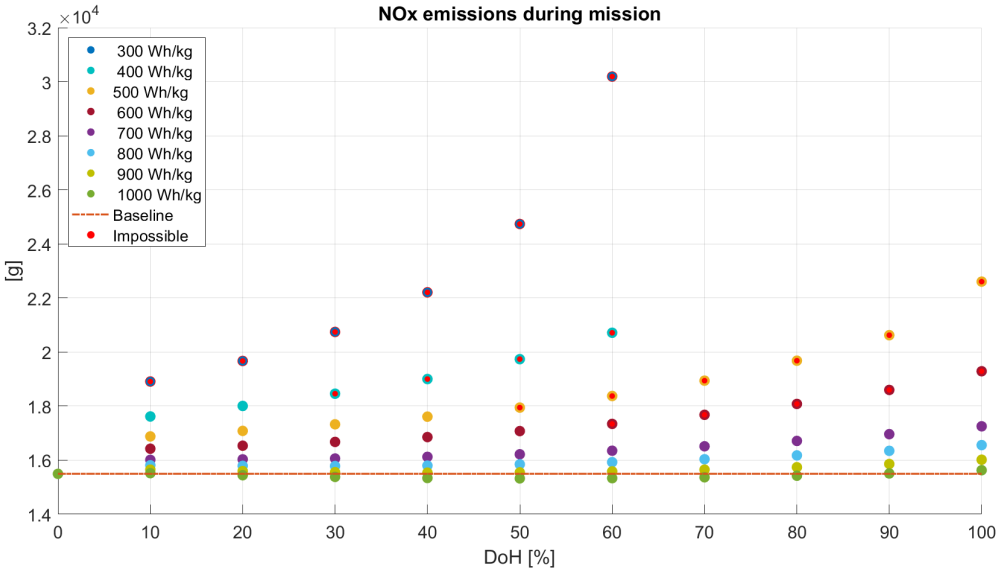

Figure 6.24: NO_x emissions during the mission (in kg) in function of the DoH for different e_{Bat}

Due to the increase of the total aircraft energy as the DoH increases, a configuration that brings together the benefits of LTO NO_x, CO and H_2O emissions reduction and the least penalty in the total energy consumption is the 10 % DoH with 1000 Wh/kg batteries (assuming that this level of battery technology can be achieved). Rephrasing, the configurations with e_{Bat} higher than 800 Wh/kg and low levels of hybridization (10 %) can reduce LTO emissions without a penalty in the energy consumption and total CO_2 emitted. However, it is essential to note that the investment that this concept would require it is not worth it to improve local air quality while it brings negligible benefits to the overall mission.

The configurations with higher DoH (higher percentage of electric assistance), for a e_{Bat} lower than 800 Wh/kg, exhibit a more significant penalty in the take-off mass, due to the significant electric mass it represents. Simultaneously, these configurations allow larger reductions in LTO emissions. Although it brings advantages in the LTO cycle, high DoH leads to significant penalties in the total CO_2 emitted and mainly on energy consumption.

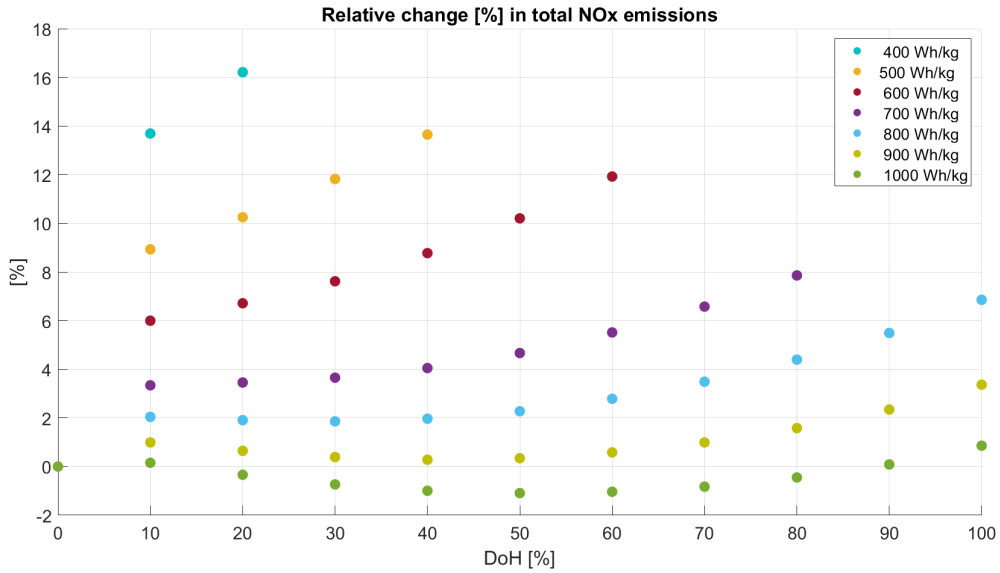

Figure 6.25: NO_x emissions during the mission (in kg) in function of the DoH for different e_{Bat}

Note that it was assumed that the electric energy is clean and that there was zero CO_2 emitted in its life-cycle. Therefore, if the real value of CO_2 is included in the analysis, the small CO_2 observed would no longer be visible.

7

Conclusions and Recommendations

In Europe, Air traffic is foreseen to rise by 42 % from 2017 to 2040. Consequently, aircraft emissions are expected to escalate, even under anticipated technology and operational improvements, leading to the search for new technologies and implementation of more stringent standards and regulations. Particularly, emissions emitted at low altitudes (including vicinity of airports) play a major role on Local Air Quality, and they have a detrimental impact on the environment and human health and welfare. NO_x and CO emissions are examples of emissions that are monitored and regulated at low altitudes, in the so-called LTO cycle. This cycle targets the emissions released below 3,000 ft (914 meters), comprising taxi, take-off, climb-out and approach and the emissions are measured.

Hybrid-electric propulsion has been investigated for the last decades as possible solution to reduce the climate impact of aviation. HEP allows several architectures, but for low levels of hybridization (partial hybridization of a mission), one that allows an easier integration (requires the least modifications in the baseline aircraft), is the parallel architecture. This architecture is also lighter and more efficient due to the least number of electric components required and least energy conversions, respectively.

As a result, this architecture has been tested in turbofan commercial aircraft (which are heavy and required to fly large ranges), but previous research have shown that this concept is highly dependent on the technology maturity scenario of electric components (mainly batteries). Thus, this research aims to investigate if this architecture could be advantageous in a relatively shorter aircraft that flies slightly shorter ranges, a regional turboprop. Moreover, due to the urge to reduce Local Air Quality emissions, this research focuses on low altitude segments.

With all the above mentioned in mind, the research of this master thesis was to assess whether an electrically assisted turboprop could play a role in diminishing the NO_x, CO and H_2O emissions in the LTO cycle.

The aircraft ATR72-600 was used as the baseline regional turboprop aircraft and simulated in an economic mission generated by `Piano-X ®`. A mission simulation routine with mission analysis was developed in `Matlab ®`. This routine uses of two modules that were also developed:

- **Turboprop Engine Module**: A model of a PW127-M (ATR72-600 certified engine) was created using the software `GSP ®`. This module gives as outputs a detailed performance of the turboprop for each operating condition, including the emission indexes of NO_x and CO that are interpolated by using a $T_{T3} - P_{T3}$ method.
- **Electric System Modelling Module**: Estimates the weight of the batteries, electric motors, inverters, transmission cabling and cooling based on the technology maturity scenario and electric Power requirements.

The hybridization strategy implemented is in line with the research goal. Taxi in and out are fully electric and the take-off, climb-out (up to 3048 meters) and approach are hybridized from 10 to 100 %.

Since this a preliminary study on the potential of low altitude hybridization in a regional aircraft, a complete re-design of the aircraft has not been performed at this stage. It is important to highlight that the re-sizing of the aircraft should be done to assess the full benefits of incorporating a hybrid-electric powertrain.

For an economic mission of 1000 Km range and fixed payload of 5,000 kg (not including the electric system weight), NO_x emissions in the LTO cycle can be reduced from 29 % up to 71 %, and CO from 15.4 % up to 21 %. As to H_2O produced in the LTO cycle, it can be reduced from 31 % up to 55%. The significant reduction observed is due to the hybridization strategy picked in this research, that focuses on electrically assistance at low altitude segments (lower than 3048 meters of altitude).

Reductions in the LTO emissions are achievable with SoA battery technology. However, it is important to look at other performance parameters of the mission. For SoA technology, the increase in the take-off mass, energy consumption, and CO_2 is such that off-sets the LTO benefits. It is not worth it to invest in an electrically assisted turboprop with the SoA technology.

Configurations with battery specific energy (e_{Bat}) higher than 800 Wh/kg bring together the advantage of NO_x and CO emissions reduction and a slight decrease in the total CO_2 emitted in the entire mission. This is possible due to a small decrease in fuel burnt achieved for these technology scenarios. However, even under such a positive scenario, there is an energy penalty associated.

For all the configurations (a combination of DoH and e_{Bat}) simulated, the aircraft TOF mass has increased (when compared to the baseline), even for fully electrically assisted powertrain (DoH= 100%), and the most optimistic battery technology scenario (1000 Wh/kg). Meaning that the electric system weight added off-sets any benefit from fuel-saving in mass. The fuel burnt mass has shown to be less than the baseline only for e_{Bat} higher than 800 Wh/kg, and even in this case, a 2% decrease is achieved.

Proportionally to the fuel burnt, a negligible reduction in the overall CO_2 emissions is detected (up to 2 %) for e_{Bat} higher than 800 Wh/kg. In this analysis, it has been assumed that the electric energy used is clean and that the battery life-cycle is carbon-free. However, it would be meaningful to compute the real carbon footprint of batteries. Most likely the little CO_2 saving observed would be off-set.

This research concludes that emissions in the LTO cycle of a regional turboprop aircraft can be reduced with the incorporation of a parallel-hybrid electric architecture. However, it is necessary to look at the whole picture and analyze the impact of such a hybridization strategy in the entire flight. Even for the optimistic values of e_{Bat}, there is a penalty in the aircraft take-off mass, energy consumption, and CO_2, H_2O and NO_x emissions of the entire flight. A revolutionary technology that could enable battery technology to go beyond 1000 Wh/kg would be necessary for parallel-hybrid electric retrofitted regional aircraft to become a beneficial concept in reducing LTO emissions without a penalty in the overall mission performance.

7.1. Recommendations for future work

Regarding the work that has been done in this research, a few upgrades could be done:

- Replace the propeller and turbine maps by their real performance maps.
- The propeller performance should be analyzed separately of GSP
- Up-date the LTO emissions table with the most recent data to obtain more accurate absolute values of Emission Index
- Develop a more accurate sizing of the electric system. Detailed performance of each electrical component at each operating point and the sizing of a thermal management system should be added in future models.
- Account for the volumetric density of the electric components and evaluate whether the volume fits in the aircraft.
- Study the behavior of a powertrain with less than 10 % of DoH

Moreover, the possibility of flying an even shorter range (shorter than 1000 Km) should be studied to compute the sensitivity of the aircraft weight, emissions, and energy consumption to the mission range.

Not only that but a switch in the design point of the engine from take-off to cruise (the operating point where the propeller is more efficient) and assist electrically the phases that have higher power requirements can theoretically bring advantages. It would allow the gas turbine to work at its optimum point constantly and

the turboprop engine to be re-designed (by delivering less power, a smaller engine and lighter is permitted).

Another recommendation would be to analyze the noise that the electrically assisted turboprop would generate since turboprops are noisy, and it is a vital parameter to analyze.

Lastly, due to HEPS's strong dependency on battery technology, its feasibility will not occur before 2040 (the predicted year for 1000 Wh/kg battery technology). As such, there is an urge to look into other alternatives. The usage of alternative fuels in regional turboprop aircraft to reduce fuel burnt could be a solution to be implemented in the short-term. Moreover, research on a more advanced turboprop engine (with higher pressure ratio) and an optimized combustion chamber (able to reduce NO_x emissions) could be a solution to achieve a fuel burn reduction and improve local air quality in the near future.

A

Appendix 1- Results

Shaft Power breakdown for different H_P and e_{Bat} of 1000 Wh/kg

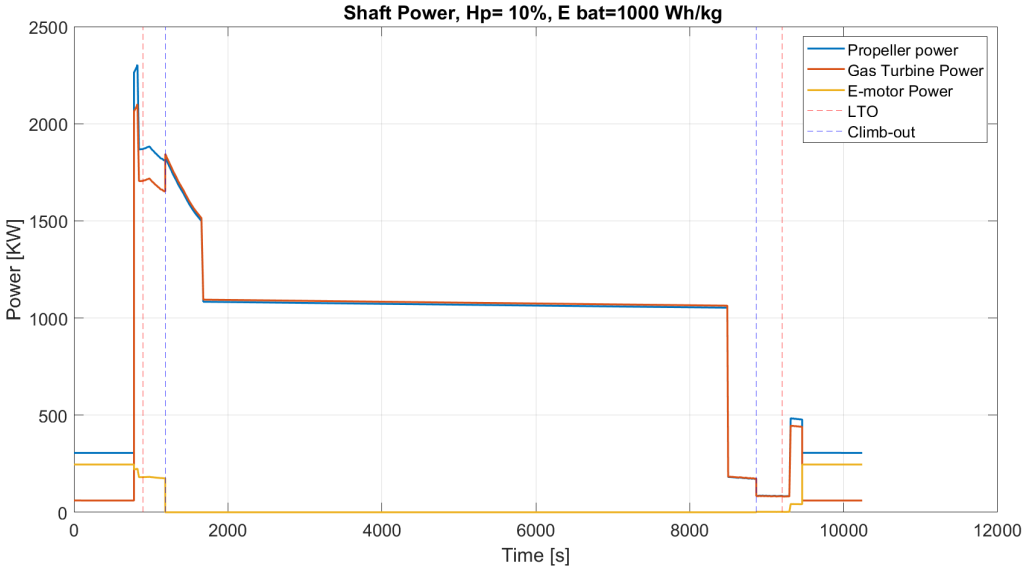

Figure A.1: Shaft Power breakdown with e_{Bat} of 1000 Wh/kg for Power Split ratio of 10%

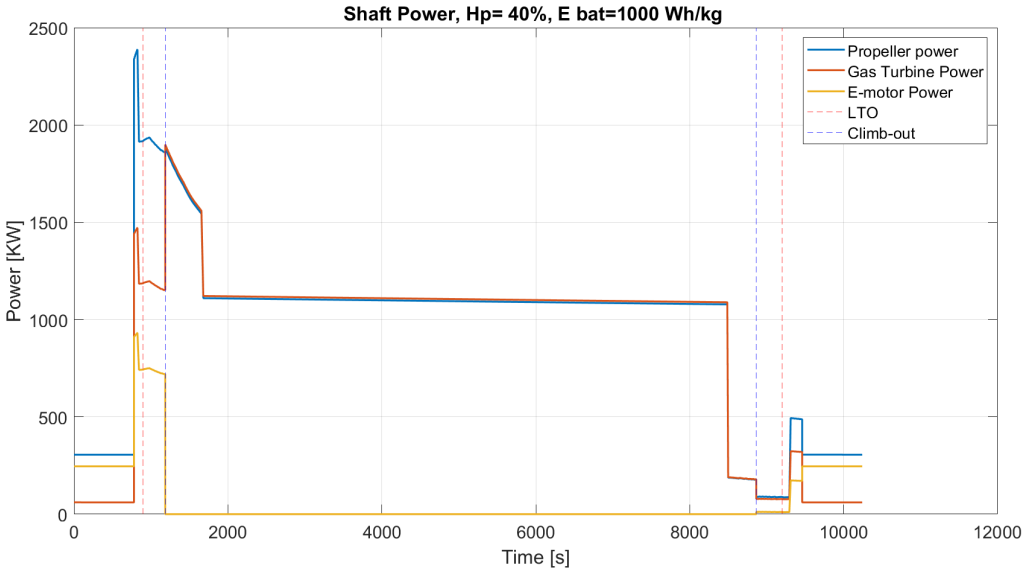

Figure A.2: Shaft Power breakdown with e_{Bat} of 1000 Wh/kg for Power Split ratio of 40%

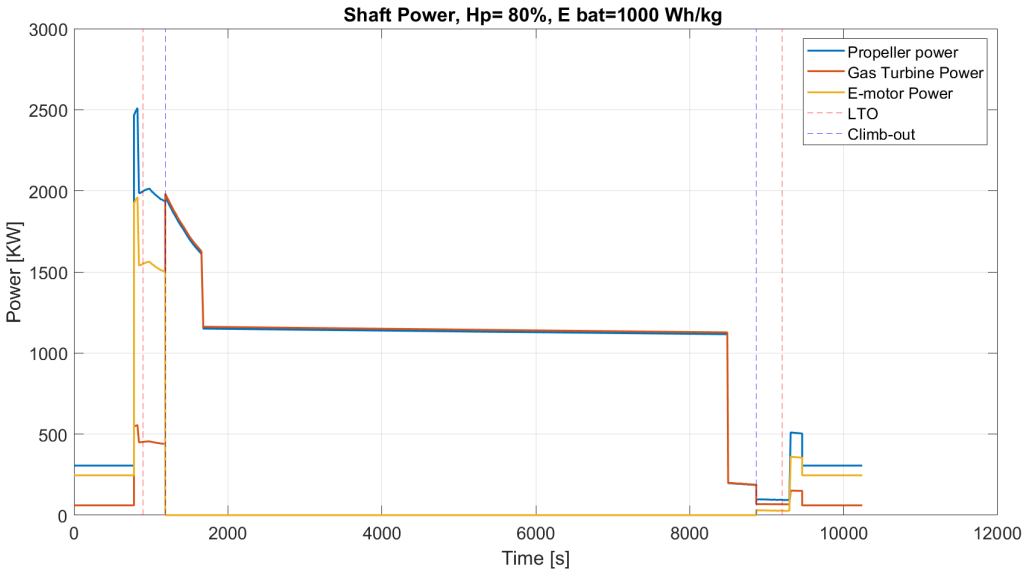

Figure A.3: Shaft Power breakdown with e_{Bat} of 1000 Wh/kg for Power Split ratio of 80%

Lift-to-drag ratio (L/D) during mission with e_{Bat} of 600, 800 and 1000 Wh/kg for different DoH

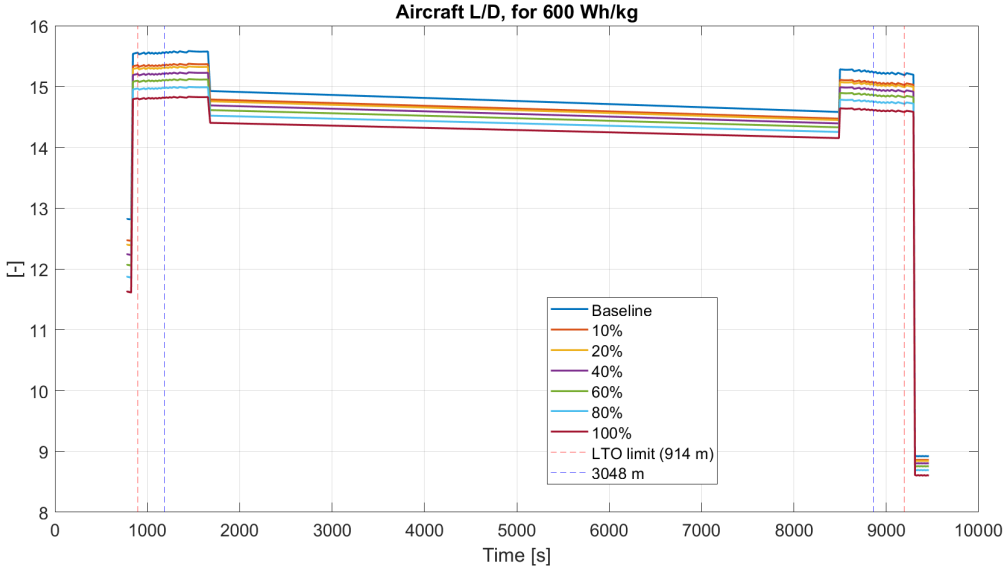

Figure A.4: Lift-to-drag ratio with e_{Bat} of 600 Wh/kg for different Power split ratios

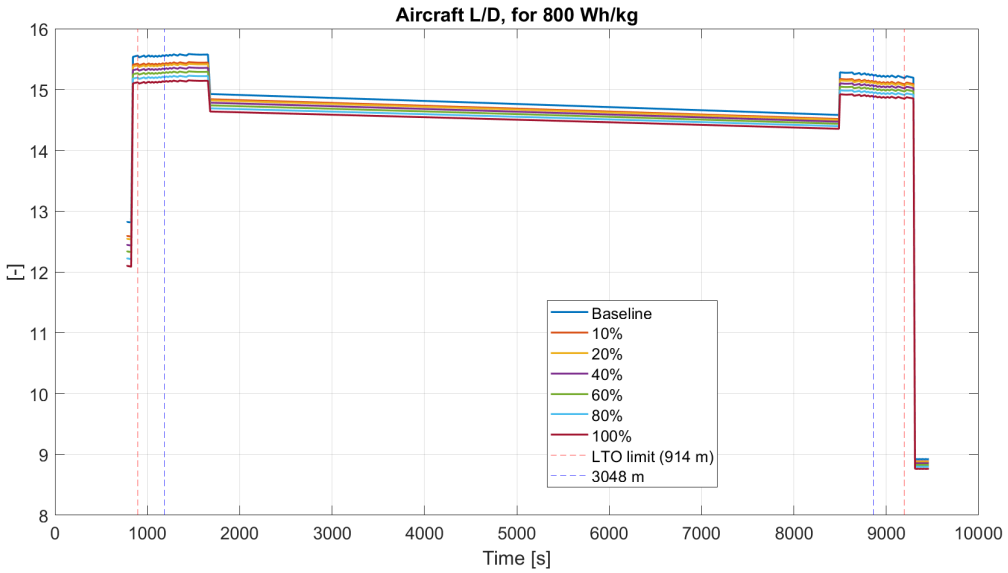

Figure A.5: Lift-to-drag ratio with e_{Bat} of 800 Wh/kg for different Power split ratio

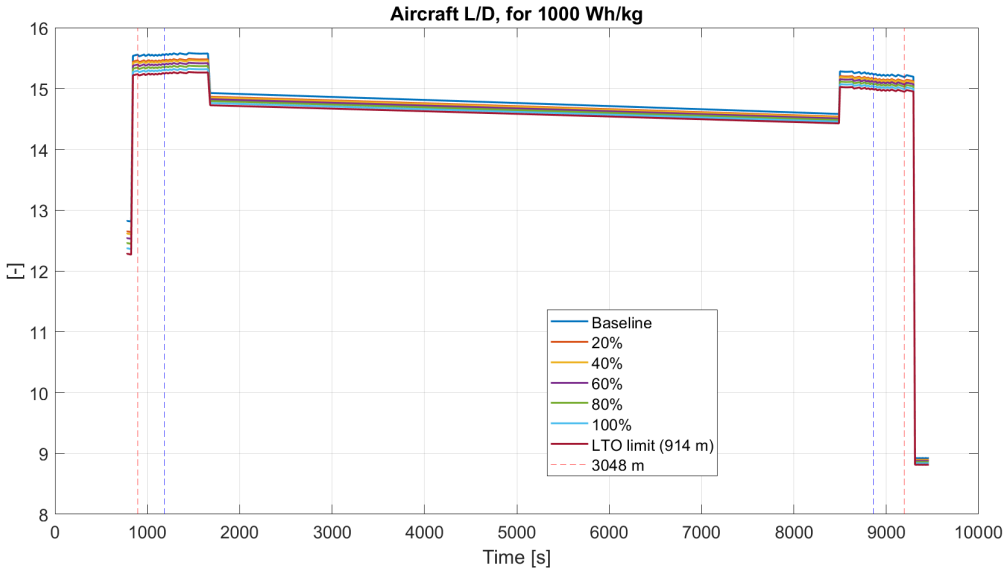

Figure A.6: Lift-to-drag ratio with e_{Bat} of 1000 Wh/kg for different Power split ratio

Fuel flow during mission with e_{Bat} of 800 Wh/kg for different DoH

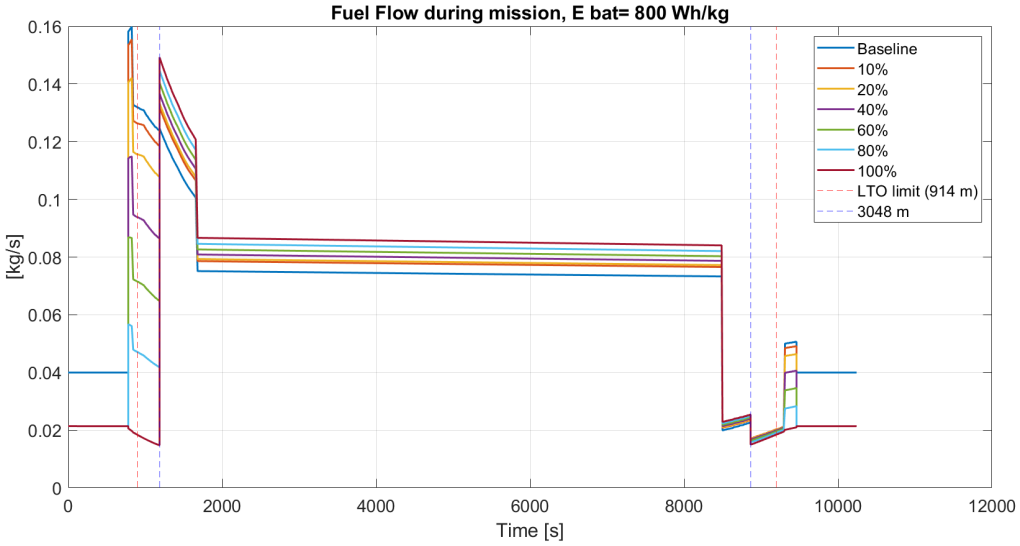

Figure A.7: Fuel flow during mission with e_{Bat} of 800 Wh/kg

Emission Index of NO_x and CO with e_{Bat} of 800 Wh/kg for different DoH

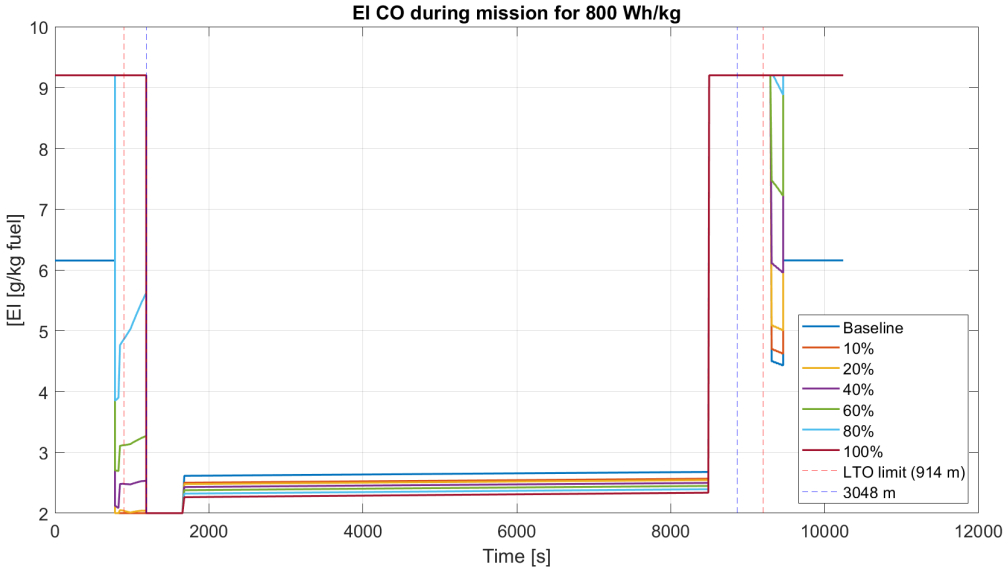

Figure A.8: Emission Index of CO during mission with e_{Bat} of 800 Wh/kg

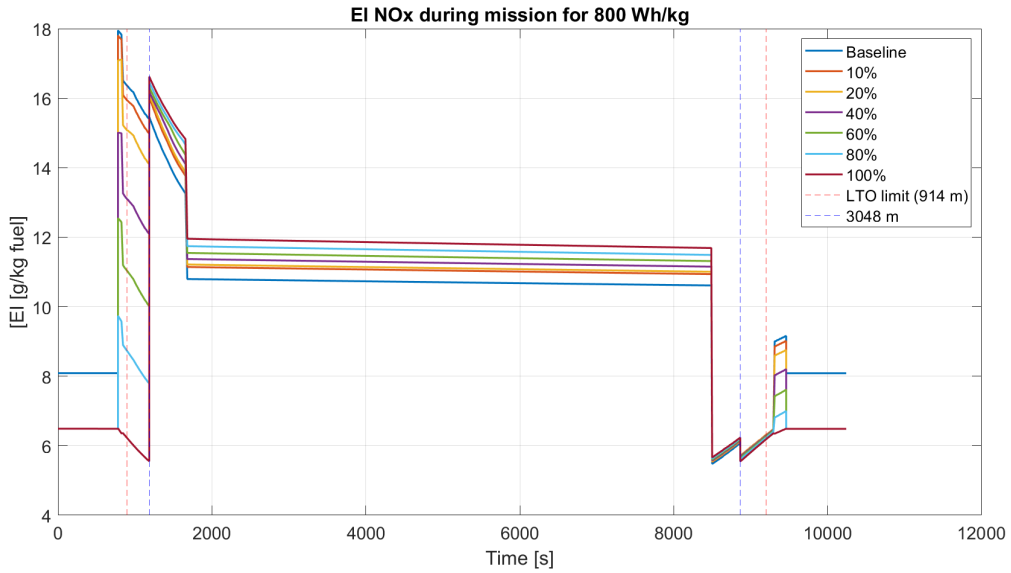

Figure A.9: Emission Index of NO_x during mission with e_{Bat} of 800 Wh/kg

Variable weight breakdown for different configurations

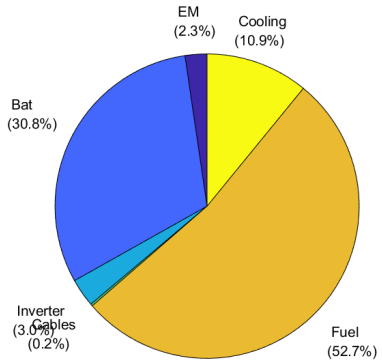

Figure A.10: Electric system plus fuel (excluding reserves) weight percentage for DoH of 20% and e_{Bat}s of 600 Wh/kg

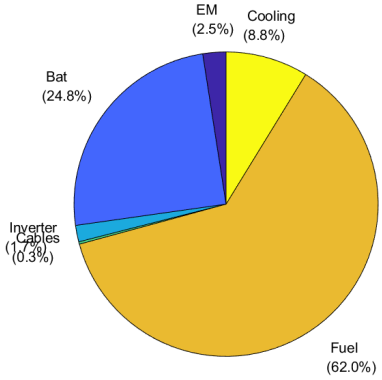

Figure A.11: Electric system plus fuel (excluding reserves) weight percentage for DoH of 20% and e_{Bat} of 800 Wh/kg

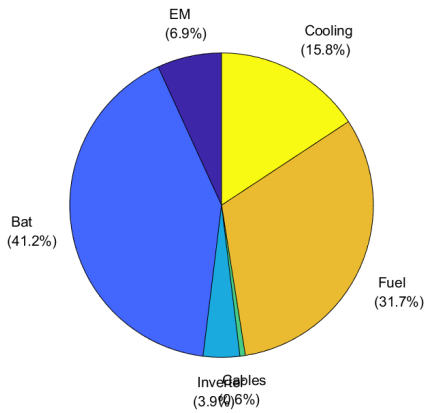

Figure A.12: Electric system plus fuel (excluding reserves) weight percentage for DoH of 60% and e_{Bat} of 400 Wh/kg

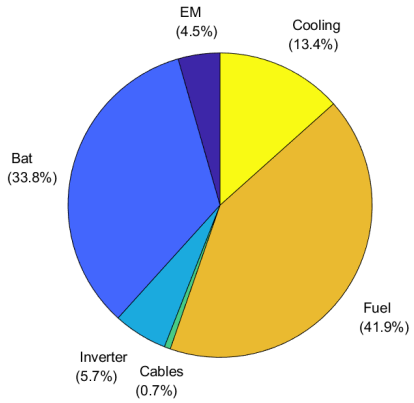

Figure A.13: Electric system plus fuel (excluding reserves) weight percentage for DoH of 60% and e_{Bat} of 600 Wh/kg

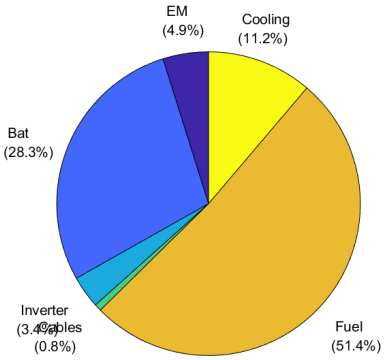

Figure A.14: Electric system plus fuel (excluding reserves) weight percentage for DoH of 60% and e_{Bat} of 800 Wh/kg

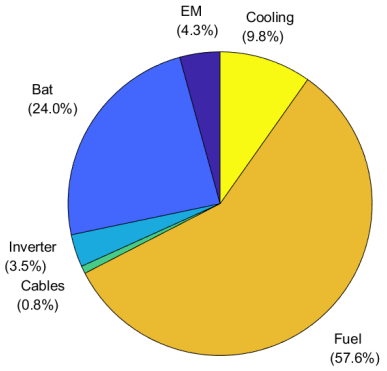

Figure A.15: Electric system plus fuel (excluding reserves) weight percentage for DoH of 60% and e_{Bat} of 1000 Wh/kg

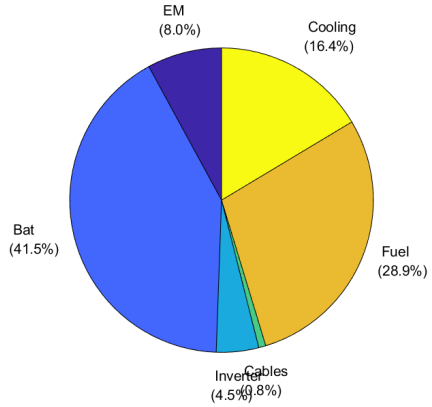

Figure A.16: Electric system plus fuel (excluding reserves) weight percentage for DoH of 80% and e_{Bat} of 400 Wh/kg

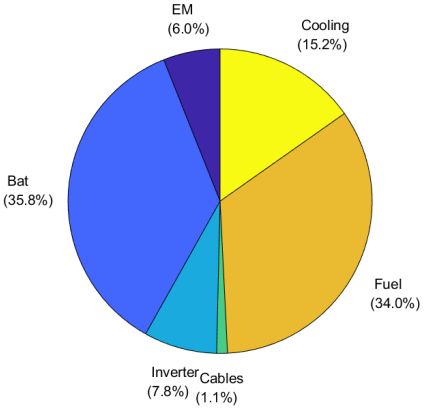

Figure A.17: Electric system plus fuel (excluding reserves) weight percentage for DoH of 80% and e_{Bat} of 600 Wh/kg

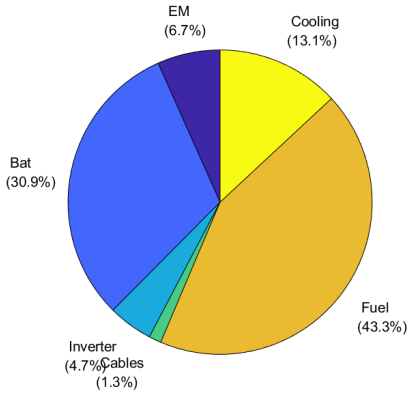

Figure A.18: Electric system plus fuel (excluding reserves) weight percentage for DoH of 80% and e_{Bat} of 800 Wh/kg

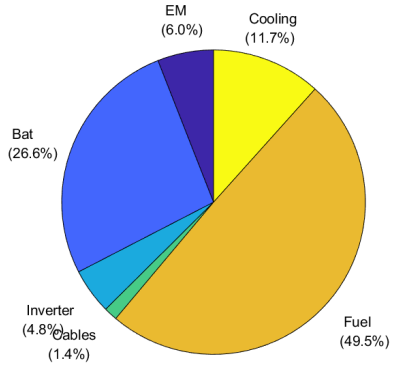

Figure A.19: Electric system plus fuel (excluding reserves) weight percentage for DoH of 80% and e_{Bat} of 1000 Wh/kg

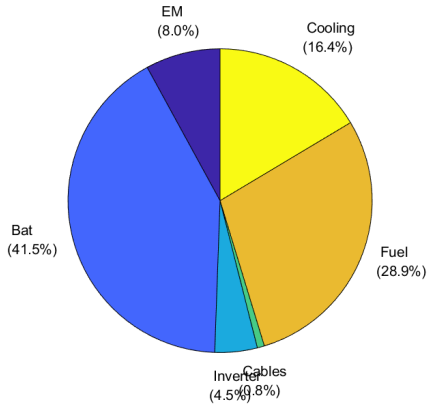

Figure A.20: Electric system plus fuel (excluding reserves) weight percentage for DoH of 100% and e_{Bat} of 400 Wh/kg

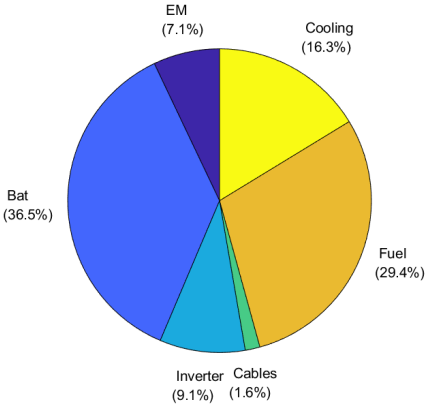

Figure A.21: Electric system plus fuel (excluding reserves) weight percentage for DoH of 100% and e_{Bat} of 600 Wh/kg

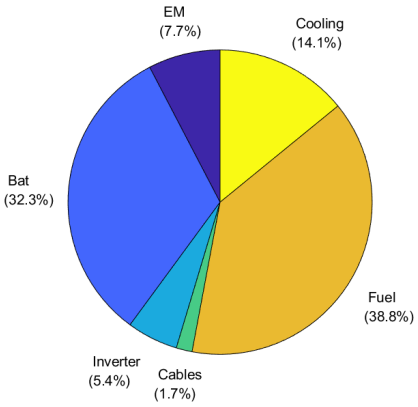

Figure A.22: Electric system plus fuel (excluding reserves) weight percentage for DoH of 100% and e_{Bat} of 800 Wh/kg

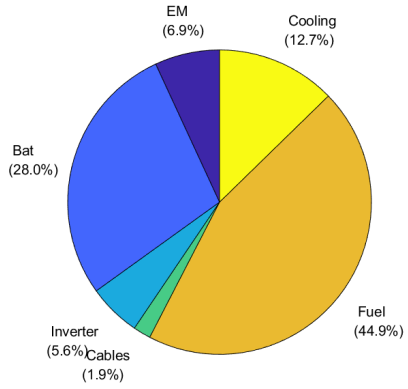

Figure A.23: Electric system plus fuel (excluding reserves) weight percentage for DoH of 100% and e_{Bat} of 1000 Wh/kg

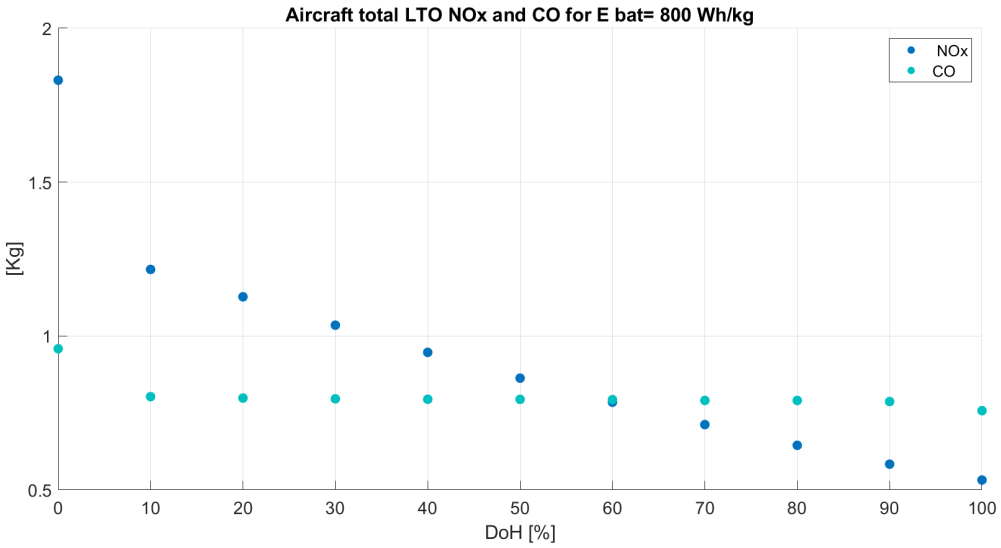

Figure A.24: NO_x and CO mass (in kg) emitted at the LTO cycle (below 914 m) in function of the DoH for e_{Bat} of 800 Wh/kg

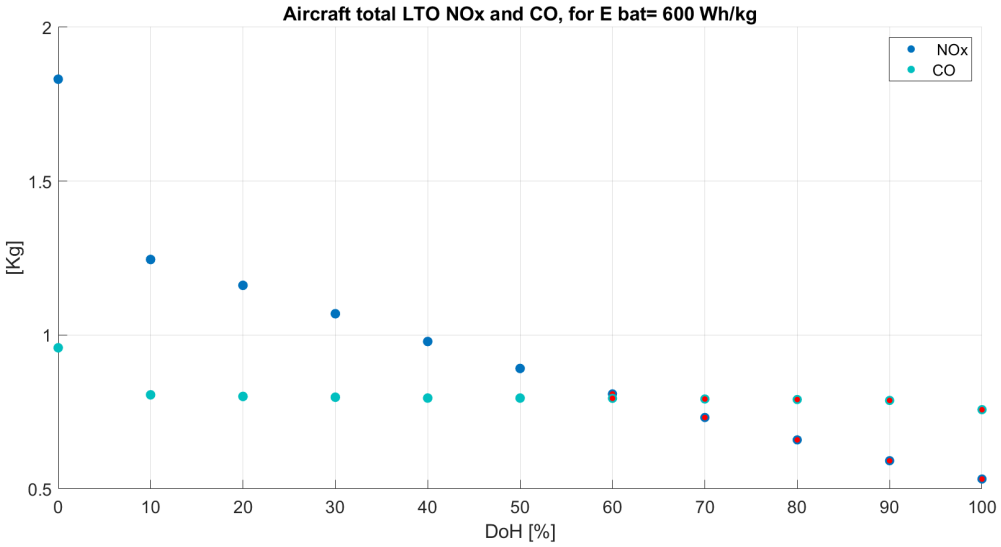

Figure A.25: NO_x and CO mass (in kg) emitted at the LTO cycle (below 914 m) in function of the DoH for e_{Bat} of 600 Wh/kg

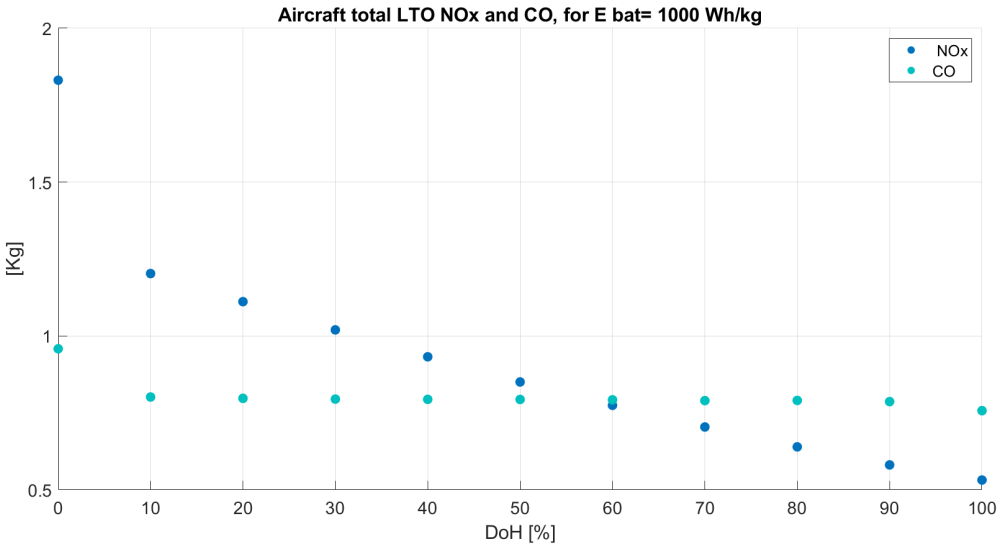

Figure A.26: NO_x and CO mass (in kg) emitted at the LTO cycle (below 914 m) in function of the DoH for e_{Bat} of 1000 Wh/kg

B

Appendix 2- Performance maps

Propeller

The propeller performance is interpolated in a propeller map (figure B.1). The four main parameters displayed in the propeller map are the propeller efficiency, advance ratio, power coefficient and pitch angle of the propeller. Advance ratio, J, is a dimensionless group used as a scaling parameter: if two propellers have the same J and are geometrically similar, have the same performance index.

After analyzing the propeller maps found in literature [15], the following conclusions can be drawn:

- Appropriate choice of the collective pitch can deliver almost constant propulsive efficiency with increasing flight speed
- Although the flight altitude has a negligible effect on the propulsive efficiency, the propeller performance depends on it

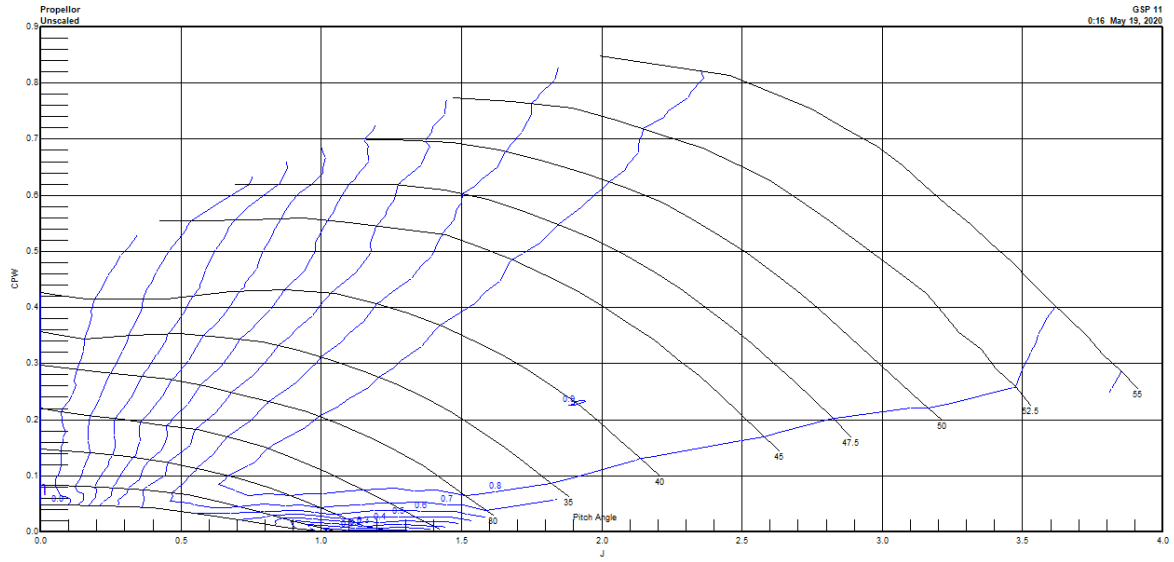

Figure B.1: Performance map from generic propeller, GSP image

$$J = \frac{U}{\Omega R} = \frac{U}{U_{tip}} \tag{B.1}$$

The **axial momentum theory**, **combined momentum** and **blade element theory** are methods used to compute the propulsive performance of an aircraft. The first one is more adequate when detailed data of the propeller in unknown and is not as accurate as the other two. However, constant speed (N) does not lead to highest efficiency at all airspeed. The advance ratio (equation B.1) varies only with flight speed for constant speed

propeller, since the diameter is kept constant, and this variation will lead to different power setting (due to change in C_p). Particularly, at low flight speed the rotational speed needs to decrease in order to keep J at higher levels because in general greater values of J shift the operating point in the propeller map towards higher efficiency zones (towards right).

The downside of variable speed propellers is that the engine to be able to operate over a range of rotational speeds, thus, increasing complexity of controls, structures and costs.

The dimensionless thrust, power and torque coefficients are given by equations B.2, B.3 and B.4, respectively.

$$C_T = \frac{T}{\rho A(\Omega R)^2} \tag{B.2}$$

$$C_P = \frac{P}{\rho A(\Omega R)^3} \tag{B.3}$$

$$C_Q = \frac{Q}{\rho A(\Omega R)^2 R} \tag{B.4}$$

For aircraft propeller driven, the tip speed U_{tip} is restricted to subsonic speeds so that vibrations, noise and losses are kept under their limits. Thus, the tip mach number, given by equation B.5), should be lower than 1.

$$M_{tip} = \frac{U_{tip}}{a} = \frac{1}{a}\sqrt{U^2 + (\Omega R)^2} \tag{B.5}$$

Compressor and Turbine

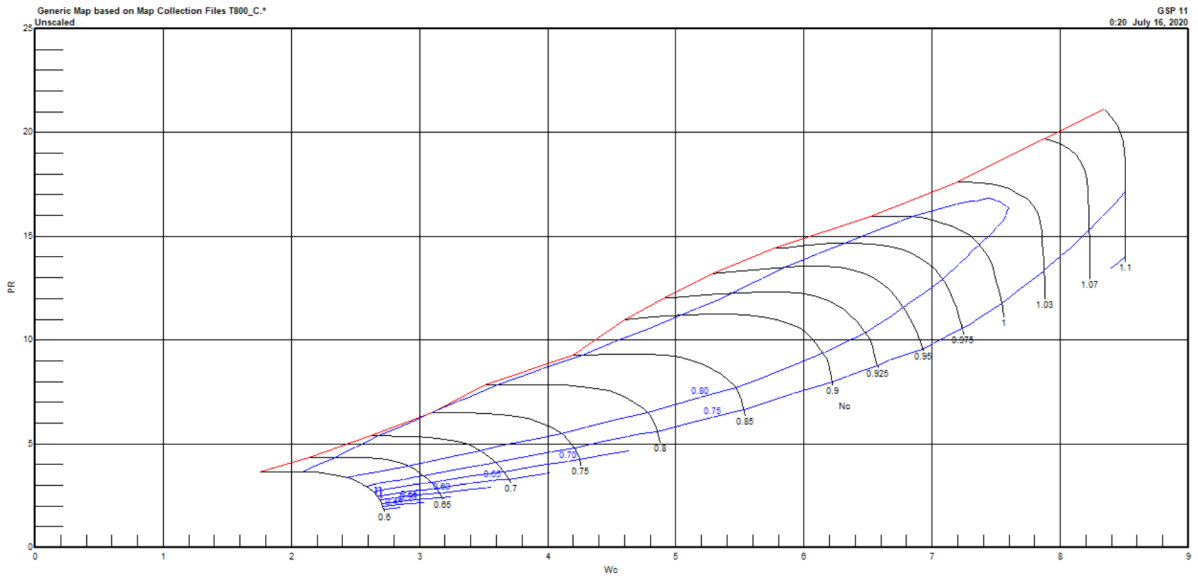

Figure B.2: Performance map from a two-stage radial compressor, GSP image

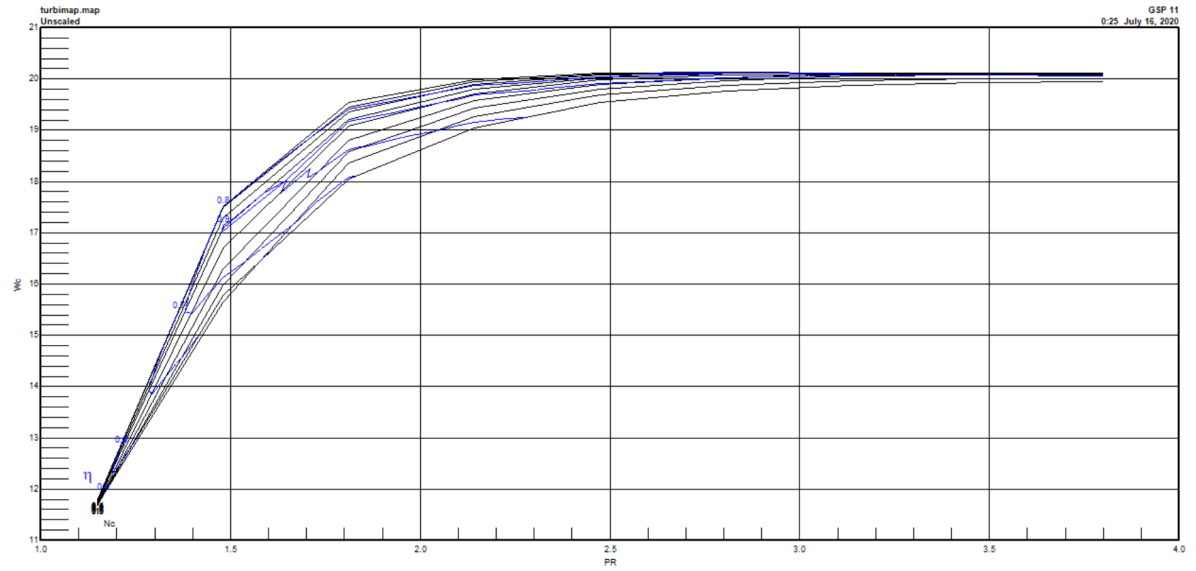

Figure B.3: Performance map from a single-stage turbine, GSP image

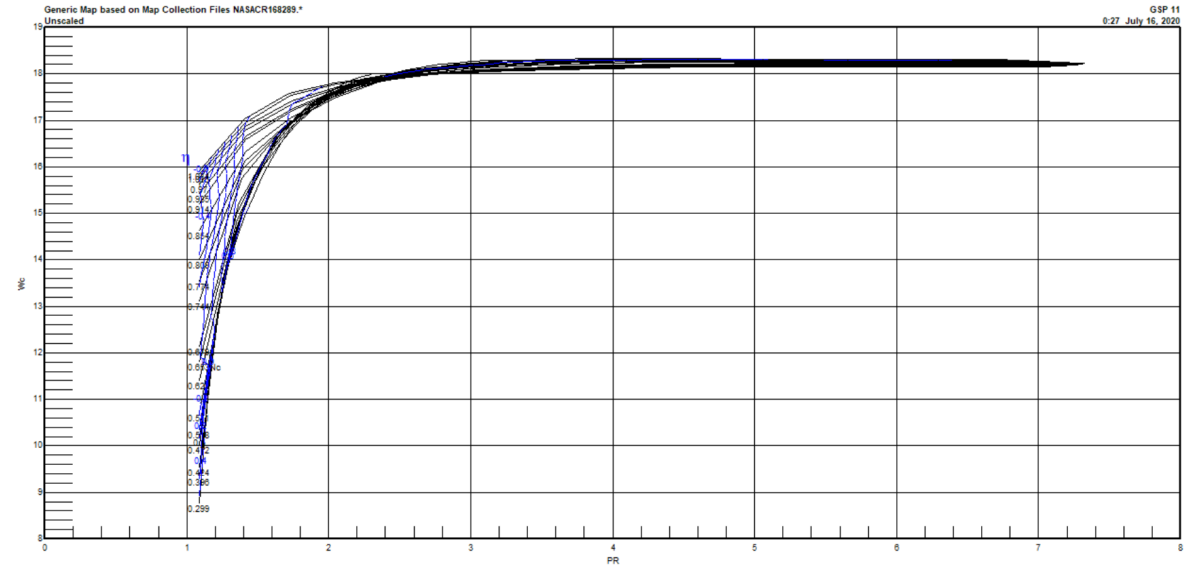

Figure B.4: Performance map from a dual-stage turbine used in the power turbine, GSP image

Bibliography

[1] *Global market forecast 2019-2038,* (2019), https://www.airbus.com/aircraft/market/global-market-forecast.html, visited 2020-03-20.

[2] *Trends in local air quality,* (2017), https://www.icao.int/environmental-protection/Pages/LAQ_Trends.aspx, visited 2020-03-19.

[3] *Atr 72-600,* http://www.atraircraft.com/products/ATR-72-600.html, visited 2020-01-15.

[4] *Pw100/pw150,* (2020), https://www.pwc.ca/en/products-and-services/products/regional-aviation-engines/pw100-150, visited 2020-04-18.

[5] D. S. Lee, D. W. Fahey, P. M. Forster, P. J. Newton, R. C. Wit, L. L. Lim, B. Owen, and R. Sausen, *Aviation and global climate change in the 21st century,* Atmospheric Environment **43**, 3520 (2009).

[6] A. H. Lefebvre and D. R. Ballal, *Gas turbine combustion: alternative fuels and emissions* (CRC, 2010).

[7] ICAO, *2019 environmental report,* https://www.icao.int/environmental-protection/pages/envrep2019.aspx, visited 2020-03-19.

[8] E. National Academies of Sciences and Medicine, *Commercial Aircraft Propulsion and Energy Systems Research: Reducing Global Carbon Emissions* (The National Academies Press, Washington, DC, 2016).

[9] P. Vratny, *Conceptual Design Methods of Electric Power Architectures for Hybrid Energy aircraft*, Ph.D. thesis, Technische Universitat Munchen (2018).

[10] P. Vratny, P. Forsbach, A. Seitz, and M. Hornung, *Investigation of universally electric propulsion systems for transport aircraft,* (2014).

[11] S.-H. Kim, *Chapter 1 - fundamentals of electric motors,* in *Electric Motor Control*, edited by S.-H. Kim (Elsevier, 2017) pp. 1 – 37.

[12] Min Chen and G. A. Rincon-Mora, *Accurate electrical battery model capable of predicting runtime and i-v performance,* IEEE Transactions on Energy Conversion **21**, 504 (2006).

[13] N. Xue, W. Du, J. Martins, and W. Shyy, *Lithium-ion batteries: Thermomechanics, performance, and design optimization,* (2015).

[14] *Method for estimating aviation fuel burnt and emissions in the framework of the EMEP/EEA air pollutant emission inventory guidebook 2016* (EUROCONTROL) https://www.eurocontrol.int, visited 2020-04-20.

[15] A. Filippone, *Advanced Aircraft Flight Performance* (2012).

[16] *Fuel saving contribute to a sustainable air transport development* (ATR, 2011).

[17] M. Voskuijl, J. van Bogaert, and A. G. Rao, *Analysis and design of hybrid electric regional turboprop aircraft,* EAS Aeronautical Journal **9**, 15 (2018).

[18] *Ar5 synthesis report,* https://www.ipcc.ch/report/ar5/syr/synthesis-report/, visited 2020-04-02.

[19] *Environmental impact of aircraft,* https://www.foi.se/en/foi/research/aeronautics-and-space-issues/environmental-impact-of-aircraft.html, visited 2020-03-10.

[20] W. Cao, B. Mecrow, G. Atkinson, J. W. Bennett, and D. J. Atkinson, *Overview of electric motor technologies used for more electric aircraft (mea),* Industrial Electronics, IEEE Transactions on **59** (2012), 10.1109/TIE.2011.2165453.

[21] P. Van den Bossche, F. Vergels, J. Van Mierlo, J. Matheys, and W. Van Autenboer, *Subat: An assessment of sustainable battery technology,* Journal of Power Sources **162**, 913 (2006).

[22] *ATR: The optimum choice for a friendly environment*, Vol. CO/EM 467/00 (ATR, 2001).

[23] J. Roskam, *Airplane design Part VI : Preliminary Calculation of Aerodynamic Thrust and Power Characteristics* (DARcorporation, 2004).

[24] *Airport air quality manual,* (2012), https://www.icao.int/environmental-protection/Documents/Publications/FINAL.Doc9889.1stEdition.alltext.en.pdf, visited 2020-03-22.

[25] *Annex 16 - environmental protection - volume ii - aircraft engine emissions,* (2017), https://store.icao.int/products/annex-16-environmental-protection-volume-ii-aircraft-engine-emissions , visited 2020-04-02.

[26] *Annex 16 - environmental protection - volume iii - aeroplane co2 emissions,* (2017), https://store.icao.int/products/annex-16-environmental-protection-volume-iii-aeroplane-co2-emissions, visited 2020-04-02.

[27] EASA, *Aircraft engine nox emissions,* EASA website (2020), https://www.easa.europa.eu/eaer/topics/technology-and-design/aircraft-engine-emissions, visited 2020-03-20.

[28] S. Ashcraft and N. G. R. Center, *Review of propulsion technologies for N+3 subsonic vehicle concepts*, NASA technical memorandum (National Aeronautics and Space Administration, Glenn Research Center, 2011).

[29] R. de Vries, M. Hoogreef, and R. Vos, *Preliminary sizing of a hybrid-electric passenger aircraft featuring over-the-wing distributed-propulsion,* (2019).

[30] B. J. Brelje and J. R. Martins, *Electric, hybrid, and turboelectric fixed-wing aircraft: A review of concepts, models, and design approaches,* Progress in Aerospace Sciences **104**, 1 (2019).

[31] A. Seitz, O. Schmitz, A. Isikveren, and M. Hornung, *Electrically powered propulsion: Comparison and contrast to gas turbines,* (2012).

[32] C. Pornet, G. , P. Vratny, A. Seitz, O. Schmitz, A. Isikveren, and M. Hornung, *Methodology for sizing and performance assessment of hybrid energy aircraft,* Journal of Aircraft **52**, 341 (2014).

[33] G. Brown, *Weights and efficiencies of electric components of a turboelectric aircraft propulsion system,* (2011).

[34] Y. Miyairi, C. Perullo, and D. Mavris, *A parametric environment for weight and sizing prediction of motor/generator for hybrid electric propulsion,* (2015).

[35] R. Berger, *Aircraft Electrical Propulsion – Onwards and Upwards* (2018).

[36] C. Friedrich and P. A. Robertson, *Design of hybrid-electric propulsion systems for light aircraft,* (2014).

[37] A. Isikveren, S. Kaiser, C. Pornet, and P. Vratny, *Pre-design strategies and sizing techniques for dual-energy aircraft,* Aircraft engineering and aerospace technology **86**, 525 (2014).

[38] C. Pornet, *Conceptual Design Methods for Sizing and Performance of Hybrid-Electric Transport Aircraft*, Ph.D. thesis, Technische Universitat Munchen (2018).

[39] A. W X Ang, A. Gangoli Rao, T. Kanakis, and W. Lammen, *Performance analysis of an electrically assisted propulsion system for a short-range civil aircraft,* Proceedings of the Institution of Mechanical Engineers, Part G: Journal of Aerospace Engineering **233**, 095441001775414 (2018).

[40] K. Antcliff, M. Guynn, T. Marien, D. Wells, S. Schneider, and M. Tong, *Mission analysis and aircraft sizing of a hybrid-electric regional aircraft,* (2016).

[41] K. Antcliff and F. Capristan, *Conceptual design of the parallel electric-gas architecture with synergistic utilization scheme (pegasus) concept,* (2017).

[42] A. Misra, *Summary of 2017 nasa workshop on assessment of advanced battery technologies for aerospace applications,* (2018).

[43] M. Hoogreef, R. de Vries, T. Sinnige, and R. Vos, *Synthesis of aero-propulsive interaction studies applied to conceptual hybrid-electric aircraft design,* (2020).

[44] *Flight data monitoring on atr aircraft 2016,* (2016), http://www.atraircraft.com/flightops_support.php , visited 2020-03-25.

[45] J. E. Penner, *Aviation and the global atmosphere* (Cambridge University Press, 1999).

[46] *NOx Sensitivities for Gas Turbine Engines Operated on Lean-Premixed Combustion and Conventional Diffusion Flames*, Turbo Expo: Power for Land, Sea, and Air, Vol. Volume 3: Coal, Biomass and Alternative Fuels; Combustion and Fuels; Oil and Gas Applications; Cycle Innovations (1992).

[47] D. Allaire and M. Astronautics, *A physics-based emissions model for aircraft gas turbine combustors,* (2007).

[48] C. Gleason and D. Bahr, *Experimental clean combustor program* (1979).

[49] *Local air quality technology standards,* (), https://www.icao.int/environmental-protection/Pages/LAQ_TechnologyStandards.aspx, visited 2020-03-18.

[50] *Icao aircraft engine emissions databank,* (), eASA website https://www.easa.europa.eu/domains/environment/icao-aircraft-engine-emissions-databank, visited 2020-04-15.

[51] A. F. El-Sayed, *Fundamentals of Aircraft and Rocket Propulsion* (Springer London, 2018).

[52] F. Yin, *Modelling and Characteristics of a Novel Multi-fuel Hybrid Engine for Future Aircraft*, Ph.D. thesis (2016).

[53] J. L. Felder, *Nasa electric propulsion system studies,* in *5th EnergyTech 2015* (Cleveland, OH, United States, 2015).

[54] A. Isikveren, S. Kaiser, C. Pornet, and P. Vratny, *Pre-design strategies and sizing techniques for dual-energy aircraft,* Aircraft engineering and aerospace technology **86**, 525 (2014).

[55] M. de Vries, R.and Brown and R. Vos, *A preliminary sizing method for hybrid-electric aircraft including aero-propulsive interaction effects,* 18th AIAA Aviation Technology, Integration, and Operations Conference (2018).

[56] J. Hung and L. Gonzalez, *On parallel hybrid-electric propulsion system for unmanned aerial vehicles,* Progress in Aerospace Sciences **51**, 1 (2012).

[57] R. Jansen, C. Bowman, A. Jankovsky, R.Dyson, and J.Felder, *Overview of nasa electrified aircraft propulsion (eap) research for large subsonic transports,* in *53rd AIAA/SAE/ASEE Joint Propulsion Conference*, AIAA Propulsion and Energy Forum (American Institute of Aeronautics and Astronautics, 2017).

[58] A. Seitz, M. Nickl, A. Stroh, and P. Vratny, *Conceptual study of a mechanically integrated parallel hybrid electric turbofan,* Proceedings of the Institution of Mechanical Engineers, Part G: Journal of Aerospace Engineering **232**, 095441001879014 (2018).

[59] J. Bijewitz, A. Seitz, and M. Hornung, *A review of recent aircraft concepts employing synergistic propulsion-airframe integration,* (2016).

[60] O. Schmitz and M. Hornung, *Unified applicable propulsion system performance metrics,* (2013).

[61] P. Vratny, H. Kuhn, and M. Hornung, *Influences of voltage variations on electric power architectures for hybrid electric aircraft,* CEAS Aeronautical Journal **8**, 31 (2017).

[62] C. Sanabria von Walter, *Design of high-torque-density synchronous drives for propulsion of rotary-wing aircraft*, Ph.D. thesis, Delft University of Technology (2016).

[63] CERN, *Superconductivity,* (2019), https://home.cern/science/engineering/superconductivity, visited 2020-03-20.

[64] K. Sivasubramaniam, T. Zhang, M. Lokhandwalla, E. Laskaris, J. Bray, B. Gerstler, M. Shah, and J. Alexander, *Development of a high speed hts generator for airborne applications,* Applied Superconductivity, IEEE Transactions on **19**, 1656 (2009).

[65] C. Luongo, P. Masson, T. Nam, D. Mavris, H. D. Kim, G. V. Brown, M. Waters, and D. Hall, *Next generation more-electric aircraft: A potential application for hts superconductors,* Applied Superconductivity, IEEE Transactions on **19**, 1055 (2009).

[66] P. Vratny, C. Gologan, C. Pornet, A. Isikveren, and M. Hornung, *Battery pack modeling methods for universally-electric aircraft,* (2013).

[67] A. Yoshino, *1 - development of the lithium-ion battery and recent technological trends,* in *Lithium-Ion Batteries*, edited by G. Pistoia (Elsevier, Amsterdam, 2014) pp. 1 – 20.

[68] D. Linden and T. B. Reddy, *Handbook of Batteries* (McGraw-Hill, New York, N.Y., 2002).

[69] J. Zamboni, R. Vos, M. Emeneth, and A. Schneegans, *A method for the conceptual design of hybrid electric aircraft,* (2019).

[70] M. Cameretti, A. Pizzo, L. Di Noia, and C. Pascarella, *Modeling and investigation of a turboprop hybrid electric propulsion system,* Aerospace (Basel) **5** (2018), 10.3390/aerospace5040123.

[71] R. de Vries, M. Brown, and R. Vos, *A preliminary sizing method for hybrid-electric aircraft including aero-propulsive interaction effects,* (2018).

[72] M. Daly, *IHS Janes aero-engines: 2015-2016* (IHS Janes, 2015).

[73] *Type-certificate data sheet no. easa.a.084 for atr 42 and atr 72,* TYPE-CERTIFICATE DATA SHEET No. EASA.A.084 (2019).

[74] J. Roskam, *Airplane design Part I :Preliminary Sizing of Airplanes* (DARcorporation, 1997).

[75] *Pw100/pw150,* (2020), https://www.pwc.ca/en/products-and-services/products/regional-aviation-engines/pw100-150, visited 2020-01-15.

[76] *ATR 72- Flight Crew Operating Manual (FCOM)* (1999).

[77] *Gas turbine simulation program,* https://www.gspteam.com, visited 2020-04-02.

[78] W. Visser and M. Broomhead, *Gsp, a generic object-oriented gas turbine simulation environment,* (2000).

[79] *type-certificate data sheet - for engine pw100 series engines,* https://www.easa.europa.eu/sites/default/files/dfu/EASAIM.E.041TCDSIssue4.pdf, visited 2020-01-15.

[80] E. Hosking, D. P. Kenny, R. I. McCormick, and S. H. Moustapha, *The pw100 engine: 20 years of gas turbine technology evolution,* in *Symposium, Design principles and methods for aircraft gas turbine engines* (NATO, 1999).

[81] R. Elodie, *Turboshaft, Turboprop and Propfan: Database Handbook* (Editions Elodie Roux, 2011).

[82] S. Stückl, *Methods for the design and evaluation of future aircraft concepts utilizing electric propulsion systems,* (2016).

[83] P. Vratny, C. Gologan, C. Pornet, A. Isikveren, and M. Hornung, *Battery pack modeling methods for universally-electric aircraft,* (2013).

[84] P. Vratny, C. Gologan, C. Pornet, A. Isikveren, and M. Hornung, *Battery pack modeling methods for universally-electric aircraft,* (2013).

[85] H. Kuhn, A. Seitz, L. Lorenz, A. T. Isikveren, and A. Sizmann, *Progress and perspectives of electric air transport,* in *28th International Congress of the International Council of the Aeronautical Sciences ICAS*, Vol. 6 (2012).

[86] T. P. Dever, K. P. Duffy, A. J. Provenza, P. L. Loyselle, B. B. Choi, C. R. Morrison, and A. M. Lowe, *Assessment of technologies for noncryogenic hybrid electric propulsion,* (2015).

[87] C. A. Luongo, P. J. Masson, T. Nam, D. Mavris, H. D. Kim, G. V. Brown, M. Waters, and D. Hall, *Next generation more-electric aircraft: A potential application for hts superconductors,* IEEE Transactions on applied superconductivity **19**, 1055 (2009).

[88] G. Brown, *Weights and efficiencies of electric components of a turboelectric aircraft propulsion system,* in *49th AIAA aerospace sciences meeting including the new horizons forum and aerospace exposition* (2011) p. 225.